Computational modelling on the final closure gaps in the Saemangeum dam, South Korea

M.B. van der Sande BSc
November 2006

Delft University of Technology
Faculty of Civil Engineering and Geosciences
Section of Hydraulic Engineering

Ministry of Transport, Public Works and Water Management
Directorate-General of Public Works and Water Management
Civil Engineering Division

Computational modelling on the final closure gaps in the Saemangeum dam, South Korea

M.B. van der Sande BSc.
Student number 1012177

November, 2006

A dissertation submitted in partial fulfilment of the requirements for the degree of Master of Science in Civil Engineering, specialisation Hydraulic Engineering and Fluid Mechanics

Examination Committee:

Prof.drs.ir. J.K. Vrijling
> Delft University of Technology, Faculty of Civil Engineering and Geosciences, Section Hydraulic Engineering

Ir. H.J. Verhagen
> Delft University of Technology, Faculty of Civil Engineering and Geosciences, Section Hydraulic Engineering

Ir. T.J. Zitman
> Delft University of Technology, Faculty of Civil Engineering and Geosciences, Section Hydraulic Engineering

Drs. R.Booij
> Delft University of Technology, Faculty of Civil Engineering and Geosciences, Section Environmental Fluid Mechanics

Dr.ir. A. Vrijburcht
> Ministry of Transport, Public Works and Water Management, Directorate-General of Public Works and Water Management, Civil Engineering Division

TUDelft
Delft University of Technology

Ministerie van Verkeer en Waterstaat
Directoraat-Generaal Rijkswaterstaat
Bouwdienst Rijkswaterstaat

Cover picture: Final closure of the Saemangeum dam. Picture has been taken during last day of closure works on April 20, 2006.

"πάντα ρεί και ουδεν μενεί"

'Everything flows and nothing stays fixed'

Heraclitus (535 BC-475 BC)

Acknowledgements

The present report is the result of the research project undertaken in order to obtain the degree of Master of Science at Delft University of Technology. During a period of two and a half months, the research has been executed at the project location in South Korea. Afterwards the results have been elaborated at Delft University of Technology in the Netherlands. The research has been sponsored by Directorate-General of Public Works and Water Management, Civil Engineering Division and the section Hydraulic Engineering of the faculty of Civil Engineering and Geosciences of Delft University of Technology.

A two and a half moth stay in South Korea appeared to be a great adventure and a very valuable experience. I would like to thank all the members of the project team Gé and Marina Beaufort, Rik Beekx, Arie Vrijburcht and Kees Dorst for their support, encouragement and companionship during the two and a half months in South Korea. My thanks also go to all the Korean authorities for their hospitality and complaisance during our stay.

I would like to thank all the staff members of the section Hydraulic Engineering and the students at my graduation office for providing a very welcome and supportive working environment during my stay at Delft University of Technology and the members of the Civil Engineering Division of the Public Works and Water Management. My special thanks go to Mr. Zijlema for his endless patience in helping me with all my Waqua troubles and to Wilco Meijerink for his assistance with the EFD.lab model and for his company during the Fridays in Utrecht.

Last but not least my thanks go to my graduation committee prof.drs.ir J.K. Vrijling, Ir. H.J. Verhagen, Ir. T.J. Zitman, Drs. R.Booij and Dr.ir. A. Vrijburcht for their kind cooperation, enthusiasm and feedback on this research project.

Delft, November 2006
Maartje van der Sande

Abstract

The flow velocities through a closure gap in the final construction stage can be relatively high because the total basin fills and empties through this closure gap. The flow velocities in this final stage are often normative for the design of the construction and the closing method. The stability of the bottom protection is of main importance during the last construction phase because scour holes that develop too close to the construction may cause the total construction to fail. The stability of a bottom protection not only depends on the mean flow velocity but on the turbulent properties of the flow as well.

EFD.lab is a three-dimensional fluid flow model that calculates a detailed pattern of the flow through a closed system, like a tube or a pipeline. EFD.lab is capable of calculating the turbulent properties in a flow. A free water surface cannot be calculated with this model but by using a pressure ceiling, a free surface flow can be modelled. To investigate the suitability of the EFD.lab model for situations with a free water surface like a closure gap, one of the final closure gaps in the Saemangeum dam has been modelled with the EFD.lab model.

Because no measurements could be executed during the closure of the dam, data about water levels at both sides of the dam, which are needed for the input of the EFD.lab model, needed to be estimated. With a storage area approach, a first estimate of the varying water level inside the basin has been made. Subsequently the water level variation during the closing period has been calculated in more detail with a two-dimensional model called Waqua. The predicted water levels have been used as input data for the three-dimensional EFD.lab model.

The storage area approach calculates a water level inside the basin and a depth average flow velocity through the remaining gaps in the dam. The water level inside the basin is assumed horizontal. No distinction has been made between the water level at different locations inside the basin or the flow velocity through the different gaps. Because no data about the varying water level at the seaside of the dam were available for a longer period, the varying water level at a location 20 km north of the closure dam has been used for the calculation. For a few days, data about water level measurements were available. The amplitude of the varying water level at the seaside of the dam was too large compared with these measurements and therefore the amplitude of the prediction of the varying water level at the basin side of the dam, appeared to be too large as well. Despite the fact that the water level variation at both sides of the dam was too large, the water level difference between the two sides of the dam did correspond well with the measured data. The predicted flow velocities through the closure gaps corresponded well with the measured flow velocities.

Waqua is a two-dimensional fluid flow model that calculates the water level and flow velocity at every point in its computational grid. For the modelling of the closure gaps in the Saemangeum dam, the total estuary and a significant part of the foreshore have been taken into account. The computational grid has been refined in the surroundings of the closure gaps. The initiation of the model has been assigned at an open boundary and exists of an in time varying water level, which has been composed by four constituents of the tidal wave. The composed water level variation in the Gunsan Outer Port has been compared with a

measured water level variation in the Gunsan Outer Port. The composed water level variations appeared to be not very accurate but because no other suitable data for the initiation of the model was available, the water level variation composed with the four constituents was used for the initiation. The results of the Waqua calculations have not been compared with real time measurements.

Closure gap number 1 has been modelled with the EFD.lab model. The geometry of the closure gap has been scaled with a factor 2.5 in both the vertical as the horizontal direction, because the computational area in EFD.lab may not exceed 1 by 1 km. Because the EFD.lab model does not calculate the water level, a water level had to be imposed beforehand. After every calculation, this imposed water level has to be adapted to the results. The flow above the sill appeared to be super critical and this instigated problems in modelling the flow. The situation with a seaside water level of 2.29m MSL and a basin side water level of 0.80m MSL has been modelled. The influence of changing several boundary conditions on the results has been investigated. To keep the Froude number in the model the same as the Froude number in the prototype the gravitational acceleration in the calculation has been adapted. The changing of the gravitational acceleration did not influence the results of the calculation. To investigate the turbulence in the model calculation, the turbulent parameters at the boundary of the model have been changed. Changing the turbulent parameters at the boundary of the model did influence the results. Lowering the turbulent values at the boundaries of the model implied less turbulence in the fluid flow. By adapting the turbulence parameters at the boundary of the model as well as in initial values in the general settings, the results were influenced in such a way that the results were no longer plausible. Finally, the influence of changing the roughness of the bottom surface has been investigated. The results of the calculation with an extra bottom roughness showed a higher maximum mean flow velocity above the sill and higher turbulence fluctuations.

The EFD.lab model appeared to be not very suitable for the modelling of fluid flows with free surfaces. Adapting the water level was time consuming and when the flow became super critical, problems arose. The parameters for the turbulent kinetic energy and the turbulent dissipation in the general settings are start values for the calculation and therefore it had not been expected that changing them would influence the results as much as they were. Before the EFD.lab model is used for turbulent calculations in a free surface flow, further investigations are recommended.

Table of contents

List of figures

List of tables

List of symbols

Symbol	Parameter	Unit
A_i	amplitude of tidal constituent	(m)
A_b	storage area of basin	(m^2)
B	widt of gap	(m)
C	Chézy coefficient	(√m/s)
C_d	wind drag coefficient	(-)
d	water depth	(m)
f	Parameter of Coriolis	(-)
Fr	Froude number	(-)
g	gravitatioal acceleration	(m/s^2)
h	depth below reference level	(m)
h_{res}	water level inside basin	(m)
h_2	downstream water level	(m)
Δh	water level difference	(m)
H	h+η	(m)
H_0	upstream energy level	(m)
I	relative turbulence intensity	(%)
k	turbulent kinetic energy	(m^2/s^2)
mu	discharge coeffiecient	(-)
p	pressure	(Pa)
p_d	height of sill	(m)
Q	discharge	(m^3/s)
S	Mass distributed external force	(kg/m^{2}s^2)
u	mean velocity in x-direction	(m/s)
u'	fluctuating velocity	(m/s)
v	mean velocity in y-direction	(m/s)
w	mean velocity in z-direction	(m/s)
α	Variable fro standard normal	(-)
δ	Kronecker delta function	(-)
ε	Turbulent dissipation	(
η	water level above reference level	(m)
ζ	water level above reference level	(m)
μ_l	dynamic viscosity	(kg/ms)
μ_t	turbulent eddy viscosity	(kg/ms)
μ	$\mu_t + \mu_l$	(kg/ms)
ν_l	kinematic viscosity	(m^2/s)
ν_t	eddy viscosity	(m^2/s)
ρ_a	density of air	(kg/m^3)
ρ_w	density of water	(kg/m^3)
τ_{ik}	viscous shear stress tensor	
τ_b	bottom stress term	
φ	phase	(rad)
ω	angular velocity	(rad/s)

1   Introduction

In 1991, the Korean government started with an extensive land reclamation project for which a large tidal estuary needed to be closed off. The Saemangeum estuary would be closed by a dam of 33 km and the enclosed area should be 400 km^2. The final execution phase of the closure dam was scheduled for the spring of 2006. The circumstances at this particular location are rather extreme because of the large tidal amplitude in front of the dam and the large area being closed off. Rijkswaterstaat Bouwdienst in the Netherlands maintains good relations with the South Korean Rural Research Institute (RRI) and the Korean Agricultural and Rural Infrastructure Cooperation (KRC) for several years now. In 2005 the Bouwdienst in cooperation with the Delft University of Technology (TU Delft), decided that participating in a project like this and gaining experience from the final closure would be very valuable.

The flow velocity through the final closure gap in the final stage of a closure can be very high because the whole basin fills and empties itself through this final closure gap. Often, the flow velocity in this final stage is normative for the design of the construction and the closing method. During the construction of a closure dam, one or more closure gaps were left open. Normally, in advance of the final closure phase, a bottom protection has been constructed in the closure gap that ensures that scour holes develop at safe distance from the construction. When these scour holes develop too close to the construction, the entire construction may collapse. Obviously, the stability of this bottom protection is of main importance during the construction phase.

For the computation of an accurate flow profile and the turbulence intensities in a final closure gap of a dam, advanced computational models are required. One of the available models is the Engineering Fluid Dynamics Lab model (EFD.lab), which is a three-dimensional flow and heat transfer model and originates from the oil and gas industry. The model is normally used for the computation of a fluid flow in pipelines and tubes and is not capable of computing a free surface flow. However, by using some adaptations, the situation of a closure gap can be approached. The Bouwdienst is investigating whether the EFD.lab model is capable to calculate correctly a situation with a free surface flow, like a closure gap in a dam,. Because the situation during the closure in Korea was rather extreme, the Bouwdienst decided to execute measurements on the flow properties during the final closure. The goal of the investigation was to compare the EFD.lab model results with the measurement executed in the closure gaps in order to investigate the applicability of the EFD.lab model on this kind of flow problems.

Unfortunately, only a few of the planned measurements were executed during the final closure and a small amount of data was collected. Because of this disappointing amount of data, it appeared to be impossible to compare the results of the EFD.lab model with measurements on the flow velocity in the final closure gaps. To be able to use the EFD.lab model and to obtain information about the usefulness of the model for situations with a free surface flow like the closure gap, data about the water levels are required for the input of the EFD.lab model. Because measurements on the water level near the closure gaps were not executed either during the final closure of the dam, a two-dimensional model is used to

generate input data for the EFD.lab model. In this way, the EFD.lab model could be used and the original objective of investigating the applicability of the EFD.lab model for situations like a closure gap could be reached.

The two-dimensional model used to obtain information about the water levels in the surroundings of the closure gaps is called Waqua. This two-dimensional fluid flow model executes calculations on among other things, the water level elevation in time over a large area. The input for this two dimensional model exists of the geometry of the estuary and its surroundings and four tidal wave components at six locations along the coast near the Saemangeum estuary. These six points are located at the boundary of the computation domain used in the Waqua model. At eleven other locations, lying inside the computational domain, the components of the tide are known as well. These eleven points were used to validate the results of the Waqua model. The computed water level near the closure gap is used as an input for the three-dimensional EFD.lab model.

Because only so little information is acquired in Korea and such a small amount of data about water levels in, flow velocities and discharges through the closure gaps is available for this investigation, a first estimate of these parameters is made. This has been done by a storage area approach, applied to the Saemangeum estuary. The results of this storage area approach give an indication of the range in which the results of the models must lie.

The setup of this report is as follows: In chapter 2, the research objectives are treated and more extensive background information on the problem and the situation in Korea will be given. The theoretical background of the problem is treated in chapter 3. This includes the basic equations for a three- and two-dimensional fluid flow as well as the formulas for turbulent fluid motion. Chapter 4 deals with the calculations executed with the storage area approach. Subsequently, the two-dimensional model Waqua is discussed in chapter 5 and the three-dimensional model EFD.lab in chapter 6. In chapter 7, the results obtained with the applied models are compared and conclusions and recommendations are presented in the last chapter, chapter 8.

2 General background

This chapter provides an overview of all background information of the research. In the introduction, the research set up and objectives are briefly treated. In this chapter, these topics will be treated more in detail. What is modelling and what kind of modelling can be used will be explained together with the models used for the design of the Saemangeum dam. Finally, some general information about the Saemangeum estuary and the situation during the final closure will be provided.

Figure 2-1 Project team in front of the Garyeok sluice gate.
From left to right: Marina Beaufort, Maartje van der Sande, Rik Beekx, Gé Beaufort, Kees Dorst and Arie Vrijburcht

2.1 Research set up

2.1.1 Problem description

To compute the fluid flow properties through a closure gap, computational models can be used. Computational modelling becomes more and more important for the hydraulic engineer every day. Often, new commercial models for the calculation of three-dimensional fluid flows enter the market, among them the program Engineering Fluid Dynamics Lab (EFD.lab). This is a new generation Computational Fluid Dynamics software based on the same mathematical principles as the conventional CFD software but differs greatly in the way it is used. It has been based on some recent developments in the aerospace engineering done by Russian scientists. For the use of conventional CFD software, the engineer has to translate the

problem into complicated computer codes but in the EFD.lab package, this is not necessary anymore. EFD.lab is three-dimensional fluid flow and heat transfer analysis software in which all simulation steps are combined. The sophisticated physical models can handle a wide range of engineering problems; from creeping non-Newtonian flows to supersonic gas flows with high Mach number. The EFD.lab model calculates the mean flow velocity but also turbulent intensities. These are very important when it comes to the stability of a bottom protection or the required rock size in the last stage of a closure.

At the location of the final Saemangeum dam in South Korea the circumstance can be called extreme. The tidal difference can be 8 m and the enclosed basin covers an area of 400 km^2. Because of the extreme conditions at the project location in South Korea, RWS Bouwdienst decided, in cooperation with the Delft University of Technology, to examine the closure works and gain as much information as possible. Not only an extensive measuring plan for the flow velocities and discharges through the closure gaps had been formulated in advance, but also a plan to execute experiments on the stability of large rocks and gabions was prepared. The location has been chosen to execute stability tests on rocks and gabions because of the extreme conditions at the project location as well. The sluice gate complexes should serve as a huge discharge flume and stability test on a 1 to 1 or 1 to 2 scale could be executed. Data about how rocks and gabions move under influence of high velocities and high turbulent intensities could be very useful for future design purposes.

Unique information could be gained when all the measurements on the flow velocities and discharges through the closure gaps had been executed. The measured data could be used to calibrate the three-dimensional EFD.lab model. A calibrated three-dimensional flow model can, among other things be used for the design of flow structures, to determine the optimal shape of structures in a flow, to calculate the discharge through flow structures and to determine the optimal shape of a closure gap like in the Saemangeum dam. For the stability of rocks in, for example, a bottom protection, the turbulence intensities can be of major importance or even critical. In a highly turbulent flow, it is possible that a bottom protection collapses while the rocks should stay in place under influence of a velocity with the magnitude of the mean flow. Due to the turbulent fluctuations, which cause locally higher velocities, the bottom protection can collapse. When a three-dimensional model is capable of calculating all these turbulent intensities in a correct way, it can be useful for the design of structures like a bottom protection.

Due to a busy schedule of the Korean counterparts, none of the proposed measurements has been executed. With the disappointing amount of data, acquired by the project team during their stay in South Korea, it is not possible to calibrate the three-dimensional EFD.lab model. Extensive research on how turbulence is implemented in the EFD.lab model is still possible. The Korean counterpart was reluctant to do the stability tests because they feared damage to the sluice complexes. After an elaborate conference, it was decided that the stability tests would not proceed. Therefore, no new data about the stability of rocks and gabions was collected.

2.1.2 Flow measurements during the final closure

Before the closure works started, an extensive measuring plan was drawn up. Purpose of this measuring plan was to gain as much information as possible about the flow properties through the closure gaps and at least all the necessary data for the calibration of the EFD.lab model. For the calibration of the three-dimensional EFD.lab model measurements on flow velocities and discharges are required. Because the EFD.lab model calculates the three-dimensional velocity profile, measurements showing also a velocity profile over the depth are preferable. An ADCP measurement device measures the velocity profile over the total depth of the water column. These kinds of measurements can be compared with the, by EFD.lab calculated velocity profile. To ensure that all the required data were obtained a measuring plan was formulated with five kinds of measurements. All the measurements had to be executed with an ADCP measuring device and preferable several times to exclude fluctuations. The following table gives the proposed measurements and their purpose.

Measurement #	Purpose of measurement
1	One measurement at the upstream side of the opening at a maximum of 500 m from the centreline of the dam: for the determination of the upstream main flow direction and the total discharge through the gap
2	One measurement at the downstream side of the opening at 1000 m from the centreline of the dam: for the determination of the contraction of the flow, the downstream main flow direction, the total discharge and the strength of large eddies next to the flow
3	One measurement in the centreline of the opening: for the determination of the flow velocities above and directly downstream of the sill in the centreline of the main flow
4	One measurement near the boundaries of the main flow at a distance of 50 m from the dam heads: for the flow velocities at the boundaries of the main flow and near the dam heads
5	One measurement through the boundaries of the main flow at a distance of 50 m from the dam heads: for the determination of the flow velocities near the dam heads, in the vortex street and in the eddies

Table 2-1 Proposed measurements on flow velocities during the final closure

The following figure shows the lines along which the proposed measurements should be executed. The measurements should preferable be executed during maximum flow velocities in both closure gaps.
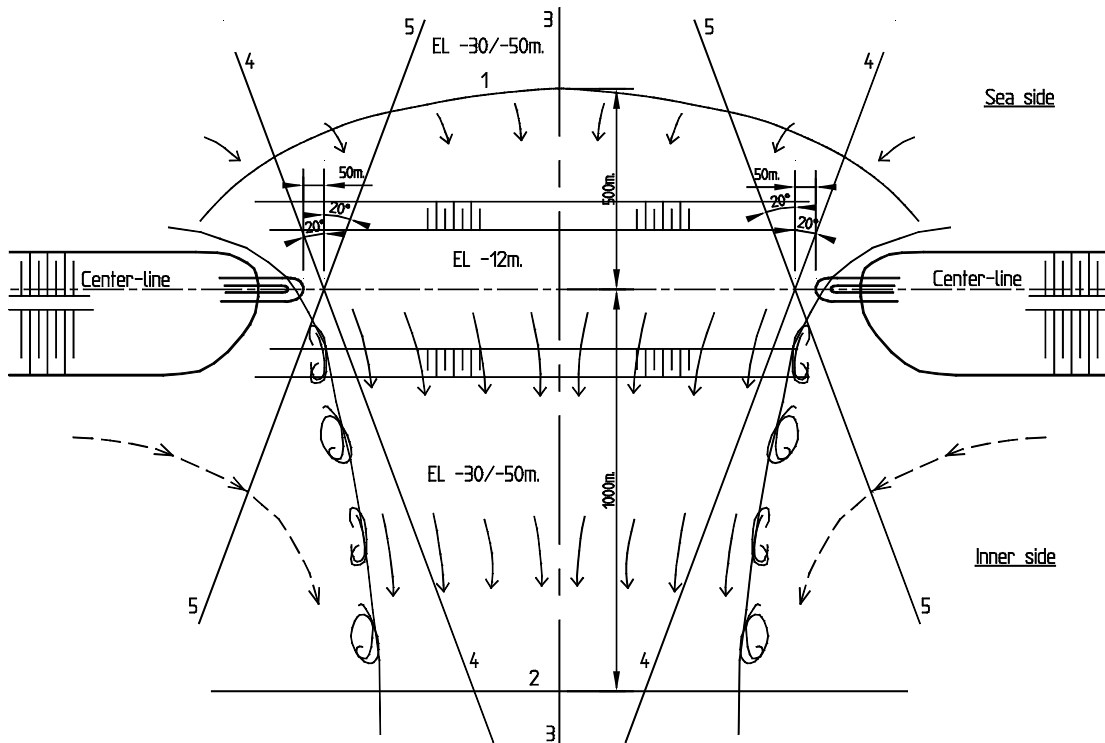
Figure 2-2 Lines along which the proposed measurements should be executed

In Figure 2-2, different parts of the flow pattern through a closure gap can be distinguished. At the seaside of the closure gap, the fluid flow contracts towards the closure gap from all directions. Above the bottom protection, the flow opening becomes smaller and the flow will start to accelerate. Because the flow velocity increases, the water level will fall. Then, the fluid flow will contract further and at the heads of the dam, the flow will separate. Above the sill, the flow velocity will increase further because the flow opening will decrease because the level of the sill is located higher than the level of the bottom protection. At the same time, the water level will fall further as well. When the flow has passed the sill, the flow opening becomes larger and the fluid flow starts to decelerate. The water level will rise again and the flow velocity will decrease. At the boundaries between the fluid flow and the stagnant water at the inner side of the dam, eddies will be formed.

Figure 2-3 Flow pattern through closure gaps

During the final closure, the executor carried out measurements on flow velocities and bottom geometry for their own use. The purpose of these measurements was to control and to monitor the flow and bottom geometry conditions during the final closure. During this phase it turned out it was not possible to execute the measurements as proposed above. Due to time stress and a lack of capacity, men and materials were not available for the execution of the extra measurements. In the following table, all the measurements on flow velocities and on bathymetry being executed during the final closure are captured.

Measurement #	Result of measurement
1	Water level at two sides of dike section 2, near both gaps with a staff gauge. These measurements were executed from March 14 until April 24, every ten minutes night and day. Water level at a distance of 2 km from the dike, at the sea side and basin side, in front of Garyeok sluice gate complex. Due to technical problems the pole at the seaside did not give any data.
2	Flow velocity with GPS floaters. Hyundai measured the flow velocity during maximum flow circumstances every day in the centreline of the closure gaps
3	During the two waiting periods, KRC measured the flow velocities through the centre line of the gaps at maximum flow conditions with an ADCP instrument
4	Before the final closure there has been executed a bathymetric survey from the surroundings of the gaps with a single beam echo sounder. During the final closure works the slope of the bottom protection was also investigated with a single beam echo sounder
5	During the waiting period extra measurements were done with GPS floaters. They not only measured the flow velocity in the centreline but also the flow velocity 100 m out of the centre line on both sides.

Table 2-2 All measurements executed during the final closure of the dam

2.1.3 Research objective

A three-dimensional flow model that gives accurate results for the mean flow properties as well as for the turbulent properties in a flow can be useful when investigating the stability of a bottom protection.

Before the disappointing results of the mission to South Korea became clear, the objective for this research was the validation of the three-dimensional flow model EFD.lab for the situation of a closure gap in a closure dam. Because almost no measurements are available, the validation of the EFD.lab model is not possible and the objective for the research has to be adjusted. A new objective has been drawn up.

The objective for this research has become to investigate the suitability of the EFD.lab model for situations with a free surface and a highly turbulent flow like the flow through a closure gap. The research will provide insight in the way turbulence is implemented in the EFD.lab model and in which way enforced boundary conditions influence the results.

Because no measurements were available that provided enough data to create the input for the EFD.lab model, other models have been used to supply this data.

2.1.4 Set up for the research

Because little data were obtained about water levels in the surrounding of the gaps and about flow velocities through the gaps, a basic calculation will be executed to get an impression of what order of magnitude can be expected for these parameters. By doing so, the water level inside the basin and the flow velocities through the closure gaps have been calculated based on the geometry of the estuary and the tidal prediction in the surrounding of the closure dam.

For the use of the three-dimensional EFD.lab model, accurate data about the geometry around the closure gaps and accurate data about the water level course through the closure gaps are required. The data about the geometry is available and used for the creation of a computational grid of 1 by 1 km. No data however, were available about the water level course through the closure gaps during the closure. To be able to use the three-dimensional model the water level course in the whole area will be calculated for the closing period. This water level course will be calculated with a two-dimension flow model called Waqua. For the creation of a computational domain for this two-dimensional model, the accurate geometry of the estuary and its surrounding is required. These data are available and have been used for the input and a computational domain of 100 by 100 km is created. To create a water level movement over the computational domain, at one border a tidal movement has been created. For this tidal movement four components of the tide were taken into account. By using the results of the Waqua model, the EFD.lab model can be used. With the EFD.lab model, several calculations will be executed with different water level courses. The turbulent properties will be investigated as well.

To ensure that the results from all these models resemble the real situation, they have to be compared with the reality. Due to the limited amount of measured data, the results of the models cannot be checked thoroughly. By using the available data as optimally as possible, a first estimate on the accuracy of the used models can be made.

The results of the storage area approach model will be compared with measurements of the water level in Gunsan Outer Port and with some GPS float measurements executed during the closure. For the input of the Waqua model, the tidal components at the border of the computational grid are used. The same tidal data are known at nine other places inside the boundaries of the computational domain. Waqua calculates a water level course in time for these nine locations and the result of this Waqua calculation will be compared with the original tidal data. To check whether the discharge coefficients for the closure gaps and sluice gates were estimated correctly in the input of Waqua, the results of the calculation for the flow velocities through the closure gaps are compared with some measured data of the flow velocities through the closure gaps.

2.2 Modelling

In the introduction, the term modelling has been used in several contexts. For the civil engineer two ways of modelling are important, namely physical and computational modelling.

The 'Van Dale' dictionary gives the following description for the word modelling. Modelling is: bring into model and to imitate on scale. In this section it will be explained how physical and computational modelling is used by the hydraulic engineer and how physical and computational modelling has been used during the realisation of the Saemangeum closure.

2.2.1 Physical modelling

During centuries, physical modelling has been of main importance in hydraulic engineering. From the beginning of the second half of the 20th century, a lot of physical modelling has been replaced by computational modelling because of the increasing capacity of computers. Although computers replaced more and more research and computational modelling became more and more important in the hydraulic engineering, physical modelling never disappeared completely. One of the advantages of physical modelling is that no assumptions are made to simplify the equations beforehand and no unknowns are neglected beforehand, which is one of the disadvantages in computational modelling. Differences with the real situation do occur during physical modelling, for example, the difference in the wall roughness used in the model and in the real situation.

Physical modelling is based on the assumption that the created situation, the model, can be compared with the real situation, the prototype. For good and reliable physical model research, similarities have to be anticipated. One of the similarities is the geometric similarity, which means that the horizontal and the vertical length scales of the model and the prototype must correspond. If the horizontal length scale is denoted by $n_h = l_m / l_p$, in which l is a horizontal length scale and the subscripts m and p stand for model and prototype, than n_h must be the same for the entire model. This also holds for the vertical length scale $n_v = l_m / l_p$. When $n_l = n_h$ are the same, the vertical and the horizontal length scale are the same and the model is called an undistorted model. When the horizontal length scale is not the same as the vertical length scale, $n_h \neq n_l$ the model is called a distorted model. A distorted model can be very useful when, for example, a very large area must be modelled. When the vertical scale would be the same as the horizontal one, the water layer in the model would just be a thin film of water.

The model must also cope with dynamic similarity. This means that the forces working on the model are comparative with the forces working on the prototype. This leads to the conclusion that the dimensionless parameter, the Froude number, of the model and the prototype must correspond. When the Froude number is considerably smaller than 1 for the prototype and the real situation, the similarity is secured. For an undistorted model, the scaling rules via the Froude number are as follows:

Froude number: $$F_r = \frac{v}{\sqrt{gd}}$$ 2.1

Velocity scale: $$n_v = \sqrt{n_l}$$ 2.2

Discharge scale: $$n_Q = n_l^{2.5}$$ 2.3

In which:

n_l = lenght scale

v = flow velocity (m/s)

g = gravitational accelaration (m/s²)

d = vertical lenght scale (depth (m))

Besides the Froude number, also the models Reynolds number $Re = \rho v l / \mu$ must lie in the same range as the Reynolds number of the prototype, although this range is quite large. [Dalrymple, 1985] Physical scale modelling is very labour intensive and expensive work. The variable cost of an experiment depends on the rent of the location and the equipment and is proportional to the number of measuring points and the number of runs. This makes physical modelling for bigger projects for which several test runs are needed, expensive and time consuming.

2.2.2   *Computational modelling*

Since almost a century and a half the mathematical formulation of the laws describing the motion of fluid are known. The so-called Navier-Stokes equations, formulated by a Frenchman called Claude Louis Marie Henry Navier (1785-1836) and an Irishman called George Gabriel Stokes (1819-1903). This system of partial differential equations governs the conservation of mass and momentum and is almost unsolvable analytically due to the high non-linearity of the equations. Only for some special cases such as a laminar flow in a simple geometry an analytical solution can be found. After some simplifications, the Navier-Stokes equations change into the Reynolds equations for a turbulent flow. A remaining problem is the closure problem, being discussed later on in this chapter. Because of the growing computer power and memory, this system of partial differential equations now can be solved by numerical methods [Zijlema 1996] [www.fluent.com]. Until the 1980's computational fluid dynamics, CFD, was the field of post doc graduates and academic researchers. Using algorithms that are more efficient and more sophisticated pre- and post processing facilities CFD is used also commercially now. One major disadvantage is that the post doc graduates and academic researchers, who used to work with the CDF programs, had an extensive knowledge of the programs and they were very conscious of the limitation of the programs. This is due to a long learning curve and extensive experience with the programs. Nowadays CFD programs are used by all kind of people, who often do not have the extensive knowledge of the post doc graduates and the academic researchers anymore. CFD programs are often used as black boxes and the users are not aware of the limitations of the model anymore. The ultimate goal of the computational fluid dynamic is to create a reliable method, which can be used as a design tool, like, for example, stress analyses. The reason why the development of such a design tool lags behind with the stress analyses is the considerable complexity of the behaviour of the underlying equations, which describe the motion of a fluid.

All commercial CFD programs contain three main elements: the pre-processor, the solver and the post-processor. The pre-processor is used for input. Often this is a user-friendly interface in which all the input data are given. This can be the geometry, the grid generation, the physical and chemical phenomena, the fluid properties and the boundary conditions. The solver is that part of the program where the actual calculation takes place. There are three numerical methods available to solve the equations that describe the motion of a fluid: the

finite difference method, the finite element method and the spectral method. The difference between these three lies in the numerical technique used to integrate the basic model equations (differential equations expressing the conservation of mass and momentum). The post processing is that part the output being visualised. Often this user-friendly interface generates graphs and diagrams of the computational results. The four main advantages of numerical computation modelling of fluids over physical modelling are a reduction of operation time and design, a possibility to study very large systems, a possibility to study systems under extreme conditions and the unlimited level of detail. [Versteeg 1995]

2.2.3   *Flow modelling for Saemangeum*

In preparation of the Saemangeum closure, several computational and physical models have been used by KRC. Not only for design purposes but also during the final closure these models were used to monitor the closure and to predict the circumstances a few days ahead, so the construction works could be adapted accordingly. During the design phase of the Saemangeum dike a large physical model has been created covering the complete estuary.

Figure 2-4 Overall scale model of Saemangeum estuary

More detailed physical modelling on the behaviour of gabions in the closure gaps was done as well. For the overall scale model, a distorted model has been used, with a horizontal scale of 1/500 and a vertical scale of 1/80. According to the similarity law of Froude, the velocity rate was 8.9 and the time scale 55.9. The model was constructed and calibrated in 1994 and since then used for several design purposes and predictions. [Eo 2003]

Figure 2-5 Detailed scale model for testing gabion behaviour

Besides the physical modelling, extensive mathematical modelling has been executed on the Saemangeum estuary. A DELFT 3D-FLOW model has been used to support the calibration of the overall Saemangeum model and to calculate the circumstances during several phases of the final construction works. HR Wallingford executed, by order of KRC, in 2002 mathematical modelling of the Saemangeum estuary and detailed physical modelling of a closure gap. The mathematical modelling has been done with a TELEMAC model. This is a two dimensional model based on the depth-integrated shallow water equations, which are solved with the finite element or finite volume method. At the seaward limit of the model, the boundary conditions were applied based on 21 harmonic tidal constituents. The model was calibrated against five sets of field data. With this model, several stages of the final closure were modelled and the maximum flow velocities in the gaps have been calculated. The physical modelling concerned a closure gap and it was focussed on the flow regime during the final 100 m closure of the gap. [HR Wallingford 2002] Professor B.H. Choi developed a 2D model based on the finite element method for the complete Yellow Sea. For the Saemangeum project, a small part of this model was extricated. Comparison with measured data showed that the model results are reasonably accurate. The model predicts the water level near the Saemangeum dike, both at the sea side and inside the basin. [Choi 2005]

2.3   The Saemangeum closure

2.3.1   General description of the Saemangeum estuary

South Korea is a mountainous country with little flat area suitable for agricultural purposes. Many successful land reclamations were executed in the past and in the polders being created, a lot of land has already been gained from the sea. The following figure shows an overview of the Korean peninsula with a detailed overview of the Saemangeum estuary, the closure dam and the last two closure gaps.

Figure 2-6 Location and overview of Saemangeum estuary with the two closure gaps

In 1991, the Korean Agricultural and Rural Infrastructure Corporation (KRC) and the Ministry of Agricultural and Forestry (MAF) started the large-scale reclamation project in the Saemangeum estuary. The Saemangeum estuary is located approximately 200 km south of Korea's capital, Seoul. The total project covers an area of 401 km^2. After the closure 283 km^2 land will be reclaimed, tidal flats and 118 km^2 desalinated water reservoir. The construction works started in 1991 and in 2000, the dam was finished, with the exception of three closure gaps. Due to heavy environmental protests the work stopped. In 2003, one of the three closure gaps has been closed off but after that, the construction work was interrupted again. In the beginning of 2005, the works restarted slowly. By then, most of the work had been executed and 90% of the sea dam was completed. Only 2.7 km of the 33 km long dam was still open. After approval of the higher court in March 2006, the construction works proceeded and in April 2006, the Saemangeum dike finally closed successfully.

Figure 2-7 Artist impression of situation in the Saemangeum estuary after closure

During the interruptions of the closure works, at both sides of the last two closure gaps huge scour holes developed. The soil on which the dam is constructed exists of a soft sand layer on top of a rock bed layer. This rock layer lies at a depth of approximately 50 meters below mean sea level. During the interruption of the construction works, the scour holes at two sides of the closure gaps developed towards this rock layer and because of the depth of these scour holes, extra precautions were taken to protect the construction from failing. A bottom protection over a length of 200m had to protect the construction. The following figure shows a cross section through one of the closure gaps. The scour holes at both sides reach to the rock bed layer and on top of the bottom protection the sill, over which the final closure will proceed, has been constructed.

Figure 2-8 Cross section of a closure gap with scour holes and bottom protection

The two final closure gaps were both located next to one of the sluice complexes. Gap1 was located next to the Garyeok sluice and Gap2 next to the Sinsi sluice. In the following table, all the properties of the two closure gaps have been captured.

		Gap 1	Gap 2
Location		Near Garyeok sluices	Next to Sinsi sluices
Starting width		1600 m	1100 m
Elevation sill		-10 m below MSL	-16 m below MSL
Progression (m/day)	Phase 1: March 24-29	21.7	73.4
Progression (m/day)	Phase 2: April 3-13	65.5	30.8
Progression (m/day)	Phase 3: April 17-24	62.5	62.5

Table 2-3 Properties of the two final closure gaps

The two closure gaps are located in the southern part of the dam near the two sluice complexes. Gap1 is the most Southern one and located next to the Garyeok sluice gate complex and gap2 is located next to the Sinsi sluice gate complex. The following figure gives an overview of the project location. Near sea dike section 2, four measuring points are indicated where the Koreans executed measurements on water levels.
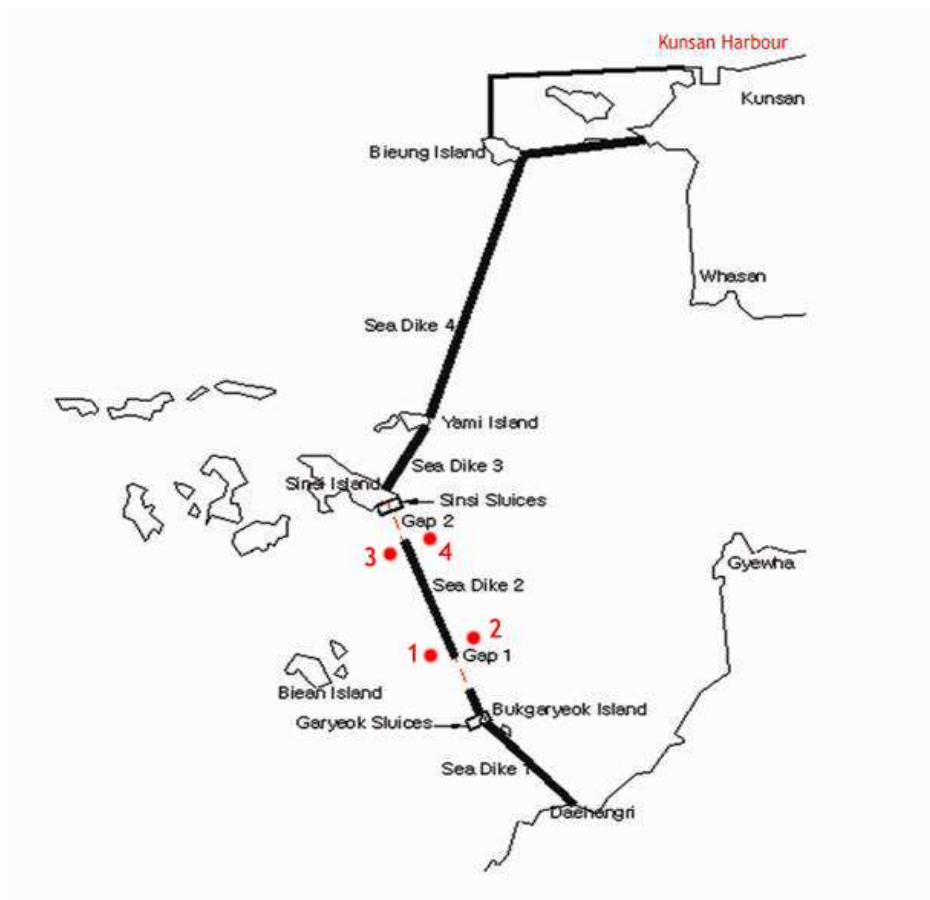
Figure 2-9 Overview of Saemangeum project
Source: HR Wallingford 2005

2.3.2 Situation during final closure

The maximum tidal amplitude at the location of the dam is approximately 8 m. The total closure period is one month, so two spring tide and two neap tide periods occur. The following figure shows the tidal elevation during the closing period at the seaside of the dam.
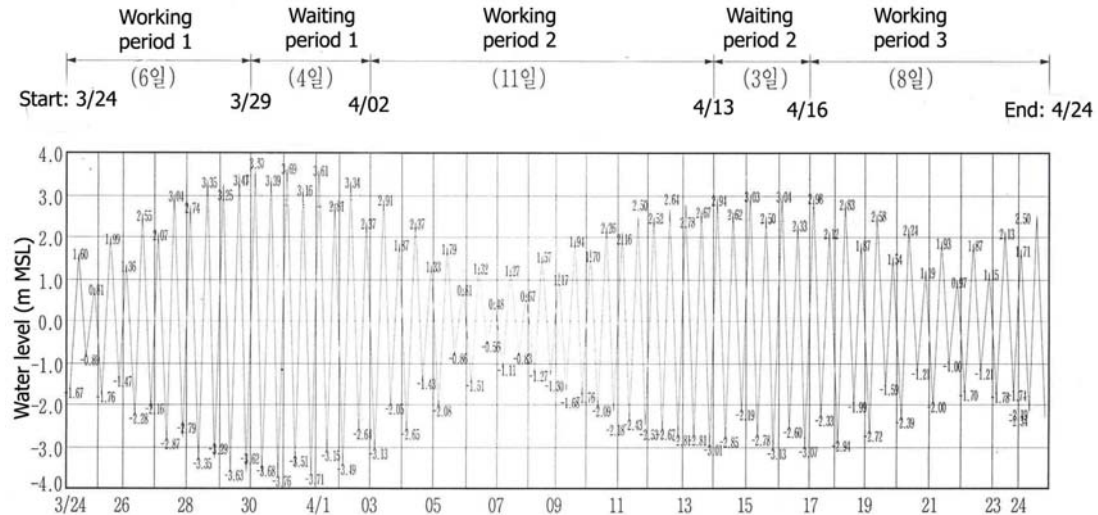
Figure 2-10 Tidal elevation at sea side of closure dam during stages of final closure

During spring tide, the maximum flow velocity through the closure gaps will be larger than during the neap tide period because the water level difference over the closure gaps will also be larger than during neap tide. The higher the flow velocity through the closure gaps is, the larger the required rocks are. Flow velocities up to 8 m/s are predicted for the different stages of the closure. The flow velocities during spring tide will be such that a significant part of the dumped materials will flush away immediately. Therefore, it was decided to insert two waiting periods during which no material is dumped into the closure gaps. The waiting periods last for a few days around the spring tide periods. In the figure above, the waiting and working periods are pointed. The first waiting period starts at spring tide and lasts four days. The second waiting period starts just before the second spring tide and lasts for three days. During the first spring tide, the tidal amplitude is larger than during the second waiting period but because the closure gaps are still bigger during the first waiting period, the occurring flow velocity during this waiting period is smaller. HR Wallingford predicted flow velocities through gap1 and gap2 of 6.29 m/s for the first waiting period and a flow velocity of 6.48 m/s for gap1 during waiting period 2 and a flow velocity of 6.68 m/s for gap2 during waiting period 2.

During the three working periods, the tidal amplitude is lower and the water level differences over the closure dam as well. Therefore, the flow velocity through the closure gaps is low enough to proceed with the dumping of rocks and gabions. During the final stage of the closing period, the velocity will increase because the flow area will be minimised. During this period, the closing periods will proceed and a considerable loss of dumped material will be accepted.

In advance of the final closure works, sufficient material for the executing of the closure works was stored on the dam. The gabions have been placed on top of each other all over the dam and the quarry material was stored on big mounds on the already finished part of the dike.

Figure 2-11 Line of trucks over dam

Figure 2-12 Dumping of material over dam head

To close the gaps a mixture of rocks and gabions is used. Depending on the different stages of the closure, a mixture of 3 to 5 ton rocks and 3-ton gabions or a mixture of 3 to 6 ton rocks and 3-ton gabions were used. The ratio of rocks and gabions differed during the different stages. In the final stage, the mixture consisted of 50 percent rocks and 50 percent gabions, while during the first stage the percentage of gabions was only 20 percent.

To gather the huge amount of rocks required for the closure a part of an island in the line pf the dam was used as a quarry. All the material was used. The quarry run was used for the dam core and the sealing. The large rocks, up to 10 ton, have been used for the surface layer

and the smaller rocks, the ones of 30 to 40 cm, were used to fabricate the gabions. For the final project a total amount of 5 million ton rocks was used. The following figures show the different rock sizes and a 3-ton gabion. A total amount of 260.000 gabions has been used.

Figure 2-13 Gabion of 3 ton

Figure 2-14 Different size of rocks used for the closure

3 Basic equations

Nowadays computational modelling replaces physical modelling more and more although physical modelling is still of major importance in hydraulic engineering. It is always important to understand the underlying equations working with a model, especially when working with advanced computational models. The motion of a fluid can be described by a set of coupled partial differential equations and depending on the circumstances, several terms can be neglected. This chapter introduces the underlying equations describing the motion of a fluid in three, two and one dimension. Some theory about discharge formulas is explained as well being relevant for calculation executed further on in the research. Finally, turbulence modelling will be discussed.

3.1 Conservation laws of fluid motion in three dimensions

The motion of a fluid in three dimensions is described by four partial differential equations; mass conservation and the conservation of momentum equations for three spatial directions. These conservation equations are derived by considering the conservation principles for a fluid element. The principle of these conservation laws can be expressed as follows for a single element:

$$Change = Input - Output + Source \qquad\qquad 3.1$$

Consider the balance of a conserved quantity G in a cubic control volume that is given by $\Delta x \Delta y \Delta z$. The change of quantity G in a time interval Δt in this volume is caused by the net transport of quantity G into this control volume. This can be expressed as:

$$G(t + \Delta t) - G(t) = G_{in}(right - left) + G_{in}(top - bottom) + G_{in}(back - front) + G_{source} \qquad 3.2$$

The following figure shows an overview of such a control volume.
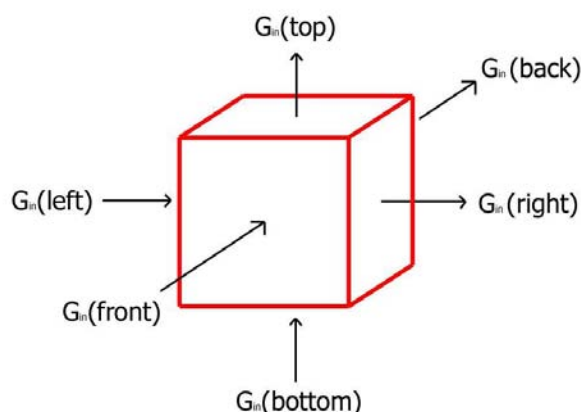
Figure 3-1 Control volume

When the above equation is divided by the volume $\Delta x \Delta y \Delta z$ and the time interval Δt, and when the limit of all Δ approach to zero, the equation can be expressed in the following way:

$$\frac{\partial c}{\partial t} + \frac{\partial(v_1 c)}{\partial x} + \frac{\partial(v_2 c)}{\partial y} + \frac{\partial(v_3 c)}{\partial z} + \frac{\partial T_1}{\partial x} + \frac{\partial T_2}{\partial y} + \frac{\partial T_3}{\partial z} + D = 0 \qquad\qquad 3.3$$

in which c is the amount of G present in the considered control volume. In the above equation, the first term at the left hand side is the time derivative of c. The second term describes the net amount transported through the sides of the cube. The third term is the diffusion term and the last term is the source term.

3.1.1 Conservation of mass

When mass is taken for the quantity G, c in the above equation can be exchanged by the density ρ, because mass considered per unit of volume is mass density. Assuming that mass cannot disappear and that mass will not reveal diffusive transport, the above equation changes in:

$$\frac{\partial \rho}{\partial t} + \nabla_i v_i \rho = 0 \qquad\qquad 3.4$$

This is the same as:

$$\frac{\partial \rho}{\partial t} + \frac{\partial(\rho v_1)}{\partial x} + \frac{\partial(\rho v_2)}{\partial y} + \frac{\partial(\rho v_3)}{\partial z} = 0 \qquad\qquad 3.5$$

For an incompressible flow, the density ρ is constant in time and space. Now the above equation changes into:

$$\frac{\partial v_1}{\partial x} + \frac{\partial v_2}{\partial y} + \frac{\partial v_3}{\partial z} = 0 \qquad\qquad 3.6$$

This is known as the continuity equation.

3.1.2 Navier-Stokes equations

The rate of change of momentum in a fluid particle equals the sum of forces on that particle. Momentum is given by multiplying the mass with the velocity. When c in the general conservation equation is replaced by ρv_i, the conservation equation becomes a conservation equation for momentum. For the first velocity component, this equation can be formulated as follows:

$$\frac{\partial}{\partial t}(\rho v_1) + \nabla_i \rho v_i v_1 = -\nabla_1 p + \eta \nabla_i^2 v_1 + k_1 \qquad\qquad 3.7$$

The first term is the rate of change of momentum, the second term is the convection term, the first two terms at the right hand side of the equation, form stresses on the fluid particle and the last term is the source term. The stresses on the surface of the fluid particle can be distinguished into a pressure related normal stress and a viscous shear stress. For a Newtonian fluid the viscous shear stresses are proportional to the velocity gradient in the

direction perpendicular to the shear stress ($\tau = \eta * \delta v_1 / \delta z$). In the same way, the momentum equations for the y and z direction of the control volume can be formulated:

$$\frac{\partial}{\partial t}(\rho v_2) + \nabla_i (\rho v_i v_2) = -\nabla_2 p + \eta \nabla_i^2 v_2 + k_2 \qquad\qquad 3.8$$

$$\frac{\partial}{\partial t}(\rho v_3) + \nabla \rho v_i v_3) = -\nabla_3 p + \eta \nabla_i^2 v_3 + k_3 \qquad\qquad 3.9$$

These three equations are known as the Navier-Stokes equations.

3.1.3 Reynolds equations

With the four equations, derived above, the motion of a fluid has been described for a fluid. It is hard to find analytical solutions because of the dominant influence of the high non-linear nature of the equations. By averaging over turbulent fluctuations, a simplification of the Navier-Stokes equations is obtained describing the mean motion of a fluid. For this purpose, both velocity and pressure are divided into a mean part and a fluctuating part. This can be written as:

$$v_i = \overline{v_i} + v_i'$$
$$p_i = \overline{p_i} + p_i' \qquad\qquad 3.10$$

in which $\overline{v_i}$ is the time averaged velocity vector and v_i' is the vector of the fluctuating velocity component. A similar notation is used for the pressure p.

When the velocity and pressure vector in the Navier-Stokes equations from paragraph 3.1.2 are replaced by the average and fluctuating part, the momentum equation in the x-direction changes, after averaging, in the following equation:

$$\frac{\partial}{\partial t}(\rho \overline{v_1}) + \nabla_i (\rho \overline{v_i v_1}) + \nabla_i (\rho \overline{v_i' v_1'}) + \nabla_1 \overline{p} - \eta \nabla_i^2 \overline{v_1} = \overline{k_1} \qquad\qquad 3.11$$

in which the over bar indicates 'time-averaged'. In the same way, the equation for the y and z direction can be formulated.

$$\frac{\partial}{\partial t}(\rho \overline{v_2}) + \nabla_i (\rho \overline{v_i v_2}) + \nabla_i (\rho \overline{v_i' v_2'}) + \nabla_2 \overline{p} - \eta \nabla_i^2 \overline{v_2} = \overline{k_2} \qquad\qquad 3.12$$

$$\frac{\partial}{\partial t}(\rho \overline{v_3}) + \nabla_i (\rho \overline{v_i v_3}) + \nabla_i (\rho \overline{v_i' v_3'}) + \nabla_3 \overline{p} - \eta \nabla_i^2 \overline{v_3} = \overline{k_3} \qquad\qquad 3.13$$

Compared with the Navier-Stokes equations, an extra term is found. This term, the third term at the left hand side, describes the effect of the fluctuating velocity on the mean motion. These effects resemble shear and normal stresses and are called Reynolds stresses. The new

equations are called the Reynolds equations. In the three directions (x, y, z-direction) six Reynolds stresses appear; three normal stresses and six shear stresses. In general, the Reynolds stresses can be written as follows:

$$\tau_{ij} = -\rho \overline{v_i' v_j'} \qquad\qquad 3.14$$

τ_{ij} is called the Reynolds stress tensor, in which i and j are the directions of the stress. The Reynolds stresses can be divided into normal stresses and shear stresses, which is showed below.

Normal stresses:

$$\tau_{xx} = -\rho \overline{v_1'^2} \qquad \tau_{yy} = -\rho \overline{v_2'^2} \qquad \tau_{zz} = -\rho \overline{v_3'^2} \qquad\qquad 3.15$$

Shear stresses:

$$\tau_{xy} = \tau_{yx} = -\rho \overline{v_1' v_2'} \;,\; \tau_{xz} = \tau_{zx} = -\rho \overline{v_1' v_3'} \;,\; \tau_{yz} = \tau_{zy} = -\rho \overline{v_2' v_3'} \qquad\qquad 3.16$$

Due to symmetry, the six shear stresses are not dependent. The three normal stresses being neglected three shear stresses remain. These three are unknown and form the basis of the so called 'closure problem'. Many decades have been spent already on finding a proper solution for these Reynolds stresses.

Further simplification of the Reynolds equations can be achieved by taking into account that the mean pressure gradient in a fully turbulent flow is significantly larger than the gradient in the normal Reynolds stresses. For flows with high Reynolds numbers, it holds that the turbulent shear stresses dominate over the viscous shear stresses. In formula form this means:

$$\nabla_j \overline{p} \gg \nabla_j \tau_{jj}$$
$$\rho \overline{v_i} \nabla_i \overline{v_j} \gg -\eta \nabla_i^2 \overline{v_j} \qquad\qquad 3.17$$

The Reynolds equation can then be formulated as follows:

$$\frac{\partial}{\partial t}(\rho \overline{v_j}) + \nabla_i(\rho \overline{v_i v_j}) + \nabla_i \tau_{ij} + \nabla_j \overline{p} = \overline{k_j} \qquad\qquad 3.18$$

The turbulent shear stress can be expressed in the same way as the viscous shear stress with the molecular viscosity replaced by a turbulent viscosity.

$$\tau_{ij} = -\rho \overline{v_i' v_j'} = -\rho v_{turb} \frac{\partial v_i}{\partial x_j} \qquad\qquad 3.19$$

Following Prandtl mixing length theory the turbulent eddy viscosity v_{turb}, can be expressed in a velocity that characterises the turbulent fluctuations and a length scale of the turbulent fluctuations, l_{mix}.

$$\tau_{ij} = \tau_{ji} = -\rho \overline{v_i' v_j'} = \rho l_{mix}^2 \left| \frac{\partial v_i}{\partial x_j} \right| \frac{\partial v_i}{\partial x_j}$$

<div align="right">3.20</div>

A new problem now arises, namely the problem of defining the mixing length l_{mix}. This mixing length is not a fluid property but depends on the flow geometry and varies for every flow.

Another way of dealing with the closure problem is the use of a k-ε model. Two additional transport equations for the turbulent kinetic energy and the turbulent dissipation are solved together with the Reynolds equations.

3.2   Conservation laws of fluid motion in two dimension

When some terms are being neglected in the three-dimensional equations for the motion of a fluid and when the equations are integrated over the depth, equations for the motion of a fluid in two dimensions are obtained. When the horizontal length scale of a system is significant larger than the vertical length scale, the pressure distribution over the vertical is approximately hydrostatic. When the water also is assumed to be incompressible, the mass balance reduces to a volume balance which is also called the continuity equation. The equation of motion gives the balance between inertia, external force and friction.

Continuity equation:

$$\frac{\partial h}{\partial t} + \frac{\partial}{\partial x}(Hv_1) + \frac{\partial}{\partial y}(Hv_2) = 0$$

<div align="right">3.21</div>

Equation of motion:

$$\frac{\partial}{\partial t}(Hv_1) + \frac{\partial}{\partial x}(Hv_1^2) + \frac{\partial}{\partial y}(Hv_1v_2) + gH\frac{\partial \eta}{\partial x} = -\tau^b$$

$$\frac{\partial}{\partial t}(Hv_2) + \frac{\partial}{\partial x}(Hv_1v_2) + \frac{\partial}{\partial y}(Hv_2^2) + gH\frac{\partial \eta}{\partial y} = -\tau^b$$

<div align="right">3.22</div>

Where:
h	= depth below reference level (m)
η	= water level above reference level (m)
H	= $h + \eta$ (m)
v	= velocity vector with components v_1 and v_2 (m/s)
τ^b	= bottom stress term

These three equations form the two dimensional shallow water equations and describe the motion of a fluid in two dimensions. The shallow water equations are known as the equations of De Saint-Venant (1871). [H. Chanson, 1999].

3.3 Storage area approach formula

The Saemangeum estuary consists of a basin with two gaps, two sluice complexes and two rivers ending into the basin. The river discharge being neglected and the tidal motion at the sea side is known, the water level inside the basin can be calculated with the storage area approach.

The storage area approach can be used the horizontal dimensions of the basin being small compared to the length of the tidal wave. In that case, the water surface within the basin is approximately horizontal although its elevation may vary in time. The flow velocity of the travelling waves inside the basin is relatively small and therefore the inertia and the friction can be neglected. Two main conditions must hold for the basin

- The length of the basin must be small compared to the length of the incoming wave, when L is the length of the incoming (mostly a tidal wave) and l is the length of the basin then it must hold that $l = 1/20\ L$. The water level in all points is almost in phase then and the water level can be presumed to be horizontal over the total length of the basin.
- There may not be any flow through the basin. The basin must be filled and emptied at one side of the basin or the inflow at one end must be significantly smaller than at the other side.

The storage area approach formula is formulated in the following way and states a relation between the inflowing or out flowing discharge and the water level inside the basin.

Storage area approach formula:

$$Q = A_b \frac{dh_b}{dt}$$

<div align="right">3.23</div>

Where:

Q	= discharge (m³/s)
A_b	= total storage area of the basin (m²)
h_b	= water level inside the basin (m)

This is called the storage area approach because the dynamics are not taken into account, only the storage inside the basin is important. [JA Battjes 2002]

3.4 Discharge formulas

In the previous paragraph the formula for the storage area approach is given. This formula contains a total discharge Q, which is the discharge in or out a basin in a certain time. To compute the water level difference over a period (dh_b/dt) the total discharge in that period must be known.

The total discharge through a closure gap depends on the geometry of the gap and on the water level. To determine the discharge through a gap one first has to determine whether the flow through the gap is a free flow, a fully submerged flow or an intermediate flow. When the flow is a free flow, the discharge is related only to the upstream water level. A certain

downstream water level being exceeded, the influence of the downstream water level becomes significant and the flow becomes submerged. The discharge of a submerged flow depends on the upstream, as well as on the downstream water level. The difference between a fully submerged flow and an intermediate flow lies in the head difference. The head difference being small, the flow is comparable with an internal flow. The water level is nearly horizontal and the velocity is small. When the head difference becomes larger, the water level is not nearly horizontal anymore. The discharge depends on the upstream and the downstream water level together. In the following figure, the different flow types are shown.
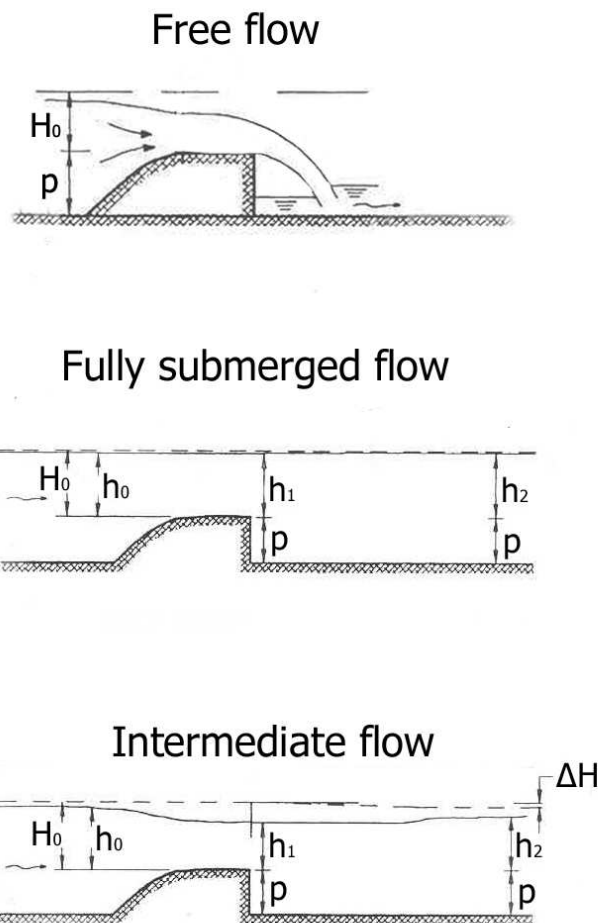
Figure 3-2 Free, fully submerged and intermediate flow

The following discharge formulas can be deduced for a free and a submerged flow. [DS Miller 1994]

- For a free flow:

$$Q = (mu)B\frac{2}{3}(H_0)\sqrt{2g\frac{1}{3}(H_0)}$$ 3.24

- For a fully submerged flow:

$$Q = B(mu)h_2\sqrt{2g(H_0 - h_2)}$$ 3.25

Where:

Q	=	Discharge (m^3/s)
mu	=	discharge coefficient
B	=	width of the gap (m)
H_0	=	upstream energy level (m) see figure 3.1
g	=	gravitational acceleration (m/s^2)
h_2	=	downstream water level (m)
p	=	height of the sill (m)

With the formulas above, the total discharge through a closure gap in a certain time period can be computed. With the computed total discharge, the water level variation can be calculated.

4 The storage area approach model

Because the amount of data about the water levels near the closure gaps and the flow velocity through the closure gaps is limited a first estimate for these parameters is made. This is done with a storage area approach, which states the water level inside a basin depends only on the amount of water that flows in or out. This means that the water inside the basin will rise water flowing in, and the water level will fall water flowing out. Because at the sea side of the basin, the water level varies with the tide, the water level inside the basin will also vary by this tidal movement of the water although with a phase and amplitude difference. Every ten minutes the water level at the seaside is known and the water level inside the basin is calculated. With the water level difference over the closure gap, the total discharge through the closure gap in the time between two water level predictions is computed and by using the storage area approach, the water level rise or fall in these ten minutes is calculated. For the period of the closure, this is repeated every ten minutes and in this way, a prediction of the water level inside the basin during the closure is made.

4.1 Boundary conditions

To predict the total discharge through the closure gap in one time interval of ten minutes the water level difference in these ten minutes must be known. The inner water level is calculated with the storage area approach and the outer, the sea side water level, is known. Therefore, the sea side water level is a boundary condition for the storage area approach. When a certain amount of water flows in or out the basin, it depends on the wet surface area in the basin how much the water level will rise or fall. The wet surface area is also a boundary condition for the storage area approach.

4.1.1 Sea side water level

To calculate the water level inside the basin the water level at the sea side must be known. Several institutes provide online predictions of high and low water levels and the according times of the high and low waters. KRC provided a tidal prediction schedule, indicating the high and low water levels for the harbour of Gunsan. Gunsan is one of the bigger harbours at the West coast of the peninsula and is located approximately 20 km north of the closure gaps.

For a decent calculation on the basin water level, not only the level of the high and low water and the time moments must be known. It is necessary to have a continuous prediction of the outer water level to calculate the water level inside the basin. Although a tidal wave never has the form of a perfect sin function, it does approach it. Therefore, it is assumed here that the tidal wave has the form of a perfect sin function. By stating that the water level varies between high and low water according to a perfect sin function, a continuous water level can be prescribed. Between a successive high and low water level prediction, the water level varies with a sin function. Between the following low and high water level, the water level varies again with a new sin function. From this continuous sin function, every ten minutes between the high and low water times a prediction of the water level is made. The predicted times for the high and low water are known, but between a successive high and low water not an exact number of ten minutes intervals is present. From the first high water prediction,

a number of ten minutes time steps have been stated. It is now said that the successive low water occur at exact n time steps of ten minutes later. Most of the time this is not the exact predicted time but then the predicted value is given to a time, which is exact n time steps later than the former high water. Now there are n time steps but only two values, one start value for high water and one end value for low water and n time steps for which the water level must be calculated. When a sin function is assumed between this successive high and low water a value for the water level can be calculated for every time step between the high and low water

$$h = h_{p,1} + \frac{h_{p,2} - h_{p,1}}{2} * (1 - cos(\frac{\pi}{n} * pos)) \qquad\qquad 4.1$$

where:

$h =$ composed water level at sea side

$h_{p,1} =$ first predicted value for water level ($h_{p,1}$ is high water then $h_{p,2}$ is low water level)

$h_{p,2} =$ second predicted value for water level ($h_{p,2}$ is high water then $h_{p,1}$ is low water level)

$n =$ number of time steps between a successive high and low water

$pos =$ position (position of time step between successive high and low water)

Now a sea side water level is composed with a value every ten minutes. To check the composed water level, it is compared with measured data from the Gunsan outer port. There are water level measurements available in Gunsan outer port for the months January and February 2006. The measured data and the composed sin function correspond well as can be seen in the following figure.
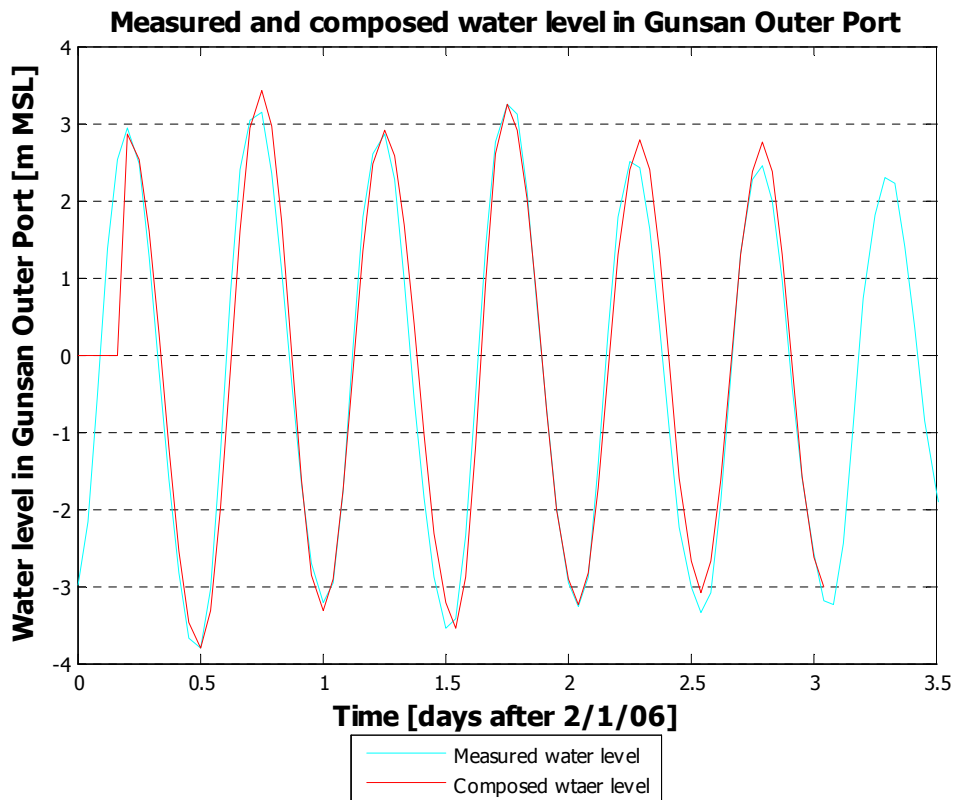
Figure 4-1 Measured and predicted water level Gunsan Outer Port

At some points, the composed and the measured water level do not completely correspond. One of the reasons can be wind set up at the location of the measuring point; wind set up is not taken into account in the composition of the water level.

4.1.2   *Wet surface area inside the basin*

The Saemangeum estuary exists of tidal wetlands. Different parts of the basin fall dry the water level inside the basin being low and they are only flooded at high tide. Therefore, the wet surface of the basin varies with the water level inside the basin. When the water level rises above + 3.5 m MSL, the wet surface does not grow anymore. This is because dikes have been constructed around the basin. The wet surface area inside the basin at different water levels is shown in the following figure.
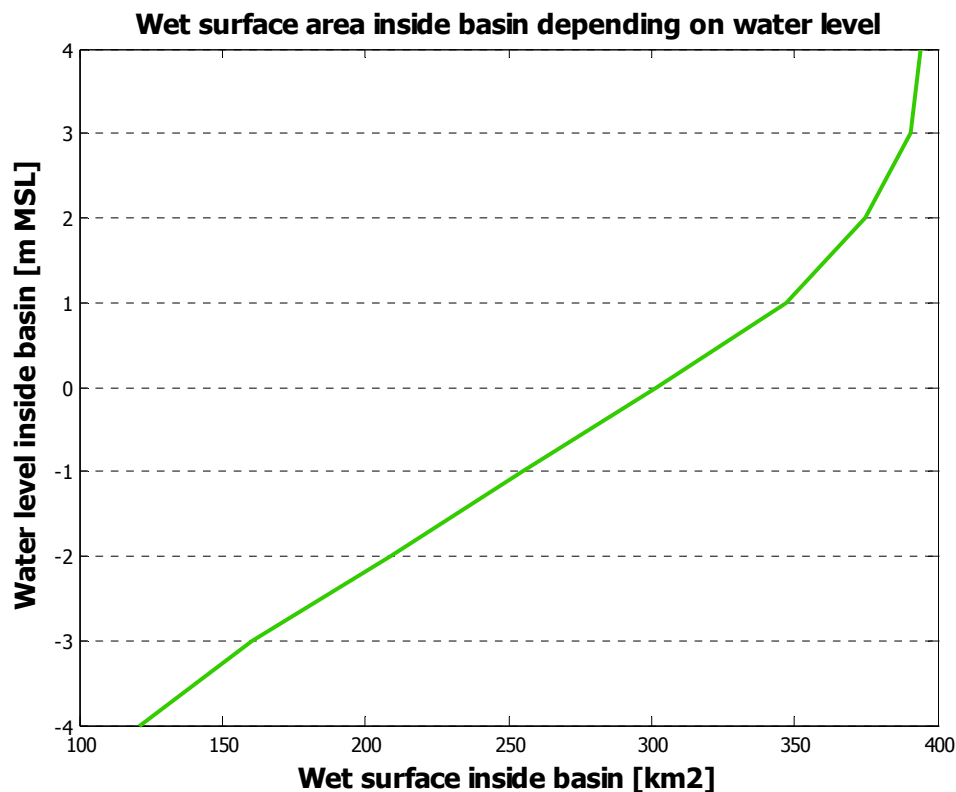
Figure 4-2 Wet surface area inside basin

The wet surface area varies almost linear with the water level inside the basin. This can be seen in the figure above. This figure is created from the following table, in which the wet surface area at different water levels is given.

Water level inside the basin(m MSL)	Wet surface area inside the basin (km^2)
-4	121.3
-3	160.5
-2	208.6
-1	254.9
0	301.7
1	347.0
2	374.7
3	390.9
4	394.0

Table 4-1 Wet surface area inside the basin

The wet surface area is assumed to be linear between two point in the above table. Figure 4.2 shows, that this is a reasonable approximation. In this way the wet surface area can be calculated for every arbitrarily water level in the basin.

4.2   Storage area approach in the Saemangeum estuary

To investigate the range, in which the outcomes of the numerical models and the physical models must be, the import factors are also calculated with the basic equations. By neglecting factors and influences, the water level in the basin and the flow velocity through the gaps can be calculated very easily. With a spreadsheet, the water level inside the basin and the flow velocity through the gaps during the closure has been calculated.

4.2.1   Applicability of storage area approach

The basin has two main branches. Both are very shallow and fall almost dry at mean sea level. The northern branch has length of 30 km from the sea dike and the southern branch has a length of 27 km. The basin itself has a length of 20 km from the sea dike. For a good approximation of the water level inside the basin, using the storage area approach, the length of the basin may not exceed 5 % of the length of a tidal wave. The average depth in the basin is 8m. The period of the tidal wave is 44700 s, so the length of the tidal wave is more or less 400 km. It must hold that *l = 1/20 L,* the basin itself suffices this condition but the two branches do not. Formally, the length of the branches exceeds the length, for which the storage area approach gives reasonable result. However, the branches fall completely dry at low water and are only little flooded during high water and therefore the storage area approach is used for the basin.

In the period of the closure, there will be little river discharge and compared to the huge storage area this discharge can be neglected. The average river discharge, for the two rivers together, in spring time is approximately 160 m^3/s. Compared to a minimum discharge amplitude through both sluices of 20 000 m^3/s after the closure, this river discharge can be neglected during the closing period. During this closing period the discharge amplitude in the basin will be even higher because water also flows through the remaining gaps then.

It is shown above that the two conditions for the storage area approach are coped with, so the water level inside the basin shall be calculated with the formulas for the storage area approach.

4.2.2 Calculation of the basin side water level

From the boundary conditions the water level at the seaside of the dam is known every ten minutes. To calculate the water level inside the basin, every ten minutes the discharge through the gaps and the sluices is calculated according to a water level difference over the dam. When the total discharge in a period is known the water level difference over this period can be calculated with the storage area approach. The water level at the sea side being known, and for $t=t_1$ the water level inside is known, the total discharge can be calculated with the discharge formula for fully submerged flow. To start the calculation the water level inside the basin must be known for $t=t_1$. This first value will be estimated.

$$Q_{total} = \mu B_g \left(h_{downstream} - h_{sill} \right) \sqrt{2g \left(h_{upstream} - h_{downstream} \right)} \qquad 4.2$$

When Q_{total} is known for $t=t_1$ the total discharge in the interval $t_1 < t < t_2$ is calculated by:

$$Q_{total,t_1-t_2} = \Delta t * Q_{total} \qquad 4.3$$

For every water level inside the basin, the total wet surface area is known. When the total discharge Q_{total,t_1-t_2} is divided by the wet surface area A_k the difference in water level in a time interval is known.

$$\frac{dh_k}{dt} = \frac{Q_{total,t_1-t_2}}{A_k} \qquad 4.4$$

The inner water level at $t = t_1$ plus the *dh/dt* gives the new water level in the basin at $t=t_2$. With this new water level at $t=t_2$ the total discharge for the next time step can be calculated in the same way.

$$h_{res} = h_2 = h_1 + \frac{Q_{total,t_1-t_2}}{A_k} \qquad 4.5$$

The water level inside the basin will follow the water level at the seaside of the dam. At both sides of the dam, the water level will follow a sinusoidal movement. During the closure, the gaps become smaller and smaller and the amplitude difference and the phase difference between the two sinusoidal movements will increase. This can be seen in Figure 4-3. At the horizontal grid line, the water level at the seaside is given and at the vertical scale, the water level at basin side is given. In the beginning, the gaps being still completely open, the water level inside the basin follows the seaside water level. After a while, when the gaps are closing and the flow area in the gaps becomes smaller, the water level inside the basin does not follow the outer water level anymore. Eventually the basin side water level keeps fluctuating

between +1.5m MSL and -1.5m MSL. The seaside water level keeps fluctuating between -4.0m MSL and +4.0 m MSL while the basin water level becomes a flat eclipse.
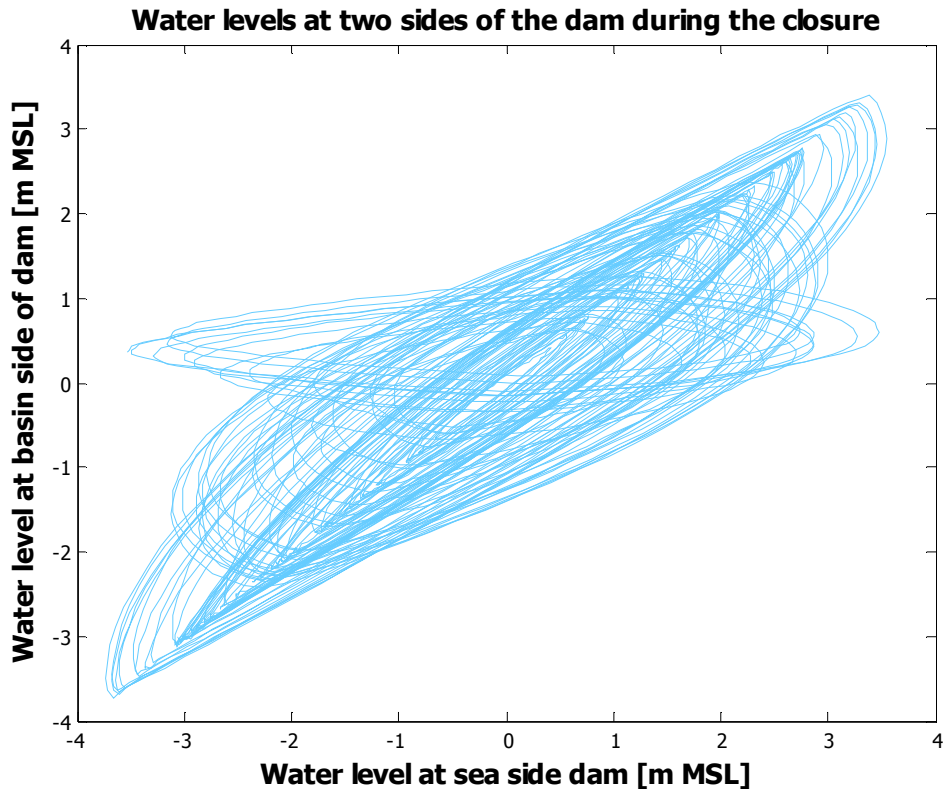
Figure 4-3 Lissajous figure of water levels at both sides of the dam during closure

The Lissajous figure shows the water level variation at both sides of the dam. The horizontal eclipse is the water level variation inside and outside the basin when the closure gaps are closed and water flows in and out the basin only through the sluices.

During the calculation the flow openings in the gaps become smaller and smaller and eventually close off completely. The sluice gates will never close, so after completing the closure, water still flows in and out the basin. From '*t= 54 days after 1/3/06*' the gaps are closed and the water only flows in and out the basin through the sluice gates. Figure 4-4 shows the water level at the sea and at the basin side during the last few days of the closing period. The blue line gives the water level at the seaside of the dam and the pink line gives the water level at the basin side of the dam. From the point '*t=54 days after 1/3/06*' the basin water level follow the tidal amplitude at the sea side with a phase difference and an amplitude variation. The basin water level varies with more or less constant amplitude of 1.5m, which can be seen in the following figure. The figure also shows that the basin is slowly filling up after the closure of the gaps.
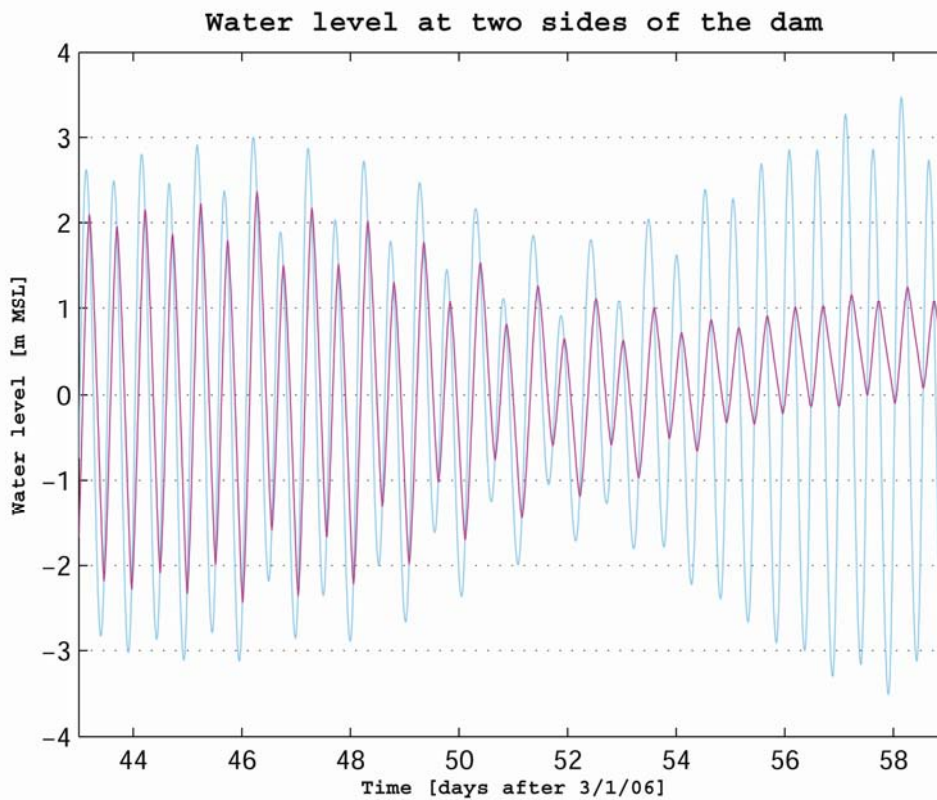
Figure 4-4 Predicted water level at seaside and basin side water level

4.2.3 Calculation of the flow velocity through the closure gaps

When the water level difference is known, the flow velocity is also known. With the basic formula, $v = \sqrt{2g\Delta h}$ the average flow velocity through all the openings in the dam can be calculated. Because only one water level difference for the total basin is calculated, also one velocity is calculated. This means that the flow velocity through both the gaps and both the sluices will be the same. This flow velocity only depends on the water level difference and not on the geometry of the gaps. In the following figure, the flow velocity has been given for the whole period.

The closure starts at *t=23* and ends at *t=54*. When the closure is completed all the water will flow through the sluices only. During the closure, the flow velocity will not exceed a value of 6.45 m/s. Figure 4-6 shows the flow velocity through the openings in the dam during the last stage of the closure.
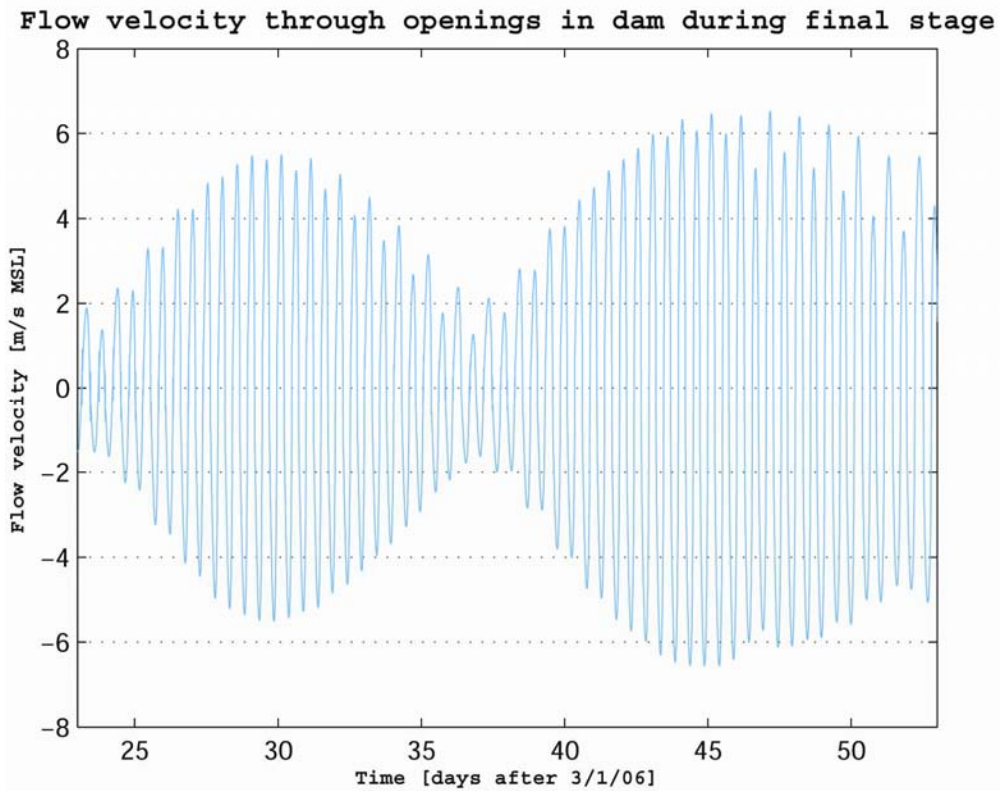
Figure 4-5 Calculated average flow velocities through openings in the dam
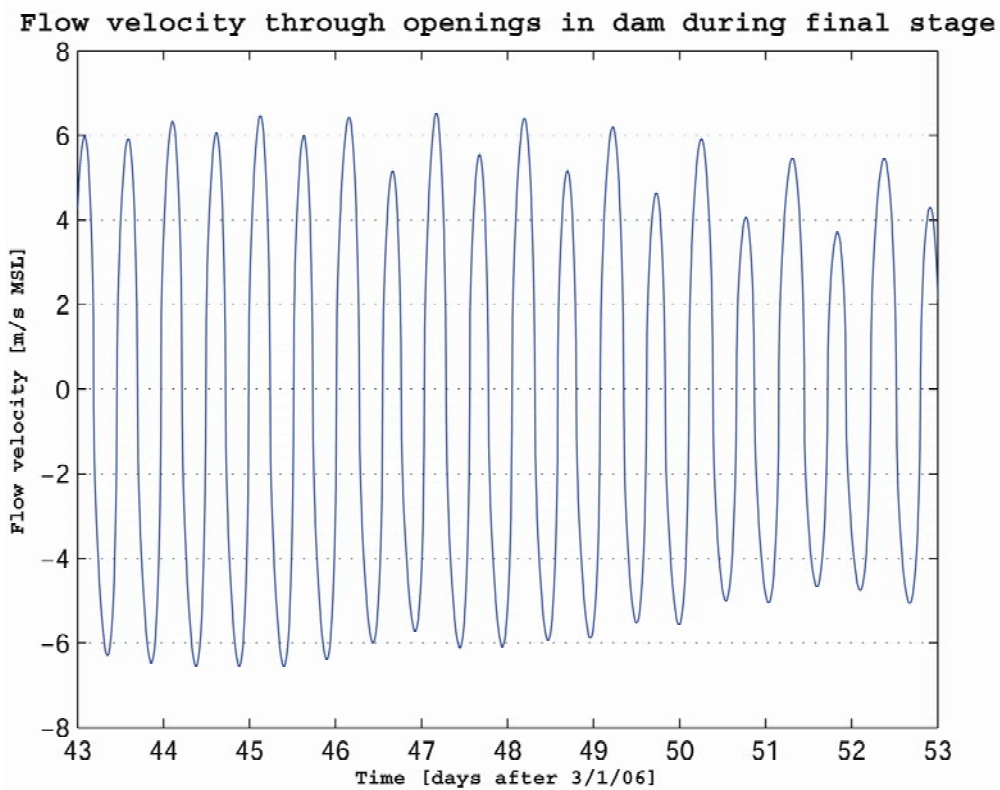
Figure 4-6 Flow velocities through gaps and sluices during end of closure

4.2.4 Sensitivity of the storage area approach

For the calculation of the discharge through the gaps in a time interval, and for the calculation of the water level rise or fall in a time interval, several parameters have been estimated. The value of all these parameters is estimated carefully but uncertainties are always present. Therefore, it is important to know in which way a parameter influences the results of the model. The following table gives the parameters and the estimated value

Parameter	Estimated value
Start value reservoir water level (h_{res})	2 m MSL
Discharge coefficient (μ)	0.9 for both gaps, 1 for the sluices
Depth of Gap1 (d_1)	-10 m MSL
Depth of Gap2 (d_2)	-16 m MSL
Wet surface area (A_{res})	Depends on water level inside basin (Table 4-1)

Table 4-2 Estimated parameters for calculation of basin side water level

To investigate the influence of the start value of the basin side water level on the prediction of the basin side water level in the time, results of calculations with different start values are investigated. The next figure shows the graph of the water level inside the basin with different start values. It can be seen that within half a day the different start values have no influence anymore. Therefore, it does not matter which start value for the water level inside the basin is taken when it is taken into account that the results can be trusted one day from the start of the simulation.
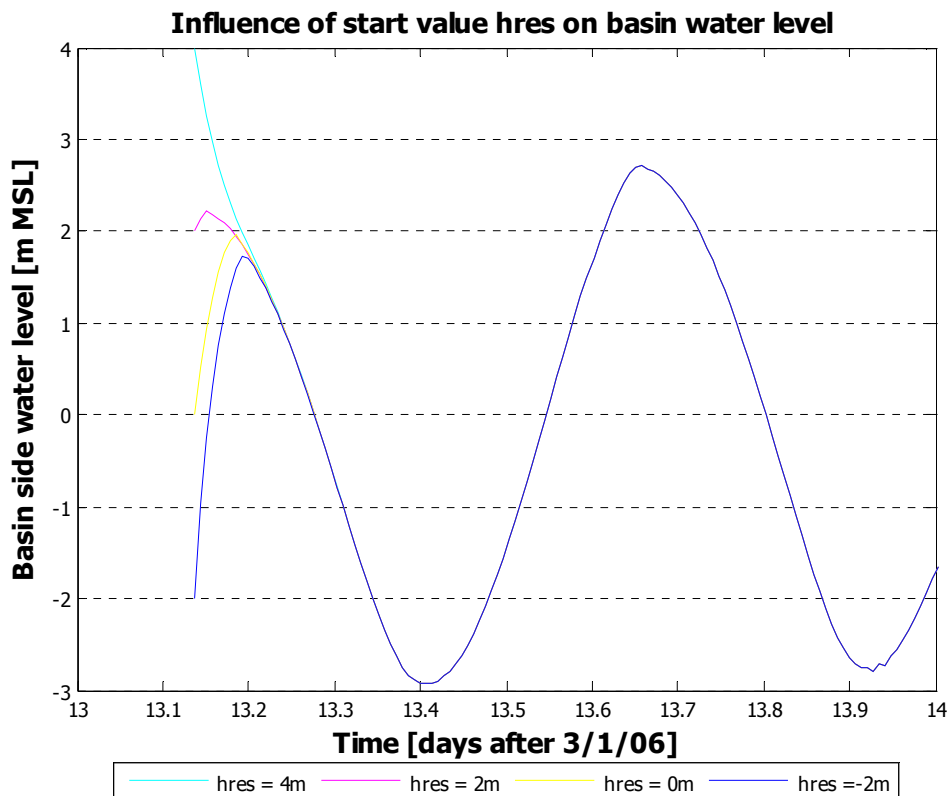
Figure 4-7 Influence of start value h_{res} on predicted water level in basic model

Via two ways, parameters can influence the predicted basin side water level. The first way is via the calculation of the discharge in a time interval and the second way is via the calculation of the water level rise or fall in a time interval. The discharge coefficient and the depth and width of the different gaps influence the prediction of the basin side water level via the discharge calculation and the wet surface area inside the basin influence the basin side water level via the calculation of the water level difference in a time interval.

The discharge coefficient μ influence the total discharge directly. See also formulas chapter 3.4. According to the Wallingford reports [Wallingford, 2005] the discharge coefficient μ can vary between 0.7 and 1.3. The common value for a closure gap is 0.9. [d'Angremond, 2001] It is also stated that the value of μ can vary during the closure because of the geometry of the gaps. This aspect is not taken into account in this investigation and one constant value for the discharge coefficient is assumed during the closure. In the following figure, the results of different calculations with different values for the discharge coefficient are showed. The smaller the gaps become, the more important the influence of a different discharge coefficient becomes.
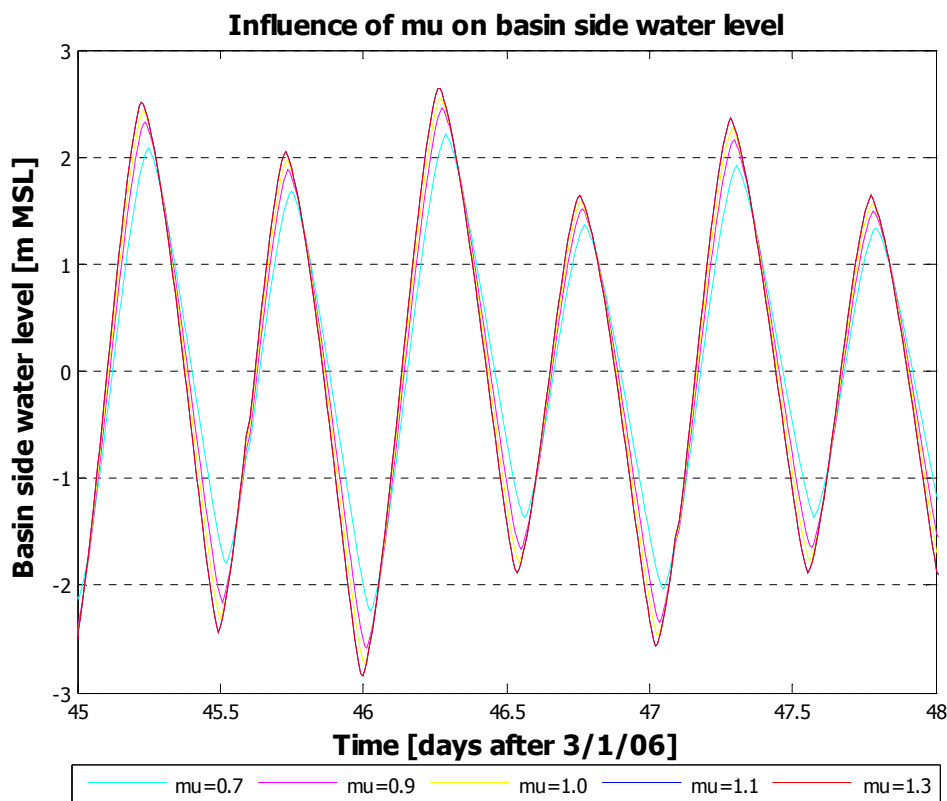
Figure 4-8 Influence of μ on predicted basin side water level

Eventually the discharge coefficients for the closure gaps are estimated on a value of 0.9(-). The discharge coefficient for the sluices is estimated on a value of 1(-).

Influence d1 on basin side water level
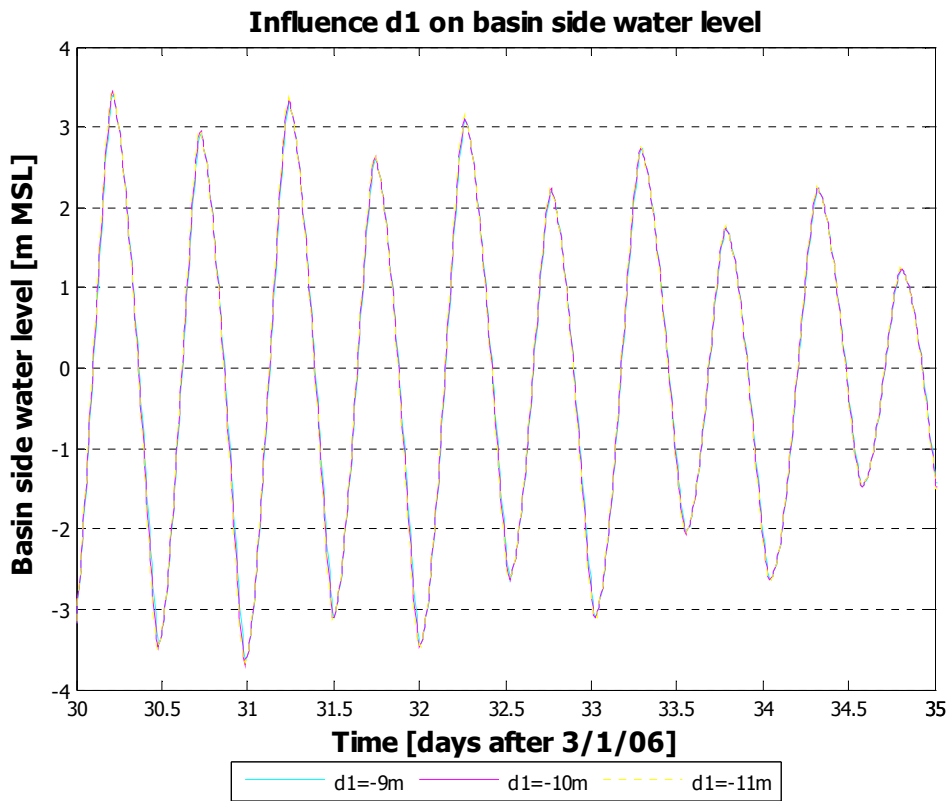
Figure 4-9 Influence of depth in Gap 1 on predicted basin side water level

Influence d2 on basin side water level
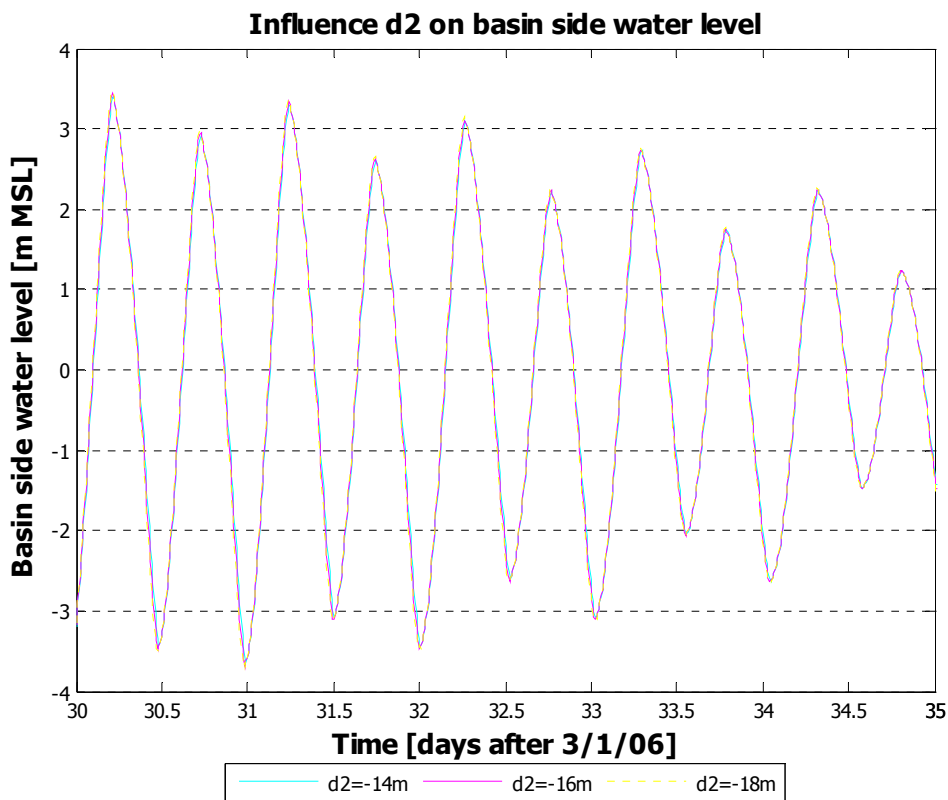
Figure 4-10 Influence of depth in Gap 2 on predicted basin side water level

Another parameter that influences the total discharge is the depth of the gaps. The depth in both gaps is measured some weeks before the beginning of the closure. According to drawings provided by KRC the average depth of gap1 respectively gap2 is -10m MSL and -16 m MSL. In advance of the closure works and during the closure works itself barges dumped loose material in the middle of the closure gaps. Because no other information is available, it is assumed that the depth of the closure gaps have the value indicated by KRC.

To investigate the influence of the depth of the closure gaps on the prediction of the basin side water level, the basin side water level was calculated with different values of the depth in gap1 and gap2. In the following figures, it is showed that the influence of the depth of the closure gaps on the predicted basin side water level is relatively small. Therefore, the final calculations are executed with the given depth of -10m and -16m MSL for gap1 and gap2 respectively.

The total discharge being known the water level rise or fall inside the basin within a certain time interval is calculated with the storage area approach formula. Now, the water level rise or fall only depends on the wet surface area inside the basin. This wet surface area is not a constant but varies with the water level inside the basin. To investigate the sensitiveness of the calculation of the water level inside the basin with the wet surface area, three model runs have been made. One with a wet surface area that is 90% of the original wet surface area, one that is 100% of the wet surface area and one with a wet surface that covers 110% of the original wet surface area. In the following figure the influence of a different wet surface area on the basin side water level can be seen.
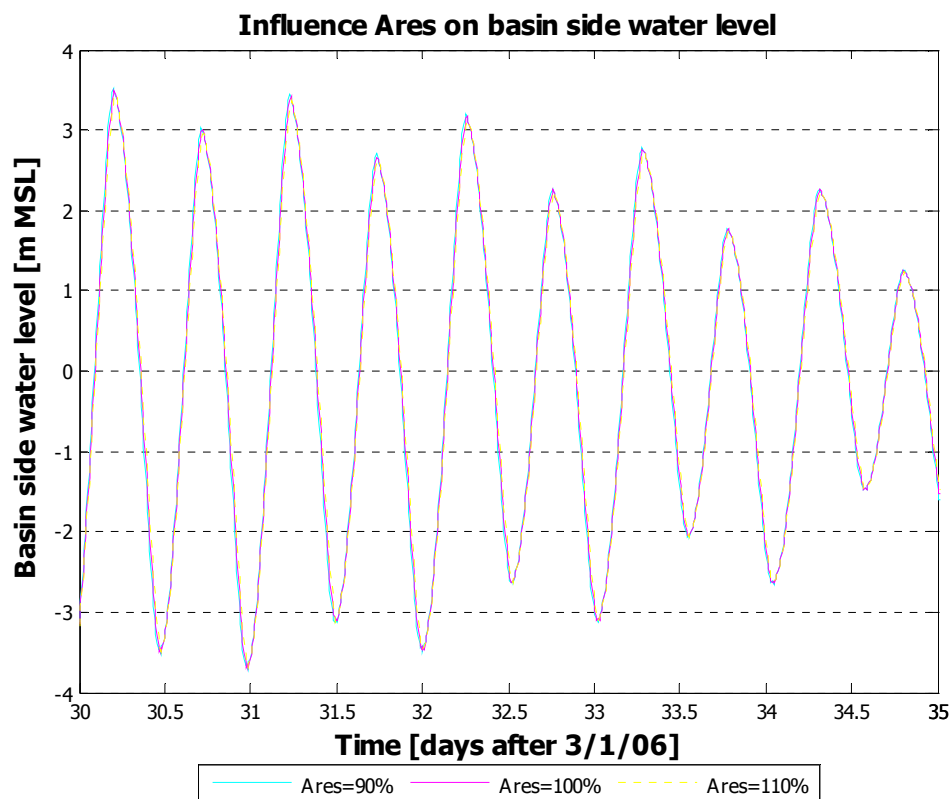
Figure 4-11 Influence of wet surface area on predicted basin side water level

If the wet surface area increases to 110%, the amplitude of the basin water level decreases. This is logical taking into account the storage area approach formula. Because the wet surface area is provided by KRC and the influence on the basin side water level is small, the original wet surface area is used.

4.3 Results of storage area approach

4.3.1 Results of water level prediction inside the basin

To investigate the accuracy of the predicted basin side water level the results of the model are compared with measured data. There is not much information governing measured data so only during one day results can be compared. By comparing the measured data with the predicted values for the basin side water level, a problem arises. The location of the measurements does not correspond with the location of the prediction. During the total closing period at four locations along the dam, measurements were executed. These four locations are indicated in the following figure.
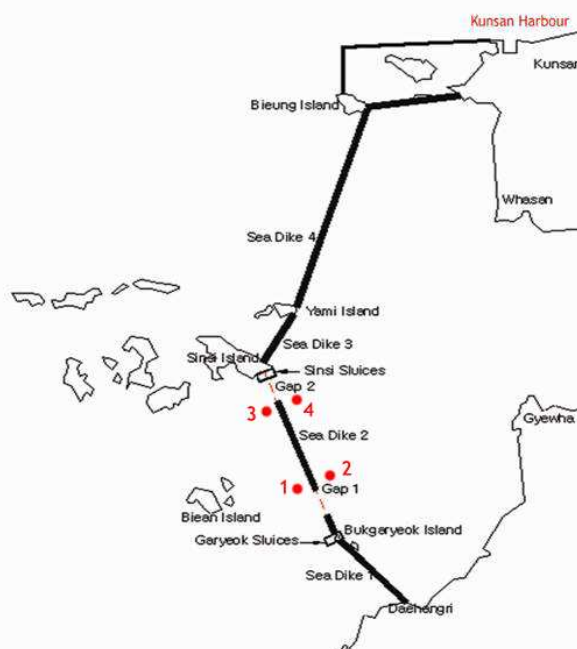
Figure 4-12 Water level measuring locations near dam section 2

The water level was measured by reading the water level from a staff gauge, which was placed near the dike at measuring point 2. A person reads the water level every ten minutes day and night. Because no telescope has been used and no information about the calibration of the staff gauges has been known, the accuracy of the measurements is not known. The form of one of the executers was photographed ad contained one day of measurements.

Figure 4-13 Staff gauge and person who read staff gauge at location 2

In the following figure the measured water level, as given on the form, is compared with the predicted basin side water level. There is a big difference between the predicted water level and the measured water level. The predicted water level is higher during high water and lower during low water so the predicted water level amplitude is larger then the measured one. The moments of the high and low waters correspond.
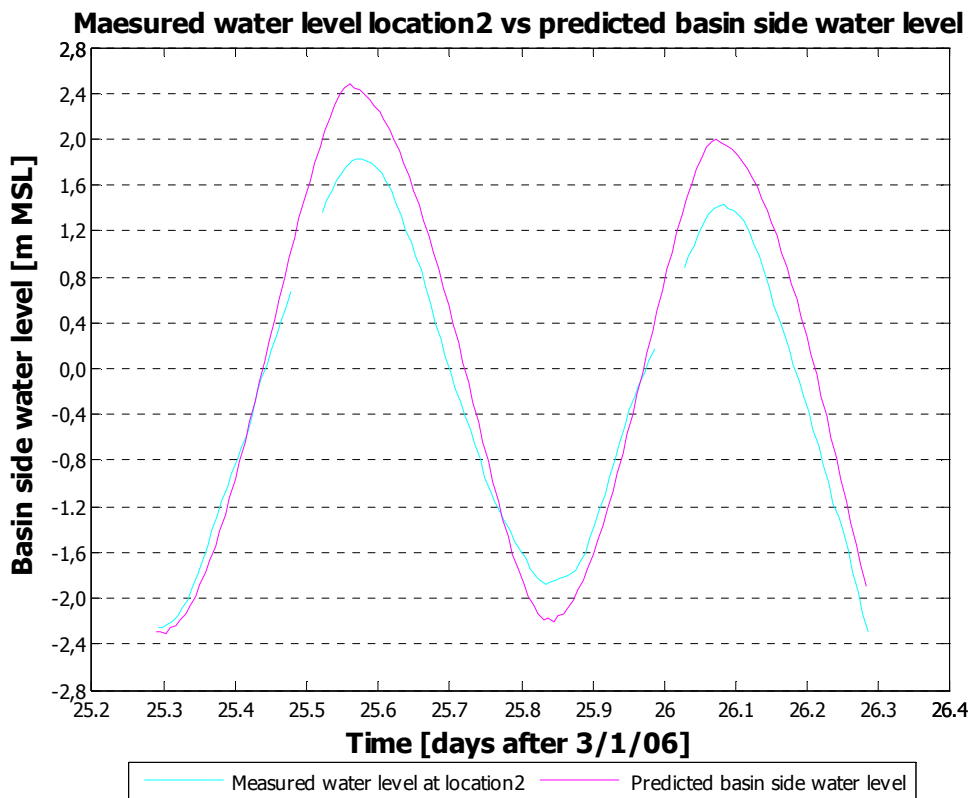
Figure 4-14 Predicted and measured basin side water level near location 2

The location of the predicted water level is Gunsan Outer Port (see paragraph 3.2.1). The measurement was executed near closure gap1 at the basin side of the dike. The distance between these two points is approximately 20 km and there is no information about how the tidal wave deforms along the coast of the Korean peninsula. According to the figure above, one can assume that the tidal amplitude at the location of the gap is smaller than in Gunsan Outer Port. The estimated parameters used for the prediction of the basin side water level will also cause a difference in the water level. By adapting these estimated parameters, an attempt has been made to let the two water levels correspond. By decreasing the flow area of the gap and by lowering the discharge coefficient μ, the tidal amplitude of the predicted water level will decrease. On the other hand, the predicted high and low water moments will shift and it will no longer correspond with the measured high and low water moments. This can be seen in the following figure.
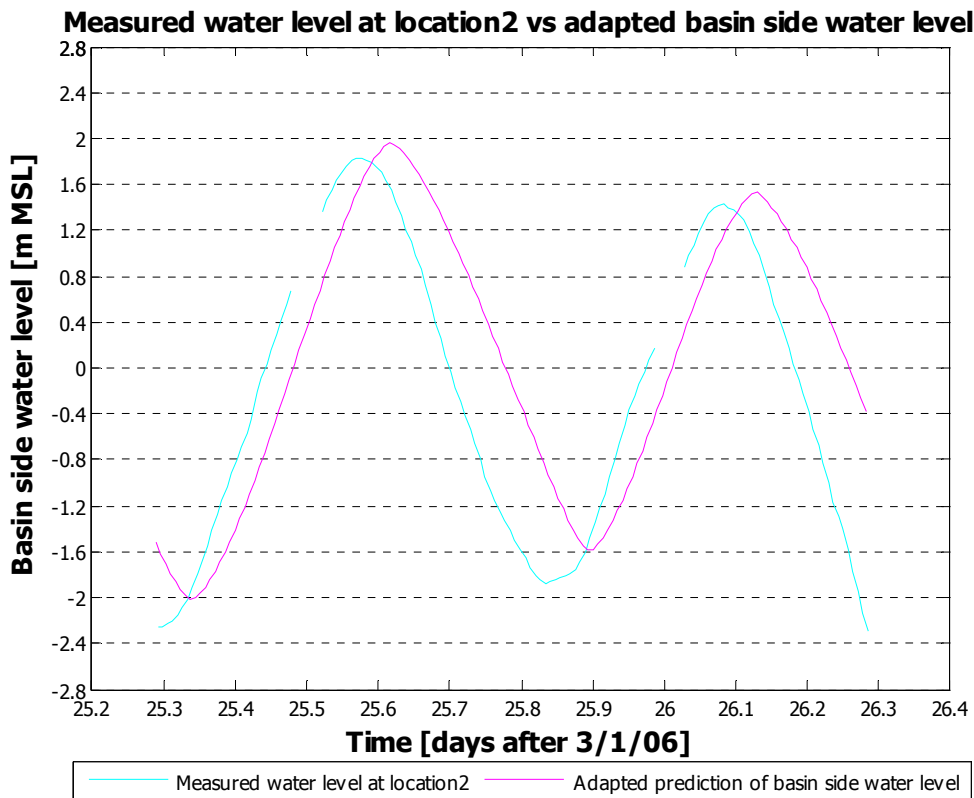
Figure 4-15 Adapted prediction and measured basin side water level near location 2

After adapting the estimated parameters, the high water level corresponds better but now, the predicted low water level is too high. The moments of high and low water no longer correspond either. Because it was not possible to let the two graphs correspond well, for further calculation, the original prediction as explained in paragraph 4.4.1 will be used.

4.3.2   Results of flow velocities through closure gaps

Wallingford [HR Wallingford 2005] states that the mid gap flow velocity calculated with their Telemac model will not exceed 6.54 m/s for Gap 1 and 6.33 m/s for Gap 2 during the closure. The maximum peak velocity according to their model is 7.41 m/s in Gap 1 and 7.08 m/s in

Gap 2. The maximum flow velocity in Gap 1 will occur just before the final closure, which is $t=54$ in the prediction, and the maximum flow velocity in Gap 2 will occur just before the third construction period, which is in $t=47$. In the prediction of the basin side water level, the water level in the basin is assumed horizontal thus the water level head over Gap 1 and Gap 2 will be the same. The calculated flow velocity is an average value for the flow velocities through the sluice gates and the closure gaps. The following figure shows the predicted flow velocities compared with the by Wallingford predicted flow velocities.
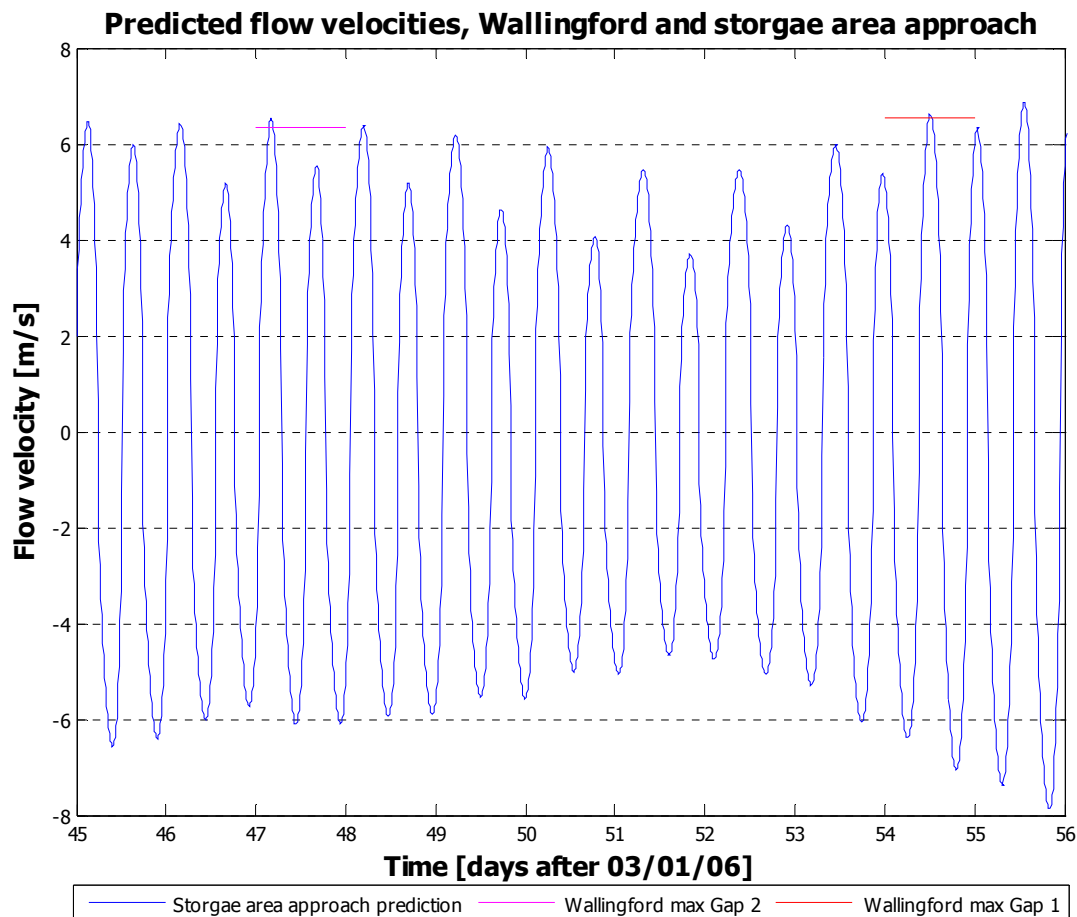
Figure 4-16 Predicted flow velocities by Wallingford and storage area approach

In Figure 4-16 the blue line is the with the storage area approach predicted flow velocity through the closure gaps. The pink line is the maximum predicted flow velocity by Wallingford for Gap 2, and the red line the predicted maximum flow velocity through Gap 1. The storage area approach does not make a distinction between the flow velocities through the gaps. It can be seen that the maximum predicted flow velocity by Wallingford correspond with the predicted flow velocity by the storage area approach.

There is one set of GPS floater measurements available. On April 16, measurements were executed with 6 GPS floats, in the centreline of gap2. For every float a series of time and average flow velocity per ten seconds is known. To get an impression of the flow velocity

course in time the maximum flow velocity and the corresponding time were compared with the predicted flow velocity. This can be seen in the following figure.

Calculated and GPS float measured flow velocity
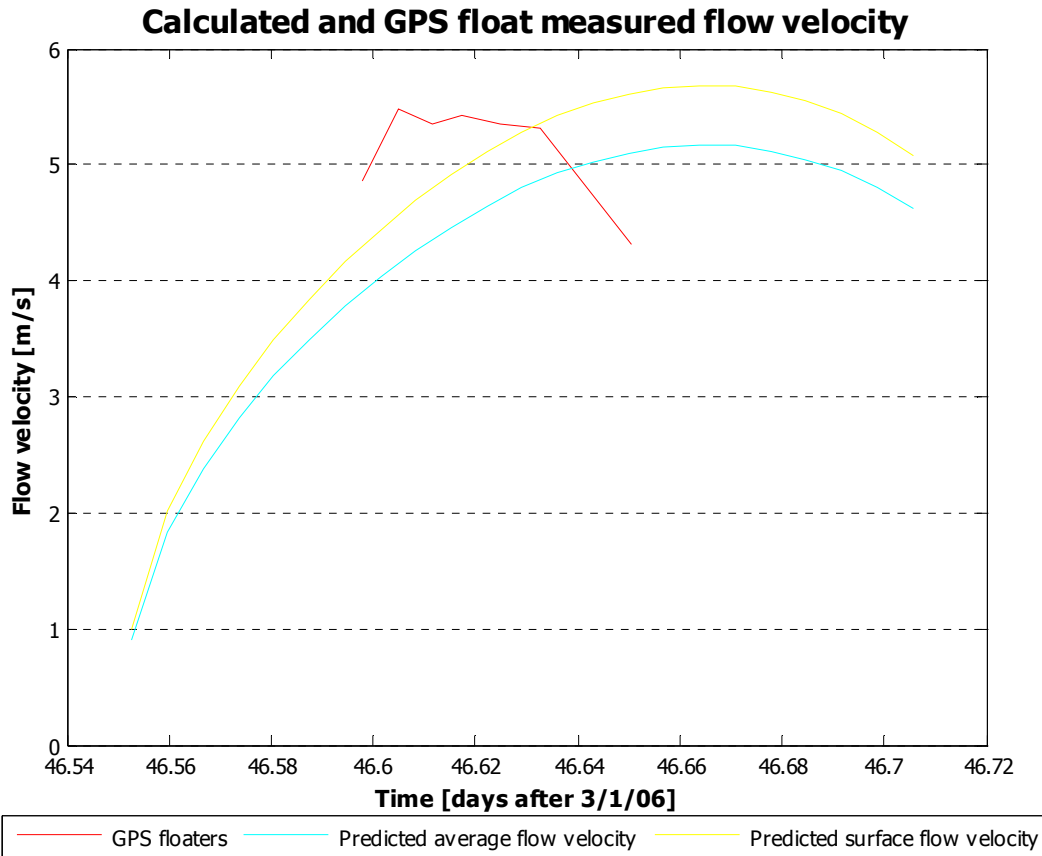
Figure 4-17 Measured surface and predicted depth average flow velocity April 16, 2006

The measured flow velocity through gap2 is larger then the predicted velocity. Because the predicted velocity is the same for all the gaps and sluices and because secondary effects as phase differences between the gaps, the detailed geometry of gap2, flows in the basin between the gaps the difference between the predicted and measured velocity can be explained. Another point is that the GPS floaters measure the flow velocity at the water surface and the predicted flow velocity is a depth average flow velocity that causes a difference of about 10%. [Schiereck 2001]

5 The Waqua model

Waqua is a two dimensional hydrodynamic and water quality simulation model which can be used for well-mixed estuaries, coastal seas and rivers. The simulation model contains three parts; the pre-processing, the processing and the post-processing part. To complete the pre-processing part, several features of Delft3D are used to generate a grid because this cannot be done using Waqua. The processing part was executed using the cluster of the Delft University of Technology and for the post-processing part, Matlab was used. With the Waqua model, the water level, the flow velocity and the discharge in every grid point of the computational domain were calculated. The results of the calculation have been compared with measurements and the model input has been adapted two times. To generate useful results with the Waqua model, the input file needs to be adapted until the results of the calculation resembles the measurements because this is not the case after the two adaptations that were done.

Because the water level is calculated in every grid point of the computational domain, the water level course through the closure gap is calculated. This water level course can be used as input for the EFD.lab model. Because the input file for the Waqua calculation needs more adaptations before it generates accurate results, the results of the executed Waqua calculations were not used as input for the EFD.lab model.

This chapter elaborates the Waqua model and the underlying mathematics are discussed first, then the pre-processing part with the generation of the computational grid and the boundary conditions for the calculation. Finally, the results of the calculation are explained.

5.1 Underlying mathematics

There are three possible types of coordinates that can be used in Waqua. The rectilinear coordinate type is the simplest modelling solution and the distance between two successive grid points in the x and y direction stays the same. When the area of interest does not cover the total modelled area, curvilinear coordinates are more suitable because then the grid can be refined in the area of interest. When a curvilinear grid is used, a grid input file is required. Waqua does not have its own grid generator so other programs are required. Besides the rectilinear coordinate and the curvilinear coordinate types, spherical coordinates are a possibility. Spherical coordinates are suitable when a considerable part of the globe is covered. To model the Saemangeum estuary curvilinear coordinates are used. Waqua uses the following form of the shallow water equations to calculate the flow velocities and water levels.

$$\frac{\partial u}{\partial t} + \frac{u}{\sqrt{g_{\xi\xi}}}\frac{\partial u}{\partial \xi} + \frac{v}{\sqrt{g_{\eta\eta}}}\frac{\partial u}{\partial \eta} + \frac{uv}{\sqrt{g_*}}\frac{\partial \sqrt{g_{\xi\xi}}}{\partial \eta} - \frac{v^2}{\sqrt{g_*}}\frac{\partial \sqrt{g_{\eta\eta}}}{\partial \xi} - fv + \frac{g}{\sqrt{g_{\xi\xi}}}\frac{\partial \zeta}{\partial \xi} + gu\frac{\sqrt{u^2 + v^2}}{C^2(h+\zeta)} =$$

$$\frac{\rho_a C_d W_\xi \sqrt{W_\xi^2 + W_\eta^2}}{\rho_w(h+\zeta)} + \frac{v}{\sqrt{g_{\xi\xi}}}\frac{\partial A}{\partial \xi} - \frac{v}{\sqrt{g_{\eta\eta}}}\frac{\partial B}{\partial \eta}$$

5.1

$$\frac{\partial v}{\partial t} + \frac{u}{\sqrt{g_{\xi\xi}}}\frac{\partial v}{\partial \xi} + \frac{v}{\sqrt{g_{\eta\eta}}}\frac{\partial v}{\partial \eta} + \frac{uv}{\sqrt{g_*}}\frac{\partial \sqrt{g_{\eta\eta}}}{\partial \xi} - \frac{u^2}{\sqrt{g_*}}\frac{\partial \sqrt{g_{\xi\xi}}}{\partial \eta} + fu + \frac{g}{\sqrt{g_{\eta\eta}}}\frac{\partial \zeta}{\partial \eta} + gv\frac{\sqrt{u^2+v^2}}{C^2(h+\zeta)} =$$

$$\frac{\rho_a C_d W_\eta \sqrt{W_\xi^2 + W_\eta^2}}{\rho_w(h+\zeta)} + \frac{v}{\sqrt{g_{\eta\eta}}}\frac{\partial A}{\partial \eta} + \frac{v}{\sqrt{g_{\xi\xi}}}\frac{\partial B}{\partial \xi}$$

5.2

$$\frac{\partial \zeta}{\partial t} + \frac{1}{\sqrt{g_*}}\frac{\partial}{\partial \xi}\left(Hu\sqrt{g_{\eta\eta}}\right) + \frac{1}{\sqrt{g_*}}\frac{\partial}{\partial \eta}\left(Hu\sqrt{g_{\xi\xi}}\right) = 0 \qquad\qquad 5.3$$

In which:

$$A = \frac{1}{\sqrt{g_*}}\left[\frac{\partial}{\partial \xi}\left(u\sqrt{g_{\eta\eta}}\right) + \frac{\partial}{\partial \eta}\left(v\sqrt{g_{\xi\xi}}\right)\right] \qquad\qquad 5.4$$

$$B = \frac{1}{\sqrt{g_*}}\left[\frac{\partial}{\partial \xi}\left(v\sqrt{g_{\eta\eta}}\right) - \frac{\partial}{\partial \eta}\left(u\sqrt{g_{\xi\xi}}\right)\right] \qquad\qquad 5.5$$

u,v	=	depth mean velocity in x and y direction (m/s)
ζ	=	water elevation above plane of reference (m)
h	=	water depth below plane of reference (m)
H	=	h+ζ (m)
f	=	parameter of Coriolis
C	=	Chézy coefficient ($\sqrt{}$m/s)
W_ξ, W_η	=	components of surface wind velocity W
C_d	=	wind drag coefficient
ρ_a, ρ_w	=	density of air and water (m³/kg)
v	=	eddy-viscosity coefficient (m²/s)
$g_{\xi\xi}$, $g_{\eta\eta}$	=	transformation coefficients
g_*	=	$g_{\xi\xi}*g_{\eta\eta}$

5.2 Creation of the model

The set-up of a Waqua model starts with the creation of a computational grid. This computational grid is enclosed by open and closed boundaries. At the open boundaries, boundary conditions concerning fluctuating water levels can be assigned. In the area of interest, which is the location of the closure gaps, the grid is refined. The open boundaries of this model should be located at such a distance that changes in, for example, the barriers coefficients assigned to the closure gaps, do not affect the boundary condition at the open boundary. The following paragraph discusses the creation of the models computational grid.

5.2.1 Generation of the grid

Because curvilinear coordinates are used, a separate input file is required. Waqua does not have its own grid generator, so another program is necessary to create the grid input file. This input file must be an *.rgf file and is created with features from the Delft3D package, RGFgrid and Quickin. For the creation of the computational grid, bottom geometry data from

measurements of the surrounding of the estuary are used. This data contains data points with coordinates in the x-direction, coordinates in the y-direction and a depth value for each data point. With RGFgrid, the computational grid in the x- and y-direction has been created in such a way that all the measured data points are used and lie inside the generated grid. The computational area governs the Saemangeum estuary and a significant part of the foreshore. The following figure shows an overview of the computation grid. At the right hand side in the computational grid, the estuary has been modelled and the two branches can be distinguished. In the area of interest, the shaded area, the two closure gaps are located.
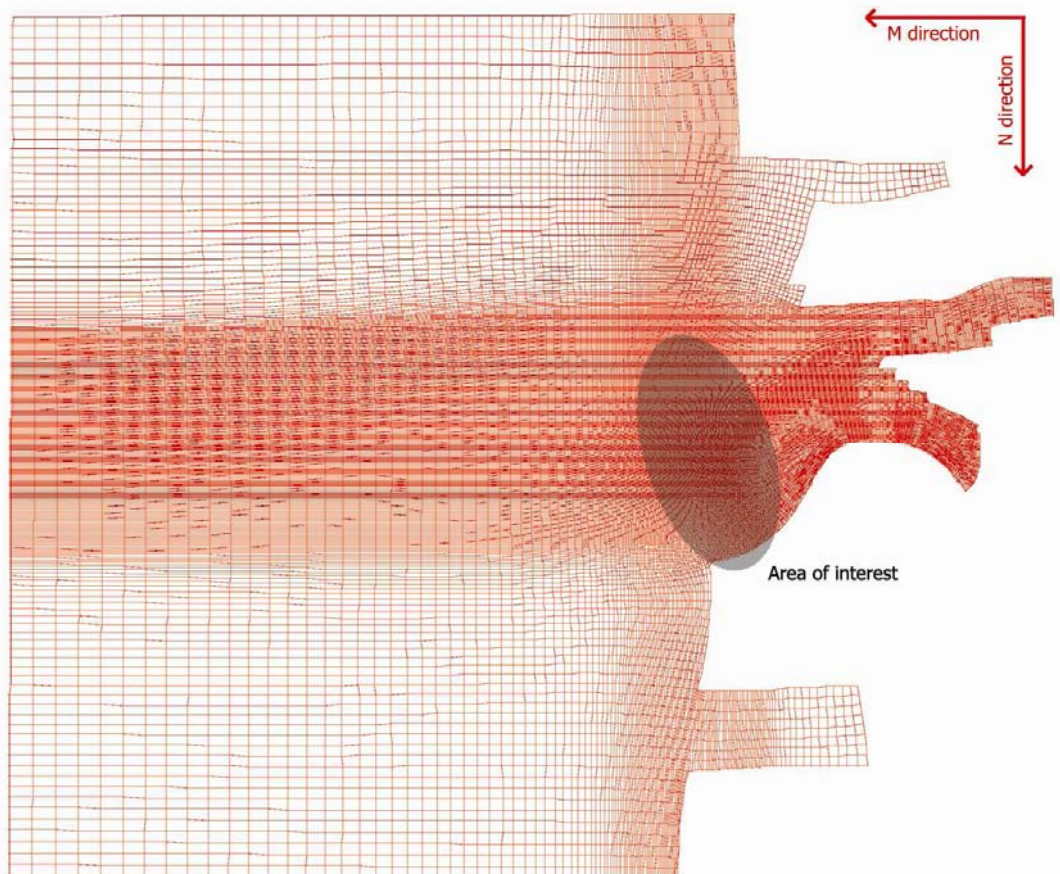
Figure 5-1 Computational grid in x (M) - and y (N)-direction of Saemangeum estuary

Figure 5-1 shows the generated grid. The grid contains 181 cells in the M-direction and 307 grid cells in the N-direction. In the area of interest, the grid is refined. The extra input file containing the information about the computational grid in the x- and y-direction, has been included in Appendix III.

To keep the numerical accuracy acceptable, the difference in size between two adjacent grid cells may not exceed 20%. This must hold in the M-direction as well as in the N-direction. The angles within a grid cell must meet the condition of 100*cos (angle) <2. This implies that the right angle between the M- and the N- lines of a grid cell may not differ more than 1.15º from 90º. Every grid point contains four basic properties, namely the water level, the depth, the u-component of the velocity (in the M-direction) and the v-component of the velocity (in the N-direction). In Figure 5-2 Physical properties of every grid point, the positions of these

basic parameters in the grid are shown. The water level grid points correspond with the grid cell points.

After generating the grid in the x- and y-direction, a depth needs to be assigned to every grid cell. The data set contains a depth value for every data point, these data points however do not correspond to a grid point. The data points are spread over the grid so for a depth value in every grid cell, the data points need to be interpolated over the grid cells. In this way a depth value is assigned to every grid cell. This is done with another feature of the Delft3D package called Quikin.
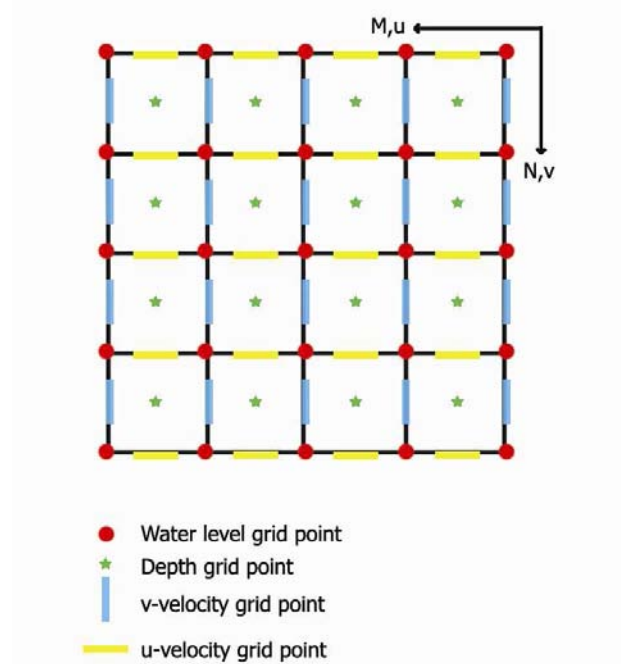
Figure 5-2 Physical properties of every grid point

Figure 5-3 shows the result of the generation of the depth file. The figure shows the varying depth over the computational domain. The right hand side the estuary and the closure gaps, with the scour holes at both side can be distinguished. At the left hand side of the figure, the colours of the depths are showed.

Bathymetry [m]
- < -47.3
- < -44.8
- < -42.3
- < -39.8
- < -37.2
- < -34.7
- < -32.2
- < -29.7
- < -27.2
- < -24.6
- < -22.1
- < -19.6
- < -17.1
- < -14.6
- < -12.0
- < -9.5
- < -7.0
- < -4.5
- < -2.0
- < 0.6
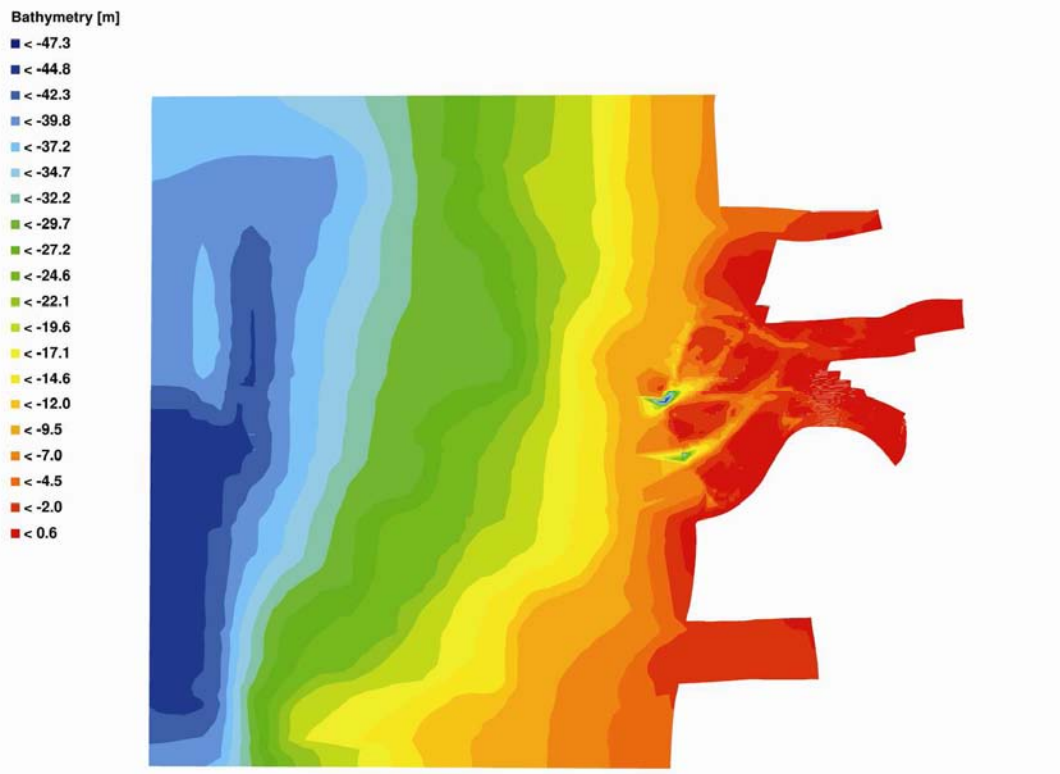
Figure 5-3 Generated depth over computational grid

The depths in every grid cell needs to be assigned manually in the Waqua input file. After the completion of the shape of the grid in the x- and y-direction and after defining a depth value to every grid cell the computational grid is finished. However, the closure dam, with the closure gaps has not been implemented yet. In the input file the grid points, where the dam is located, are assigned as dam points. This means that the depth value for this location is overwritten and the point is permanently dry. At the location of the closure gaps and the sluices gates barrier points are created. Parameters have to be assigned to these barrier points. This will be elaborated in the section boundary conditions.

With the x- and y-coordinates of the grid cells and the depth value in every grid cell a three dimensional view of the computational area is created. This is showed in Figure 5-4. The axis of the figure do not all has the same scale. The x- and y-axis show the coordinates in these directions and the z-axis shows the level of the bottom compared to MSL.
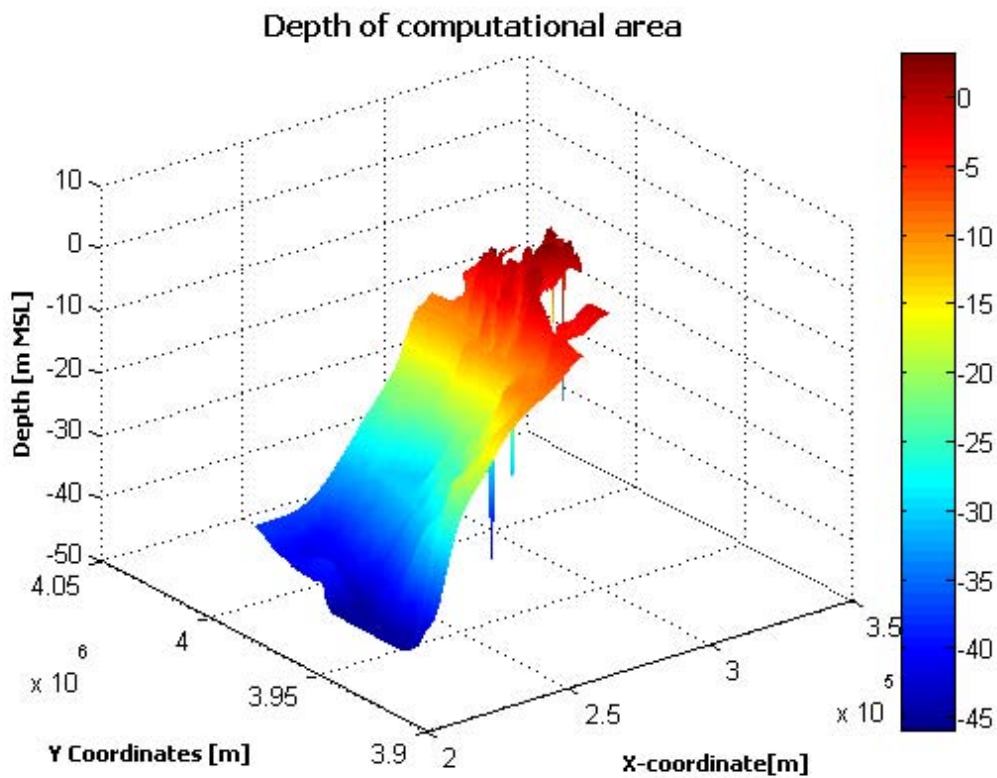
Figure 5-4 Three-dimensional view of Saemangeum estuary computational domain
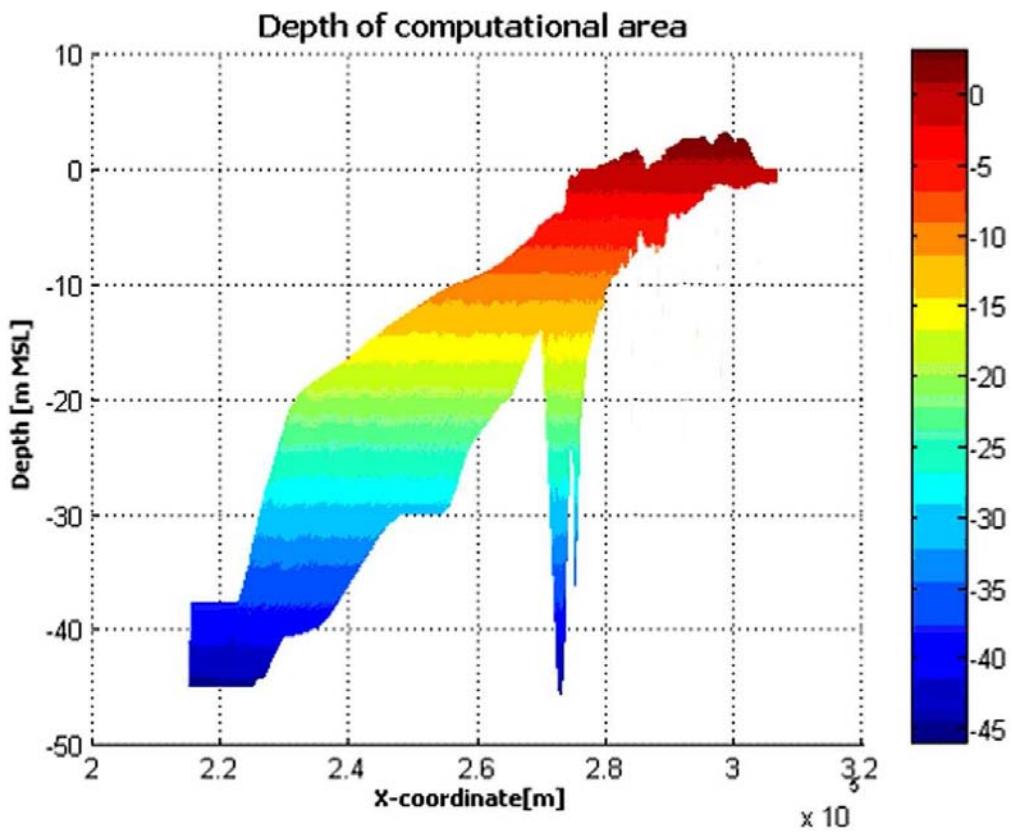
Figure 5-5 Side view of depth in computation grid, side view

Figure 5-5 shows a side view of the computation domain. The highest levels and the lowest levels over the x-axis of the computational domain are shown. The scour holes can now distinguished.

5.2.2 Generation of the input file

Waqua is based on SIMONA, which is a concept for the development of computational software. The major part of the Waqua system is written in FORTRAN77. For this thesis, all calculations are executed on a cluster, located at the faculty of Civil Engineering at Delft University of Technology. The input file for Waqua is a structured ASCII file. During the pre-processing the input file will be transformed into a SDS file which is required for the actual calculation. During the calculation, all results will be written to this SDS file. The input file is divided into several blocks, each can be subdivided into sub-blocks. Every (sub) block is separated with a keyword and the structure of the total file is hierarchical. Only after all the required information between two keywords is assigned, a block is completely defined. The information concerning a certain block must be assigned in that specific block and cannot be assigned elsewhere in the input file. There are thirteen main keywords, from which three are mandatory and ten optional. The three main, mandatory keywords are:

- IDENTIFICATION: In this block, the general information for the run is specified. The experiment name and title must be generated and the kind of model that should be used needs to be selected.

- MESH: The mesh block specifies the total geometry of the model. The grid file is assigned and the kind of coordinates is specified. User points are created, which can be used in another part of the input file. This is purely for the convenience of the user. When points are created they can be referred to instead of to the grid points. The user points can be used for the definition of openings, barriers checkpoints etc. Just like user points, user curves can be defined here, which can also be used later on in the input. Boundaries, such as enclosures, openings and barriers are specified in this block, using the points and curves defined earlier. An important sub-block is the block, where the depth is assigned to the grid points. Every grid cell receives a value for the depth in that particular grid cell.

- FLOW: the flow part is subdivided into three sub-blocks and contains all the information for the hydrodynamic model. The three sub-blocks are a problem block, a forcing block and a checkpoints block. In the problem sub-block, all the parameters and coefficients that are required for the calculation are defined. These can be for example start date, time step, friction and viscosity.

    The forcing sub-part contains information about the initial values and the boundary conditions. Here, the initial water level and velocities, and the boundary conditions on the openings are specified.

The remaining ten optional keywords are depth control, restart, general, transport, densities, turbulence model, displays, sds output, print output and ignore. In Appendix IV. the complete input file is shown.

5.3 Boundary conditions

In the input file, which is used for the calculation all the boundary conditions are implemented. Besides the geometry of the estuary and the surrounding, many other boundary conditions have to be taken into account.

In the section 'GENERAL' of the input file, the physical parameters of the model need to be assigned. The following values for these parameters are assigned:

Gravity = 9.81 m/s^2
Water density = 1023 kg/m^3
Air density = 1.225 kg/m^3
Dynamic viscosity = 0.001 kg/ms

In the section 'FLOW' the following input parameters have been assigned:

Starting time of calculation = March 14, 2006
Period of the calculation = 66240 minutes
Formula for friction = Manning
Value for Manning parameter = 0.0260 m$^{-1/3}$ in u and v direction
Eddy viscosity = 1 m^2/s (Same value as used in Waqua calculations for the Eastern Scheldt [Dijkzeul 1998])
Barrier coefficient barrier 1 = 0.9 (closure gap1)
Barrier coefficient barrier 2 = 0.9 (closure gap2)
Barrier coefficient barrier 3 = 1.0 (Gareyok sluices)
Barrier coefficient barrier 4 = 1.0 (Sinsi sluices)

In the section 'FORCING' the following input parameters have been assigned:

Initial value for water level = 2.0m MSL
Initial velocity in u-direction = 0.0 m/s
Initial velocity in v-direction = 0.0 m/s

To create a forcing of the water level, a Fourier series has to be applied to the open boundary. This Fourier series correspond to the tidal movement of the water level at this open border. At seventeen locations in and near the computation grid, four of the main tidal components are known. The seventeen locations in and around the computational grid are shown in Figure 5-6.

The water level in the 17 locations has been composed out of the four constituents with the following formula:

$$h(t) = H_0 + \sum_{i=1}^{n} (A_i (cos((\omega_i t) + \phi_i)) \qquad 5.6$$

where:
$h(t)$ = water level at time t (m)
H_0 = average water level (m)
A_i = amplitude of component i (m)
ω_i = angular velocity of component i (rad/s)
φ_i = phase of component i (rad)
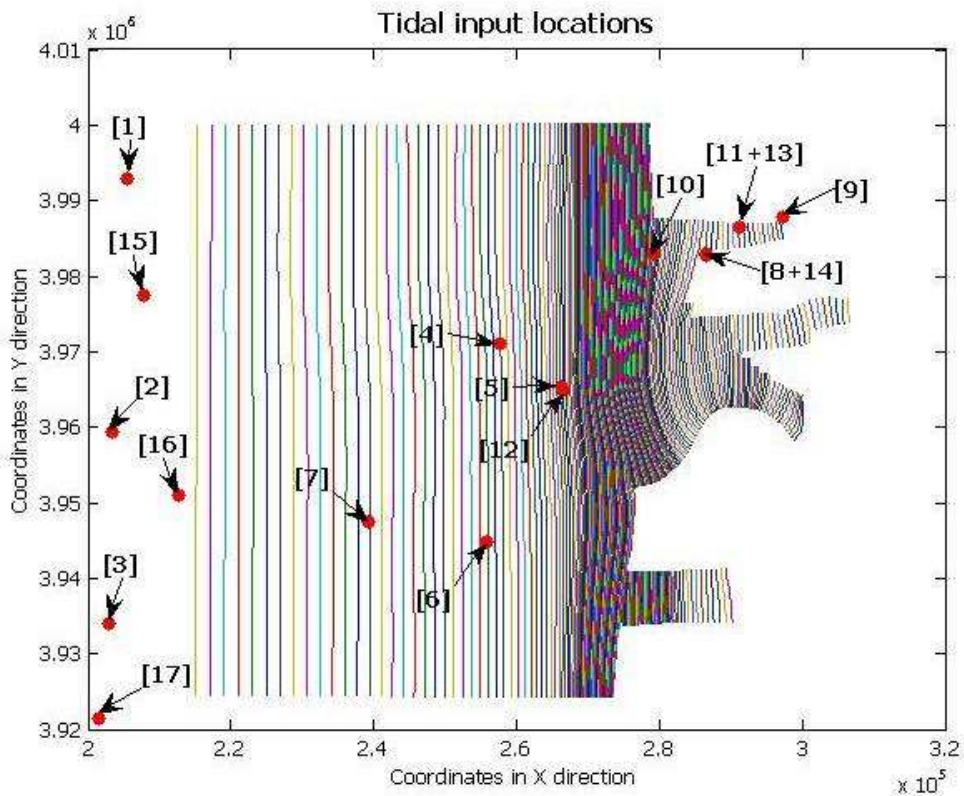
Figure 5-6 Location in which tidal constituents are known, in the computation domain

The amplitude and the phase of each of the components vary over the different locations, but the angular velocity of the constituents is a constant. The following table gives an overview of the different constituents and the angular velocity.

Tidal constituent		Angular velocity (rad/s)
M2	Principal lunar semi-diurnal constituent	0.000140518
S2	Principal solar semi-diurnal constituent	0.000145444
O1	Lunar diurnal constituent	0.000067597
K1	Lunisolar diurnal constituent	0.00007292

Table 5-1 Tidal constituents used for composition of tidal movement
Source: www.getij.nl

In Appendix V. all the 17 constituents, their locations and the amplitude and phases have been listed.

To investigate the accuracy of the water level composition with four tidal constituents, which will be used for the initiation of the model, this prediction was compared with the water level variation in Gunsan Outer Port. Location 8, from Figure 5-6, gives the location of the Gunsan Outer Port.

For the water level prediction executed with the storage area approach, the water level variation in the Gunsan Outer Port has been composed with predictions for the high and low water levels. This composed water level was compared with measured data and the two water level variations corresponded well. This has been explained in Chapter 4. Because of this good correspondence, the composed water level as used in chapter 4 is assumed accurate and therefore, the water level variation composed with the four tidal constituents, will be compared with the predicted water level variation as used in the storage area approach.

The phase of the two predictions cannot be compared because no start value of water level variation composed with the four tidal constituents is known. The amplitude and the shape of the two water level variations can be compared.

Figure 5-7 shows the water level variation in the Gunsan Outer Port. The blue line is the water level variation as used in the storage area approach and is the most accurate water level variation. The pink line is the water level variation composed with the four tidal constituents for location 8 from Figure 5-6. The amplitude of the water level variation composed with the four tidal constituents is smaller than the water level variation predicted in the Gunsan Outer Port. Figure 5-7 shows the water level variations during spring tide. During neap tide, the water level variations of the composed water level with the four constituents did not correspond with the predicted water level in Gunsan Outer Port.

Despite of the differences between the water level variation composed with the four constituents and the predicted water level variation in Gunsan Outer Port, for the initiation of the Waqua model a composition of the water level with the four constituents will be used because no other data is available.

water level variation in Gunsan Outer Port
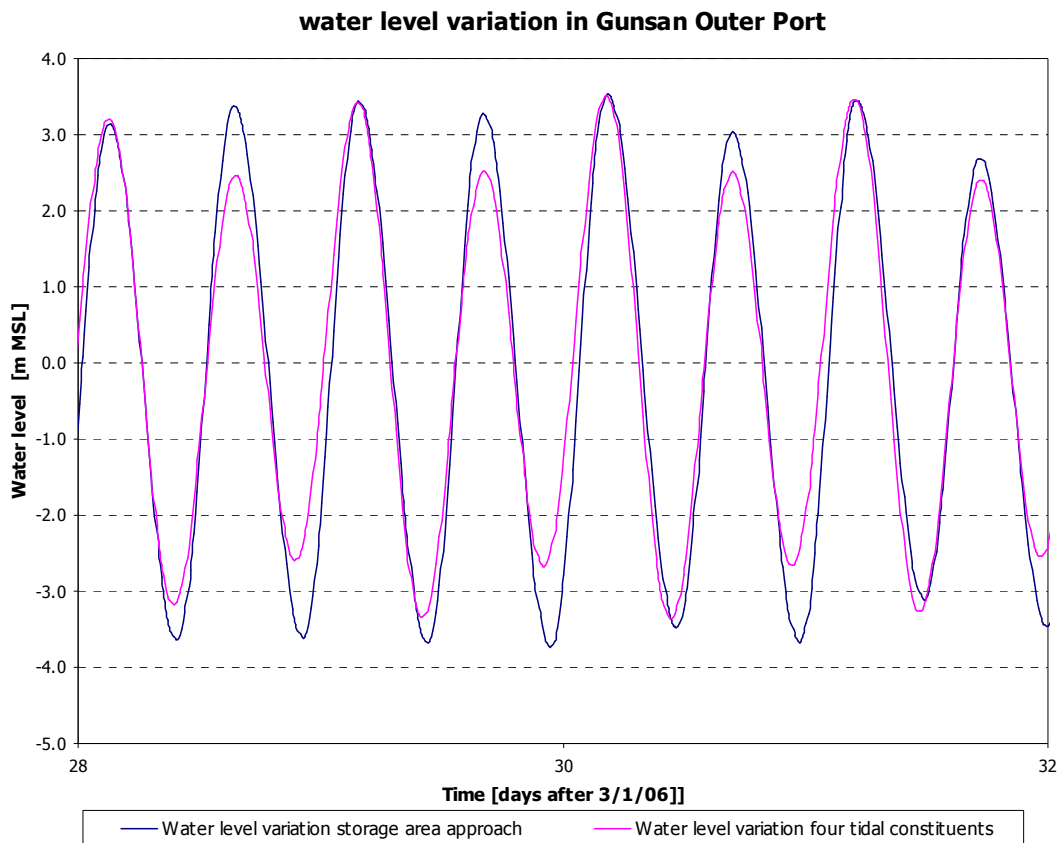
Figure 5-7 Comparison of water level in Gunsan Outer Port

At the left hand side of the computation grid, an open boundary is enforced and at this open boundary a Fourier series, that contains the four tidal constituents, is assigned. The six points that lie at the left hand side of the computational domain (number 1, 15, 2, 16, 3, 17) can be used for the input. The six locations have different amplitudes and phases and the water level in the six points will vary. In the following figure, the water level in the six locations is shown.

Tidal movement at locations at the border of compuational grid
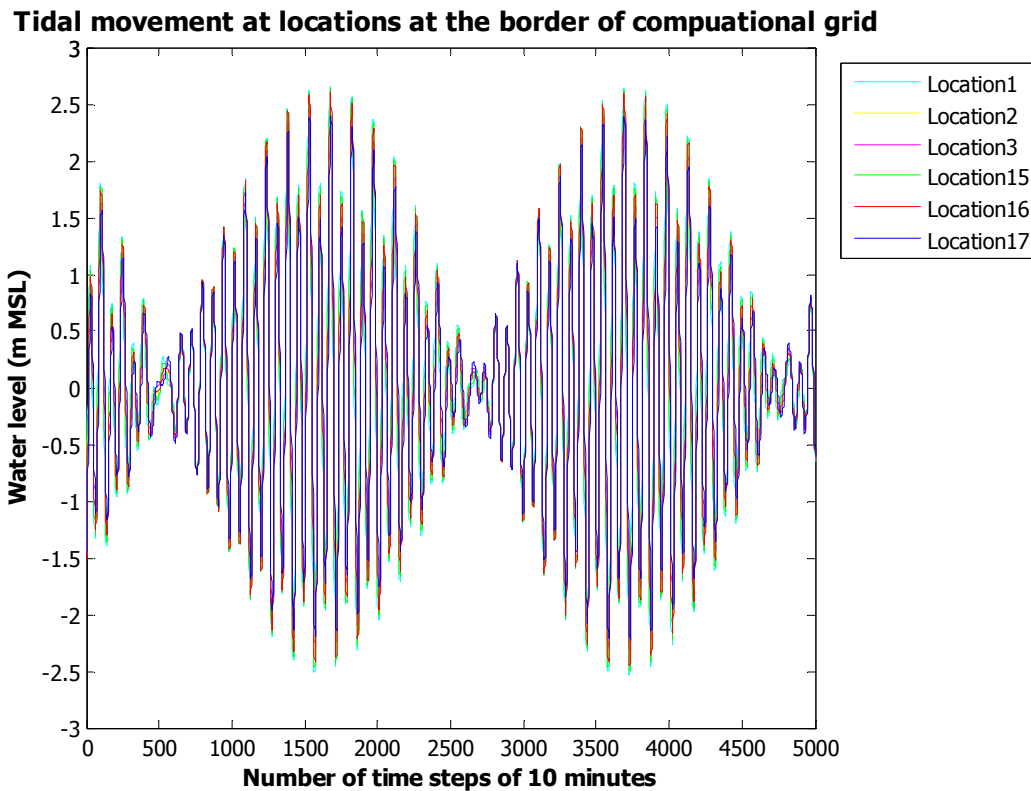
Figure 5-8 Tidal movement at six locations at the boundary of the computational domain

At the boundary of the computational grid, one open boundary is created so only one Fourier series can be assigned. As shown in the figure above, the water level varies along the boundary of the computational grid. Location number 1 is the most northern location and number 17 the most southern one. The tidal wave deforms along the coast and has the highest amplitude in the north and the smallest amplitude in the south. The phase difference between these two points is small, which can be seen in figure 5-7. This figure shows a more detailed view of the water level in the different locations at the boundary of the computational grid. Because only one of these six tidal waves can be used for the input of the model, the one that is closest to the average of the six tidal waves, has been used. This is the tidal wave in location 2.

The properties of the tidal wave in location number 2 are listed in the following table. The amplitude A and the phase P are given for the four constituents.

M2 A	M2 P	S2 A	S2 P	O1 A	O1 P	K1 A	K1 P
(m)	°	(m)	°	(m)	°	(m)	°
1.082	174.93	1.020	265.37	0.197	100.70	0.321	141.28

Table 5-2 Tidal constituents at location 2, used for input of Waqua model

Detail of water level at boundary compuational grid
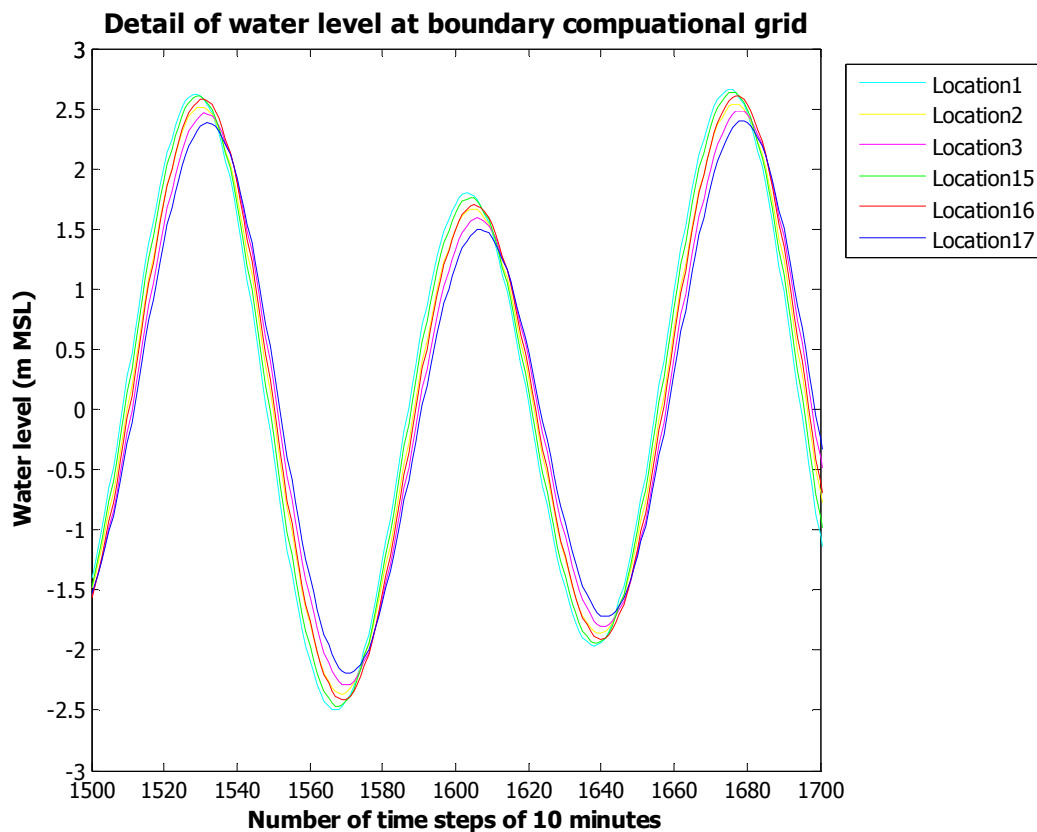
Figure 5-9 Detailed plot of the water level at the boundary of the computational grid

The other eleven locations from Figure 5-9 that lie inside the computation grid have been used to investigate the results of the calculation. This will be explained later on.

5.4 Results

When the calculation is finished all the data are stored in the SDS file. To obtain this data and to be able to use it, post-processing is necessary. During the post-processing part, all data stored in the SDS file are converted into a well-ordered data set that can be used for the creation of graphs and prints. During the post-processing, time series with the water level variation in specific locations are generated and overviews of the water level over the total computational domain at certain moments.

5.4.1 Accuracy of the results

Before the result of the calculation can be used as input for the EFD.lab model, the accuracy must be known. To investigate the accuracy of the results, the water level at several locations has been compared with the water level in those locations. In section 5.3 the initiation of the model by means of a tidal wave has been explained. The tidal wave is composed with the four main constituents. At 17 locations, the amplitude and phase of these four constituents are known. Six of the seventeen locations lie at the boundary of the model and have been used for the initiation. The other eleven locations can be used to investigate the accuracy of the water level prediction with the Waqua model.

In the Waqua input files, the grid points that correspond with the locations where the tidal wave is known, have been enumerated and for all these point, well ordered files, which contains the time and the water level, can be subtracted from the SDS file. The water level in these grid points have been compared with the tidal composition in these locations. How the tidal wave is composed is explained in section 5.3.

The following figure shows the Waqua results in the points P116 and P117 (see Appendix IV. for the Waqua input file) These point correspond to the tidal input locations number 4 and 5 from Figure 5-6.
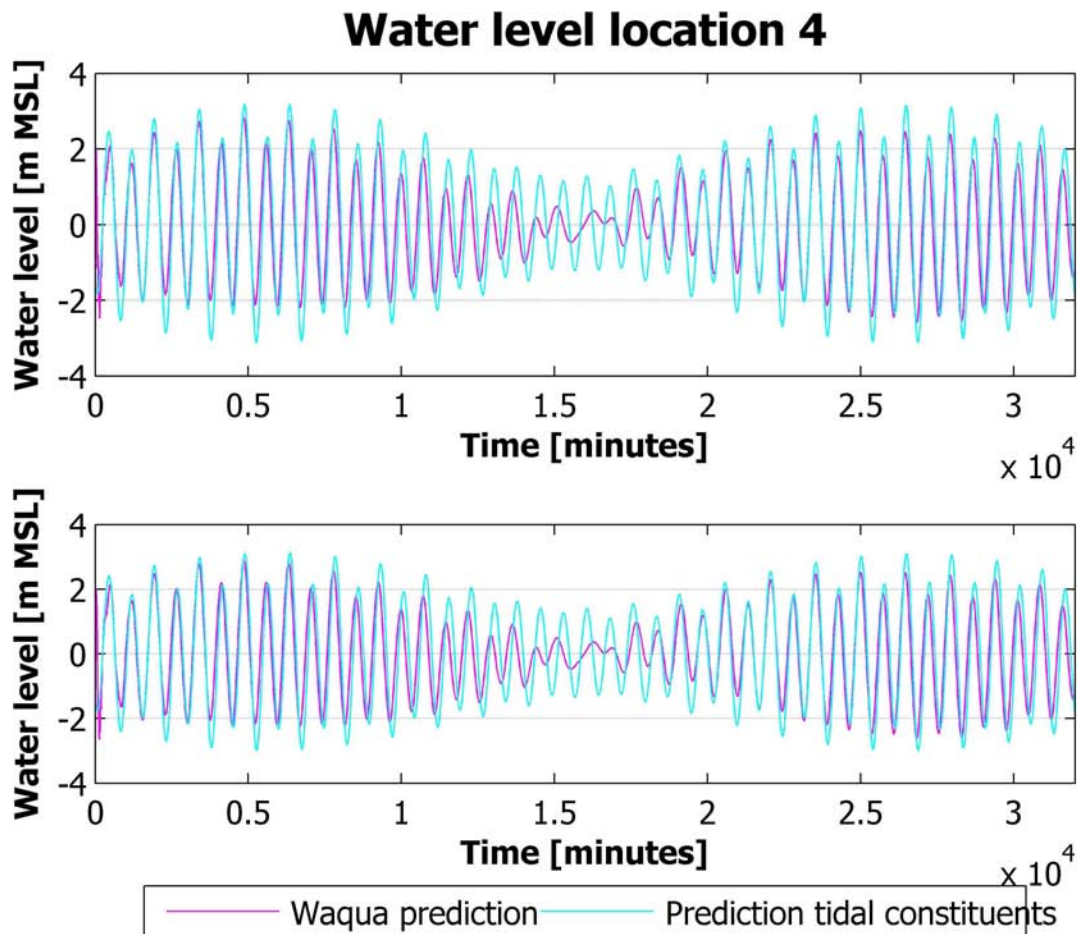
Figure 5-10 Water level variation at location number 4 and 5, Manning factor 0.026 m$^{-1/3}$

The pink line in Figure 5-10 shows the with the Waqua model calculated water level and the blue line the composed water level. The figure shows the differences between these two water level variations. During neap tide, the water level variation composed with the tidal components is larger then the water level variation calculated with the Waqua model. During spring tide, the water level variation of the composed tidal wave is larger as well but the differences are significantly smaller.

To create the input file for the Waqua model, several parameters had to be estimated. Because the amplitude of prediction with the Waqua model is smaller then the amplitude of the tidal wave composed with the components it is tried to let these two water level

variations correspond by adapting some parameters in the input file. The predicted water level is too low and therefore the Manning parameter has been lowered. In the first calculation, the factor for the Manning bottom friction was estimated on 0.026 m$^{-1/3}$. (See Appendix IV. By lowering the Manning factor to 0.024 m$^{-1/3}$, a smoother bottom is created so the water will experience less friction.

The following figure shows the results of the calculation with a Manning factor of 0.024 m$^{-1/3}$.
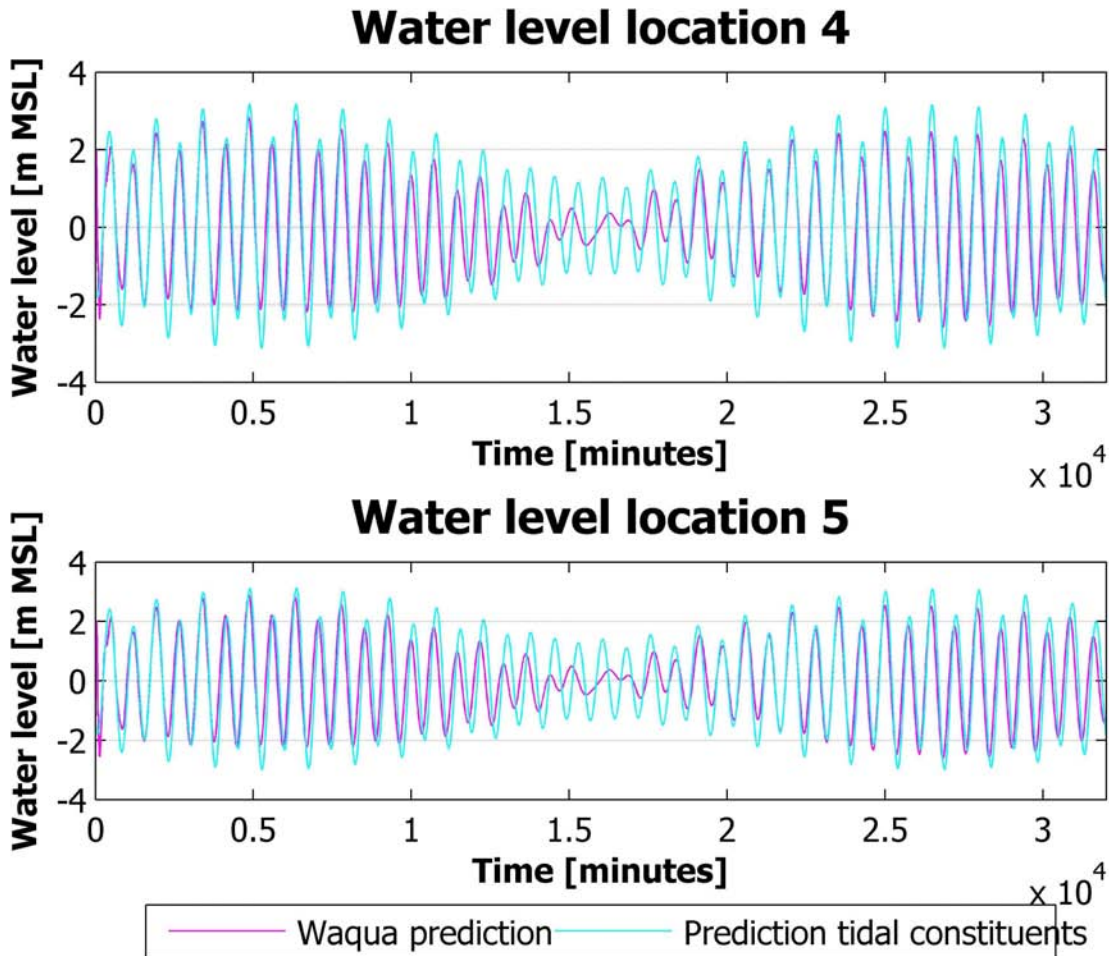
Figure 5-11 Water level variation at location number 4 and 5, Manning factor 0.024 m$^{-1/3}$

In the figure, the pink line is again the water level predicted with the Waqua model and the blue line the result of the composition of the tidal constituents. The two water level variations in Figure 5-11 correspond better than the water level variations in Figure 5-10. Because the water level variation in the composed tidal wave is still larger than the water level variation calculated with the Waqua model, the Manning factor has been lowered to 0.022 m$^{-1/3}$ to investigate whether the water level variations correspond better.

Figure 5-12 shows the results of this calculation. Again, the pink line is the Waqua prediction and the blue line the tidal wave composed with the constituents. When the results of the two calculations are compared, almost no differences can be observed.

Water level location 4

Water level location 5
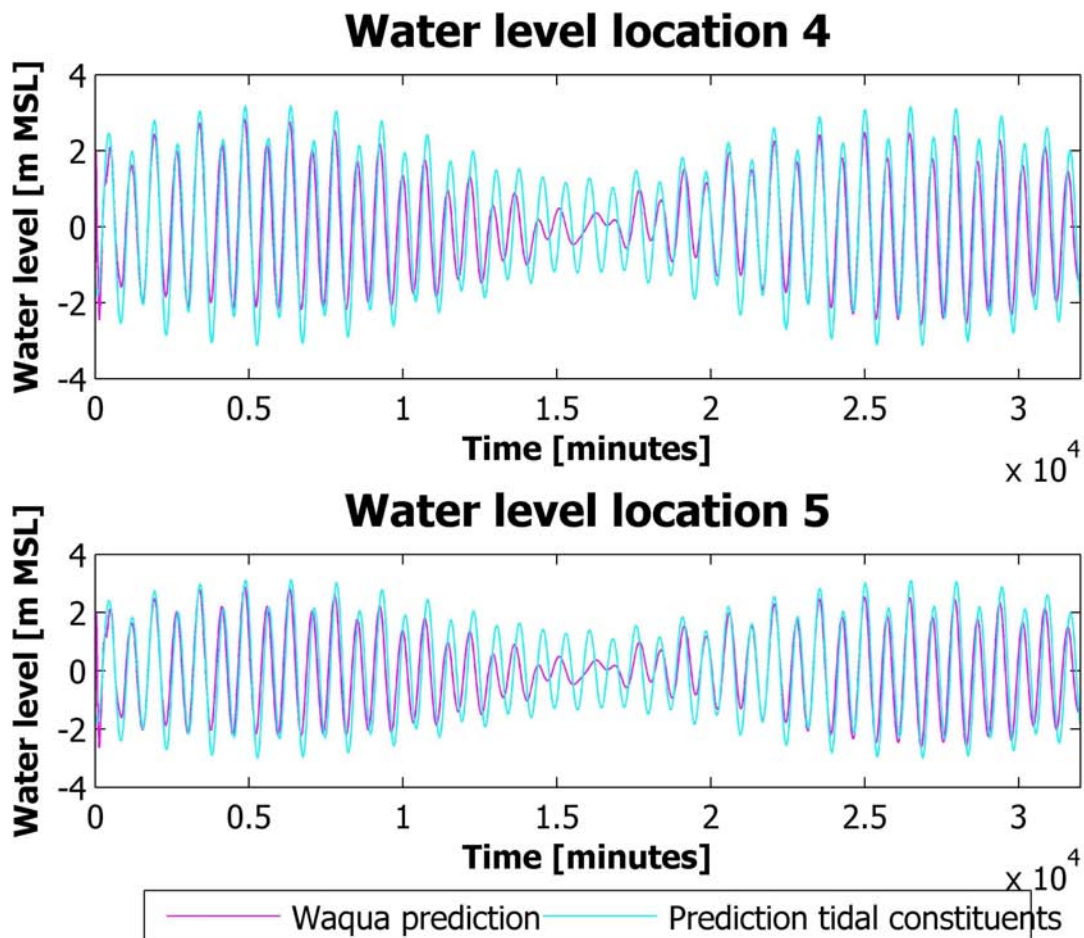
Figure 5-12 Water level variation at location number 4 and 5, Manning factor 0.022 m$^{-1/3}$

The two water level variations still not correspond completely. Especially during neap tide, the water level variation predicted with the tidal constituents is larger than the calculated water level variation with Waqua. During neap tide the influences of the shallow water constituents appear to have more influence. During spring tide the flow velocities through the gaps in the dam are larger then during neap tide and these maximum flow velocities are important for the further research. The water level variation during spring tide corresponds reasonably. The differences between the two water level variations are larger in location 4 than they are in location 5.

5.4.2   Water level over total basin

The water level in the total computation basin can be plotted at a certain moment. The following figure shows the water level in the basin at two moments during the calculation. The top frame is the water level in the computational area when t=1320 and the lower frame is the water level in the computational area when t=1980. The rectangular part of the figure is the foreshore and the estuary with the two branches is located at the right side of the figure.

The water level in the foreshore in the top frame varies between -1.4 m MSL and -1.2 m MSL. The water level inside the basin, the water level is significant higher. At the lower frame, the

water level at the foreshore side varies between 0.5 m MSL and 1.5 m MSL and the water level inside the basin is significant lower. this implies that the water level variation inside the basin lacks behind at the water level at the foreshore. This has also been seen during the calculations of the basin side water level with the storage area approach in Chapter 4.
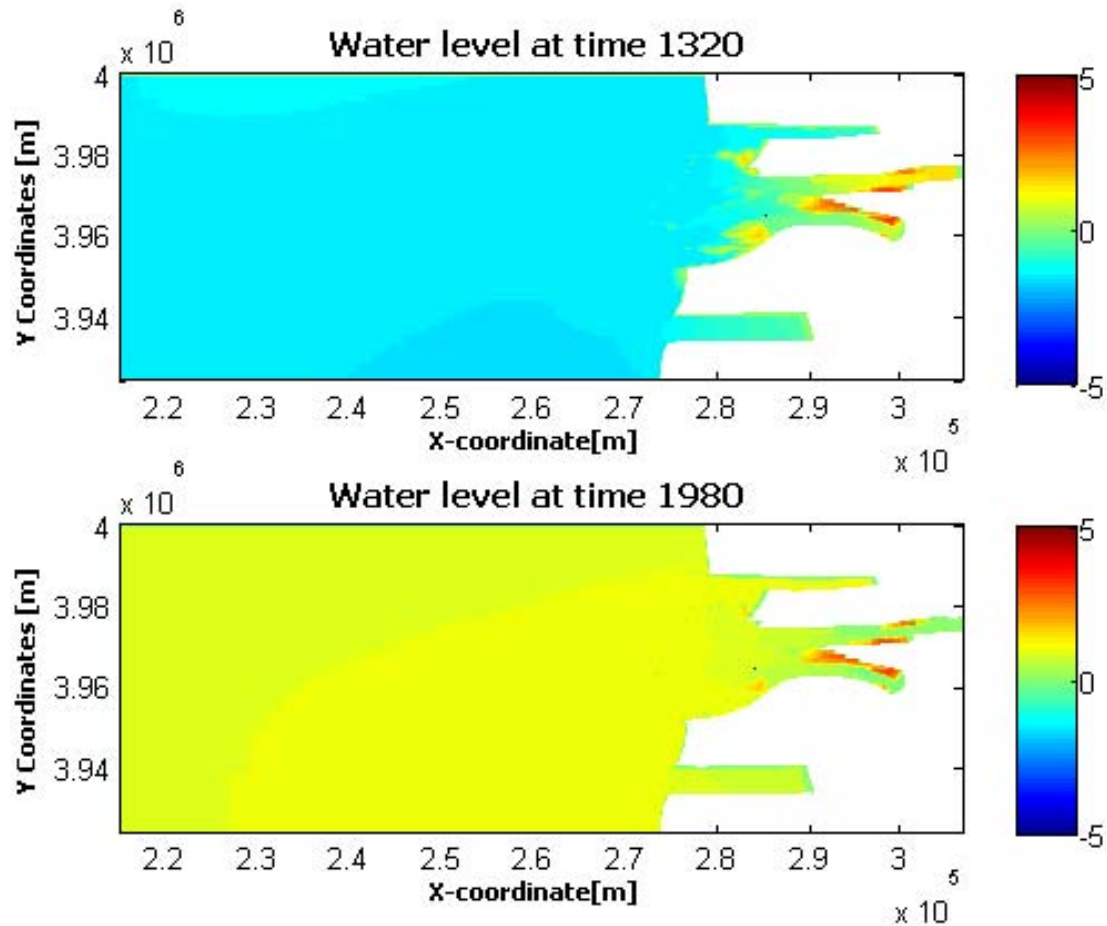
Figure 5-13 Water level variation over the total computational area

5.4.3 *Water level variation in the closure gap*

Because the EFD.lab model cannot calculate a flow with a free surface, the water level course in the closure gap must be enforced. Waqua calculates the water level in every grid cell and thus the water level course through the closure gap has been calculated during the calculation. In the centre line of the closure gap 10 point have been defined in the input file. By plotting the water level in these ten points at the same time with the location of the points, the water level course in the closure gap can be visualized.

The following figure shows the water level course through closure Gap 1 for three time steps. At the horizontal axis, the coordinate in the X-direction is given and the vertical axis gives the water level. The left hand side is the seaside and the right hand side is the basin side.
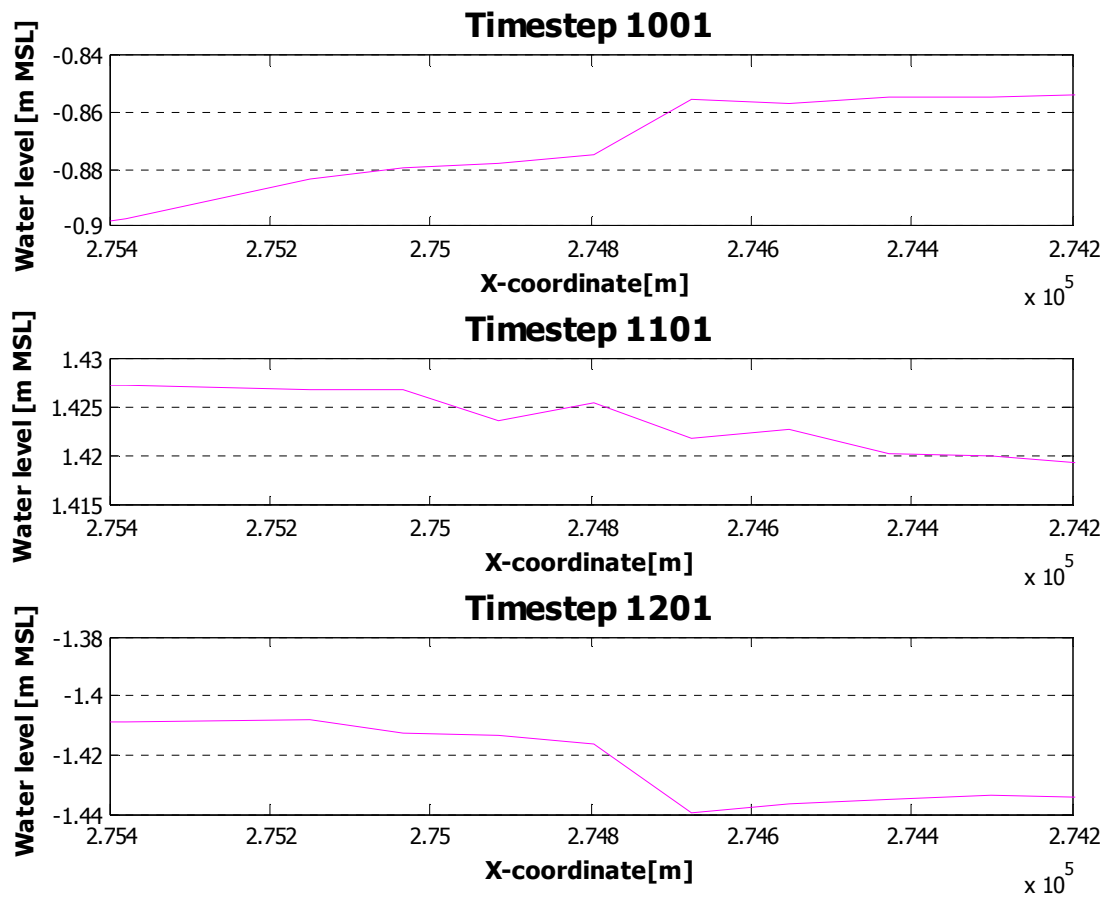
Figure 5-14 Water level course in closure Gap 1 at different times

In Figure 5-14 it can be seen that the water level varies the most around x=2.748 *10^{5}m. This is the location of the bottom protection and the sill. The flow will accelerate at this location and the water level will drop.

For every arbitrarily timestep during the calculation, a graph can be subtracted from the results. So far, no steep water level courses in Gap 1 have been observed. By adapting parameters in the input file, the water level prediction over the total computational domain will change and the water level course in closure Gap 1 as well.

5.4.4 Flow velocity in the closure gap

In every grid point, the flow velocity has been calculated. The flow velocity has a component in the x-direction and a component in the y-direction. The colour bar at right hand side gives the water level inside the basin. the blue arrows give the flow direction in the computational domain.
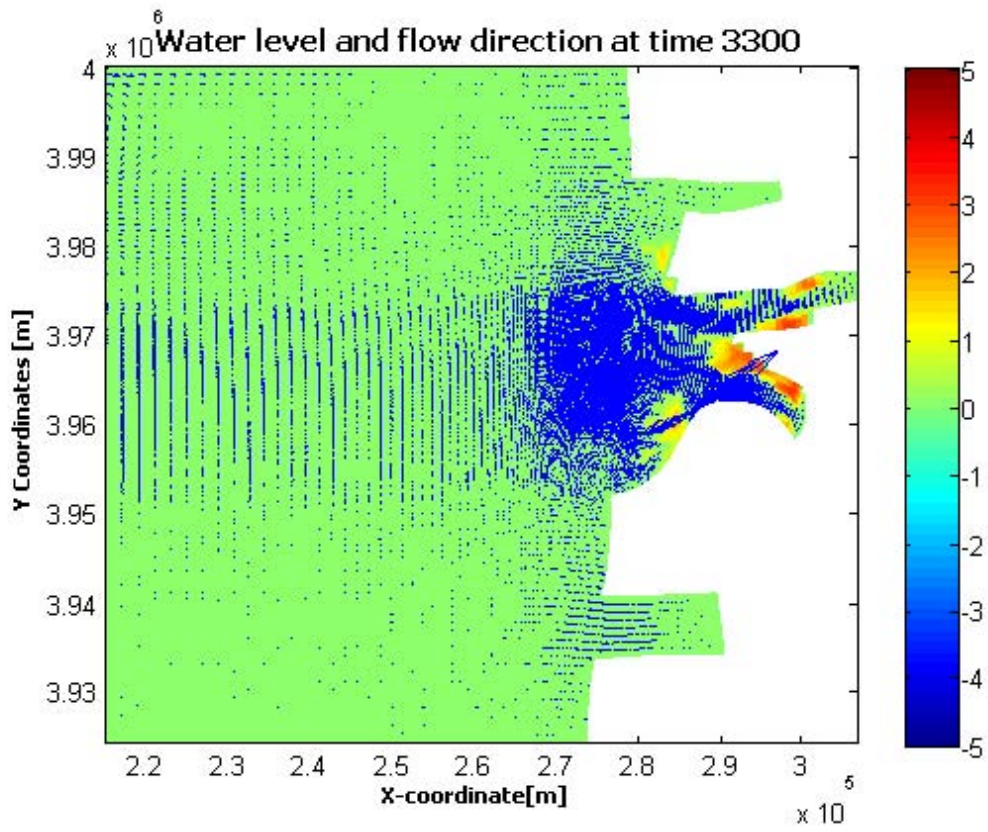
Figure 5-15 Water level and flow velocity direction

6   The EFD model

6.1   Introduction

EFD.lab is a three dimensional fluid flow and heat transfer analysis software in which all simulation steps are combined. The EFD.lab model has been developed by the company NIKA in 1999, was first supplied as an addition to a Solid Work package, and it was called Flow Works. From 2001 on, EFD.lab has been supplied apart from the Solid Work package. The model has been created in a Solid Work surrounding and a special EFD.lab plug-in governs the calculation part. In Solid Work, a model is an assembly and contains several parts. Each part contains one piece of the model, for example a dam or a bottom geometry, and added together in one assembly, they form the system for the calculation. EFD.lab is not developed for the calculation of a free surface flow. Free surface flow calculations can however be executed by introducing a pressure ceiling that resembles the water level. This pressure ceiling is a separate part in the assembly. Due to the calculation limitations of EFD.lab the maximum dimensions of a model are 1X1X1 km. Because the area of interest for the Saemangeum case exceeds this area, the dimensions of the model have been scaled. EFD.lab is expensive in computer resources and one calculation will take about 24 hours. This chapter elaborates on the underlying mathematics, the creation of a model and the accompanying boundary conditions. The results of the calculations executed with the EFD.lab model will be discussed as well. Several calculations have been executed, the first calculations were necessary to achieve the right water level. More calculations have been executed to investigate the influence of scaling the gravitational acceleration on the results of the calculations. The influence of changing the turbulent parameters in the boundaries of the model on the calculations results has been investigated as well. Finally, the influence of a large wall friction at the bottom geometry has been investigated.

6.2   Underlying mathematics

To calculate the properties of a fluid flow, EFD.lab solves the Navier-Stokes equations and the energy equation, which are suitable for laminar and turbulent flows. Most of the flows encountered in engineering practice are turbulent flows so the EFD.lab is mainly developed to calculate and study turbulent flows. To deal with turbulent flows, the Reynolds average Navier-Stokes equations are used. To close the system of equations EFD.lab uses transport equations for the turbulent kinetic energy k and the turbulent dissipation rate ε; this is the so-called k-ε model. The k-ε model will be discussed in more detail in Appendix II. Besides the k-ε model, EFD.lab uses a laminar or turbulent boundary layer model to describe the fluid flows in the surrounding of the walls.

EFD.lab uses the following notation for the conservation laws of mass and momentum in a Cartesian coordinate system:

$$\frac{\partial \rho}{\partial t} + \frac{\partial}{\partial x_k}(\rho u_k) = 0 \qquad\qquad 6.1$$

$$\frac{\partial \rho u_i}{\partial t} + \frac{\partial}{\partial x_k}(\rho u_i u_k - \tau_{ik}) + \frac{\partial P}{\partial x_i} = S_i \qquad\qquad 6.2$$

where:

u = fluid velocity (m/s)
ρ = fluid density (kg/m^3)
p = pressure (Pa)
S_i = mass distributed external force per unit mass
E = total energy per unit mass
Q_H = heat source per unit volume
τ_{ik} = viscous shear stress tensor
q_i = diffusive heat flux
i,j,k = subscripts to denote direction of coordinate axis

The Reynolds stresses in the EFD.lab model for Newtonian fluids are defined as follows:

$$\tau_{ij} = \mu\left(\frac{\partial u_i}{\partial x_j} + \frac{\partial u_j}{\partial x_i} - \frac{2}{3}\frac{\partial u_l}{\partial x_l}\delta_{ij}\right) - \frac{2}{3}\rho k \delta_{ij} \qquad\qquad 6.3$$

Where:

μ = $\mu_l + \mu_t$
δ_{ij} = Kronecker delta function (when i=j it is unity and zero otherwise)
μ_l = dynamic viscosity (kg/ms)
μ_t = turbulent eddy viscosity (kg/ms) (=0 for laminar flows)
k = turbulent kinetic energy (m^2/s^2) (=0 for laminar flows)

The dynamic viscosity is a fluid property and has a value depending on the temperature of the fluid. The turbulent eddy viscosity is zero for a pure laminar flow and is defined using the two turbulence properties in the k-ε model, namely the turbulent kinetic energy k and the turbulent dissipation ε. The eddy viscosity is not a fluid property but a flow property and is defined as follows:

$$\mu_t = \frac{C_\mu \rho k^2}{\varepsilon} \qquad\qquad 6.4$$

The two transport equations for the turbulence parameters in EFD.lab are defined as follows:

$$\frac{\partial \rho k}{\partial t} + \frac{\partial}{\partial x_k}(\rho u_k k) = \frac{\partial}{\partial x_k}\left(\left(\mu_l + \frac{\mu_t}{\sigma_k}\right)\frac{\partial k}{\partial x_k}\right) + S_k \qquad\qquad 6.5$$

$$\frac{\partial \rho \varepsilon}{\partial t} + \frac{\partial}{\partial x_k}(\rho u_k \varepsilon) = \frac{\partial}{\partial x_k}\left(\left(\mu_l + \frac{\mu_t}{\sigma_\varepsilon}\right)\frac{\partial \varepsilon}{\partial x_k}\right) + S_\varepsilon \qquad\qquad 6.6$$

In which S_k and S_ε are source terms for respectively the turbulent kinetic energy and the turbulent dissipation and are defined as follows:

$$S_k = \tau_{ij}^R \frac{\partial u_i}{\partial x_j} - \rho\varepsilon + \mu_t P_B \qquad\qquad 6.7$$

$$S_\varepsilon = C_{\varepsilon1} \frac{\varepsilon}{k}\left(f_1 \tau_{ij}^R \frac{\partial u_i}{\partial x_j} + \mu_t C_B P_B \right) - C_{\varepsilon2} f_2 \frac{\rho\varepsilon^2}{k} \qquad\qquad 6.8$$

where P_B represents the turbulent generation due to buoyancy forces and is give by:

$$P_B = -\frac{g_i}{\sigma_B}\frac{1}{\rho}\frac{\partial\rho}{\partial x_i} \qquad\qquad 6.9$$

and where:

g_i = component of gravitational acceleration in direction xi
σ_B = constant with a value 0.9
C_B = constant (1 when $P_B>0$ and 0 when $P_B<0$)
f_1 = constant with value 1.000125
f_2 = constant with value 1
$C_{\varepsilon1}$ = empirical defined constant with value 1.44
$C_{\varepsilon2}$ = empirical defined constant with value 1.92
C_μ = empirical defined constant with value 0.009
σ_ε = empirical defined constant with value 1.3
σ_k = empirical defined constant with value 1

The k-ε model uses the above equations to deal with the closure problem. The turbulent kinetic energy and the turbulent dissipation are calculated as an output parameter during an EFD.lab calculation. Other turbulent parameters are formulated in the following way:

Turbulent length:

$$L_t = \frac{C_\mu^{0.75} k^{3/2}}{\varepsilon} \qquad\qquad 6.10$$

With: C_μ=0.09 (-) and L_L (m)

Turbulence intensity:

$$I_t = 100\% \frac{\sqrt{2/3\,k}}{V} \qquad\qquad 6.11$$

With V= time average fluid velocity (m/s) and I (%)

Turbulent kinetic energy:

$$k = \frac{1}{2}\sum_{i=1}^{3} u_i' u_i' \qquad\qquad 6.12$$

With u' fluctuating velocity and k (m²/s²)

6.3   Creation of a model

The EFD.lab model uses Solid Works as a graphic tool for the compilation of a model. A model is build up out of several parts. Each part is created separately, can be adapted apart from the rest and contains a part of the whole model, for example a dam or a sill. When the origins of all different parts correspond, adding all parts together will produce an assembly. The assembly forms the final model for the calculation. Before starting the calculation, the boundary conditions and calculation goals have to be assigned. Because EFD.lab can only execute a calculation when a pressure difference or a discharge is given for an object with a closed geometry (for example a tube, box), the assembly must form a closed box. EFD.lab is not capable of calculating a flow with a free surface. For the calculation of a free surface flow, a fixed ceiling that resembles the free water level is required. After the first calculation, this pressure ceiling must be adapted to the results and the calculation needs to be redone. After several adaptations, the artificial ceiling will lie at the right level and the final results are obtained. The process of adapting the water level will be explained more extensive in section 6.5. The following figure shows several parts of the assembly including the water level part.
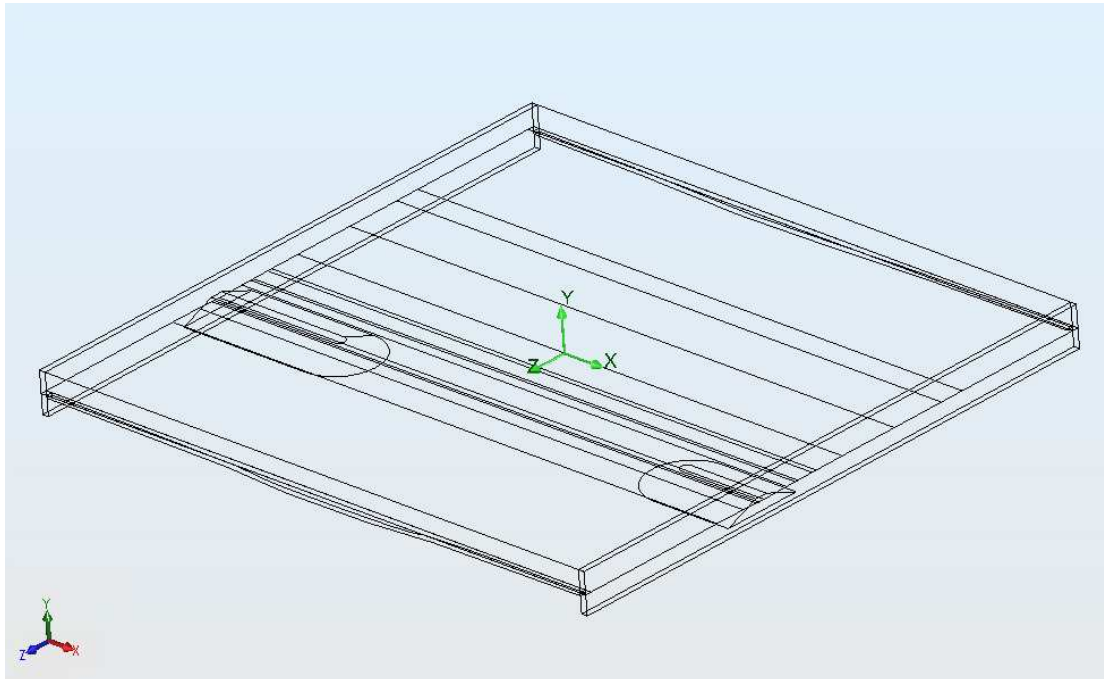
Figure 6-1 Different parts of the model with on top the water level ceiling part

Due to calculation limitations, EFD.lab is only capable of calculating an area of 1x1x1 km. Because the area of interest in the Saemangeum dam case exceeds this 1 by 1 km, a scaled model is necessary. The data used for the creation of the bottom part, originates from measurements executed in the Saemangeum estuary. The data file is available in a *.xyz file and cannot be used for the bottom geometry directly. For the creation of a bottom geometry part parallel lines with data points are required. The data points of the measurements do not lie on parallel lines but are random points in the surrounding of the closure gap. The random located data points have been used to generate fifty parallel lines perpendicular to the closure gap. These lines have been scaled with a factor 2.5, both in the horizontal and vertical direction. The fifty parallel lines form a plane that follows the bottom geometry. To create a

solid part, the created plane has been transformed into a part of a box. Figure 6-2 shows the solid bottom part with the fifty parallel lines.
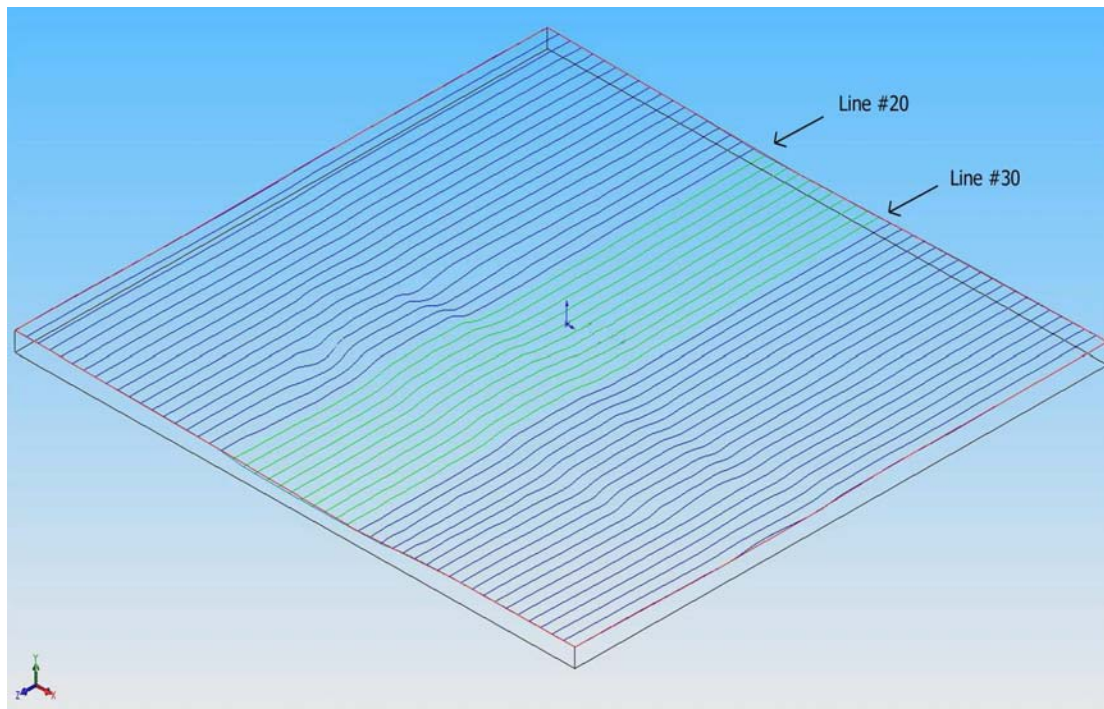
Figure 6-2 Bottom geometry build up out of fifty parallel lines

The dimension of the model in the flow direction, the models z-direction, is 944m, 317m in front of the closure dam and 627m behind the closure dam. The width of the model in the x-direction is 980 m and the gap. The gap between the two dam heads is 496m and the depth varies between 16m and 4m.

Because the horizontal dimensions are considerably larger than the vertical dimensions, the cross section profile cannot be distinguished very easily. The cross section of the model in the flow direction at the centre line of the closure gap contains two big scour holes, at both sides of the dam, a bottom protection over a length of one hundred meters and on top of this bottom protection a small sill over which the final closure proceeded. Figure 6-3 shows the middle 10 parallel lines (number 20-30) of the fifty lines that form the bottom geometry. On top of the bottom geometry part, a dam part is placed. This dike extends until a height of 8m so no water will flow over the dam and all the water has to flow through the closure gap.
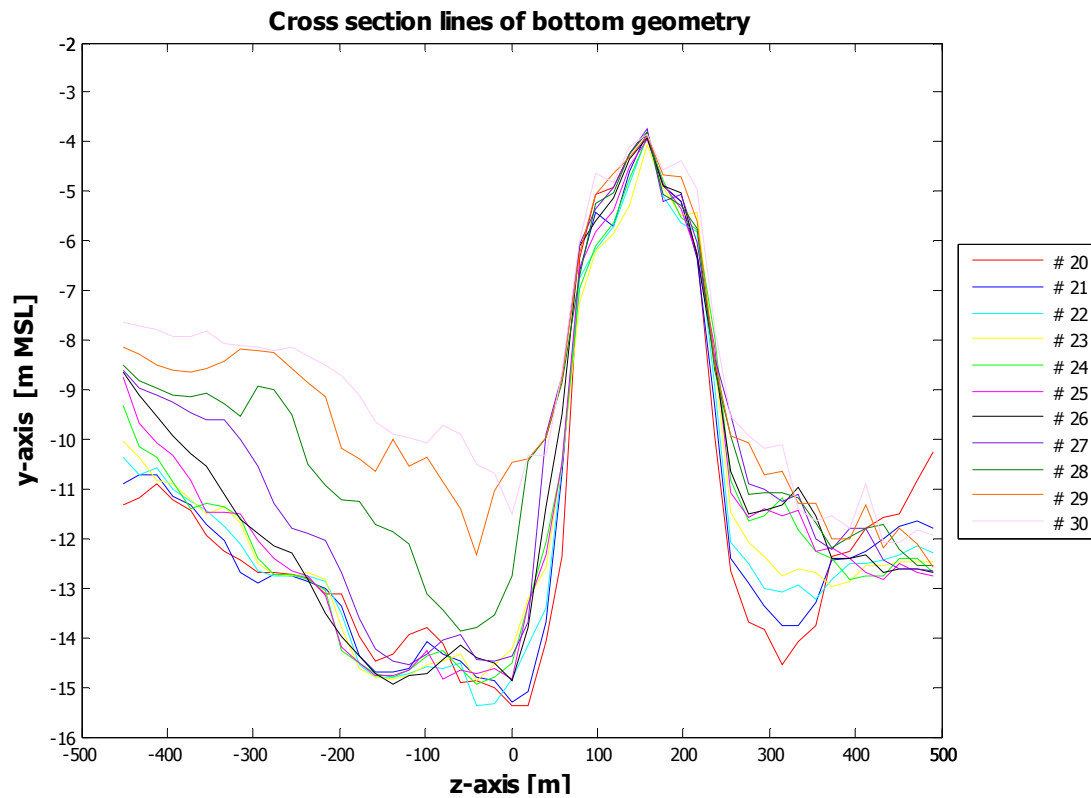
Figure 6-3 Ten middle lines of bottom profile of the closure gap

To create a closed box for the calculation, two walls parallel to the flow direction close off the box at both sides, these are the orange and yellow parts in Figure 6-4. To finalise the model, an inflow and an outflow part are necessary. Through these two parts, the water flows in and out of the model and boundary conditions have to be assigned on these parts. The red part is the inflow part and the blue part is the outflow part. The following figure shows the whole assembly.
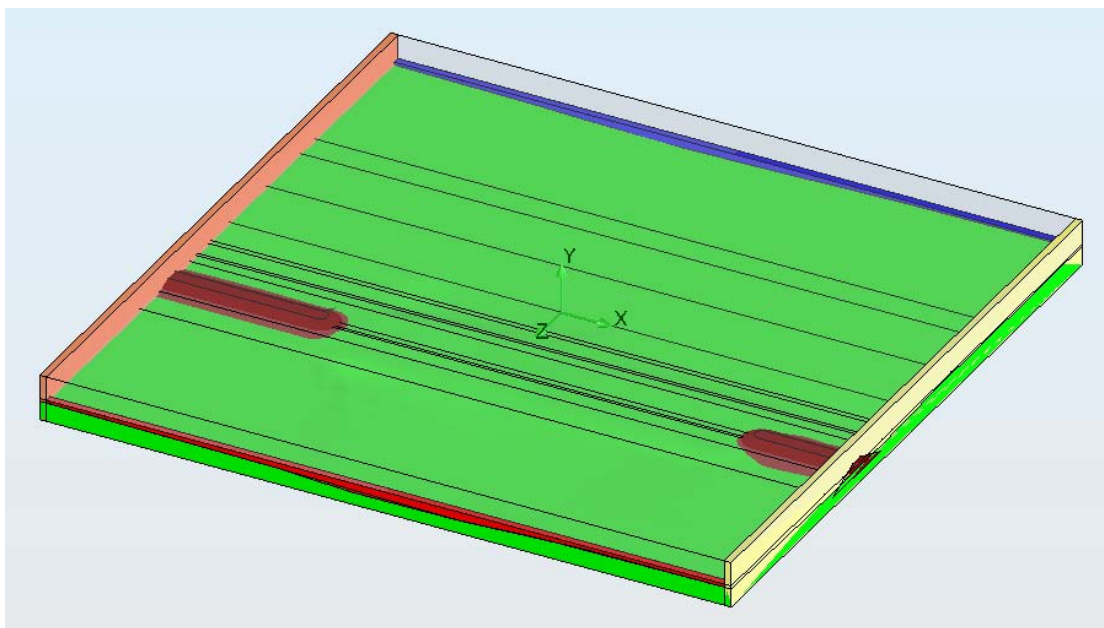
Figure 6-4 Model assembly with all the different parts

6.4 Boundary conditions

6.4.1 Computational domain

When the model has been created, EFD.lab generates a computational domain by itself. Based on the largest flow cross section in the three directions, a rectangle box is determined. This is the computation domain and within this computational domain the computational mesh will be created. It is possible to use the automatic generation of the computation domain as a check for the model geometry. When the geometry contains sharp edges or is not a completely closed box, EFD.lab will encounter problems in perceiving the computational domain. This often results in a computation domain that does not lie inside the model boundaries. When the computational domain is generated according expectations, the geometry of the model is finished.

6.4.2 Computational mesh

Within the computational domain, EFD.lab can generate a mesh automatic or manual. In this case, the number of grid cells has been assigned manually. The height of the computational domain is several times smaller than the length scale of the computational domain and when an automatically generation of the mesh is used the number of grid cells over the height will be limited. This will influence the accuracy of the model results. The number of grid cells in the three model directions is variable. Eventually the number of grid cells over the height is set to 20 and to 200 over the width and length of the computation domain. The choice of the number of grid cells is a deliberation between the accuracy of the outcomes and the necessary calculation time. The total length in the x direction is 980m so the average width of a grid cell in the x-direction is 4.9m. The length in the z-direction of the model is 944m so the average width of a grid cell in this direction is 4.72m. In the vertical direction, the grid cells have an average height of 1.25m.

6.4.3 Pressure

Because free water surface cannot be simulated, a pressure ceiling has to be created. The pressure at the boundaries of the model has to be assigned. The pressure is related to the pressure at the origin of the model. The free water level is located in the origin and the pressure in the origin is the atmospheric pressure. To model a water level that is not located in the origin the pressure at the boundaries has to be adapted. The pressure in the origin in such a case is no longer the atmospheric pressure but the atmospheric pressure plus or minus a pressure difference, depending on the height of the free water level compared to the origin. The pressure at the boundaries can be calculated by using the following formula.

$$p_{boundary} = p_{h=0} + h_{boundary} g \rho \qquad\qquad 6.13$$

In which:

$p_{boundary}$ = the pressure at the boundary when hydrostatic pressure is assumed

$p_{h=0}$ = atmospheric pressure (101325 Pa)

$h_{boundary}$ = water level at boundary (m MSL)

ρ = mass density of the fluid (1000 kg/m^3)

g = gravitational acceleration (9.81 m/s^2)

In the following figure, the pressure difference at the boundary is explained.
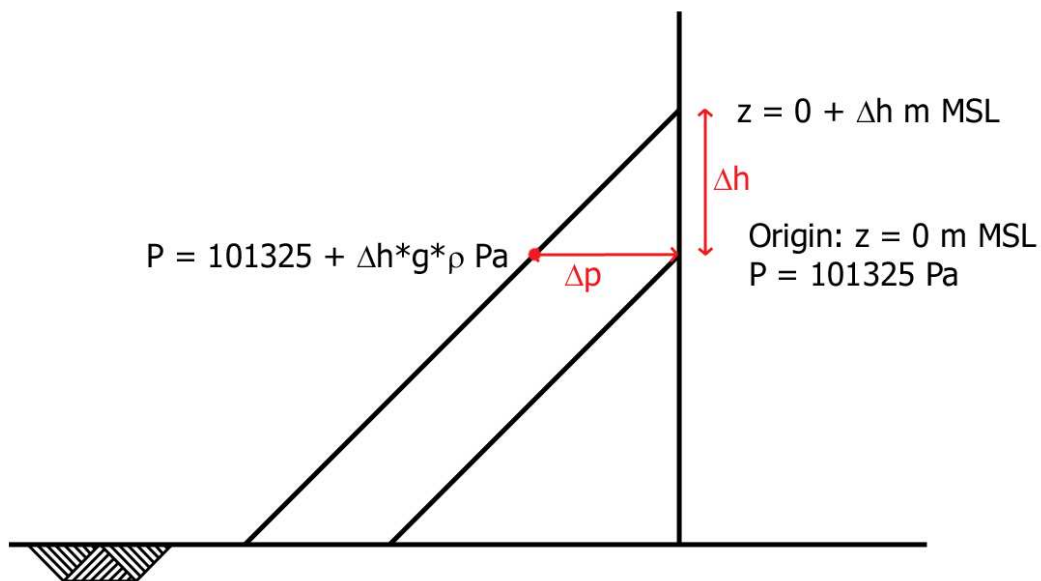
Figure 6-5 Pressure distribution at boundaries of the EFD model

The water level at the boundaries of the model for the first calculation has been extracted from the storage area approach. Two values, one for the inflow water level and one for the outflow water level have been used. The inflow water is 2.29 m MSL before scaling and the outflow water level is 0.80 m MSL. The vertical scale of the model is also 2.5 so the water levels used in the model are 0.916 m MSL at the inflow and 0.32 m MSL at the outflow.

The value for the pressure at the inflow boundary becomes:

$$p_{inflow} = 101325\,Pa + 0.916\,m * 9.81\,m\,/\,s^2 * 1000\,kg\,/\,m^3 = 110310.96\,Pa$$

The value for the pressure at the outflow boundary becomes:

$$p_{outflow} = 101325\,Pa + 0.32\,m * 9.81\,m\,/\,s^2 * 1000\,kg\,/\,m^3 = 104464.20\,Pa$$

The ceiling of the model has been assigned as an ideal wall, which means that there is no friction between the water and the wall

6.4.4   Turbulence parameters

At the inflow and outflow boundaries, turbulence parameters can be assigned. When no value is assigned, the default value will be used. The turbulent kinetic energy k and the turbulent dissipation rate ε can be assigned. To be able to assign a value to these parameters several calculations with the default values have been executed. The influence of assigning a value to these two parameters will be investigated.

Not only at the boundaries a value for the turbulent kinetic energy and the dissipation rate has to be assigned but also in the general settings. The influence of changing these parameters in the general settings will also be investigated.

At the inflow boundaries and in the general settings, a value for the turbulent kinetic energy and a value for the turbulent dissipation rate have to. be assigned. To estimate these values the average flow velocity is required. Because several calculations with the default values have been executed, an average flow velocity can be subtracted from the results of these calculations. With the following formulas an estimation for the values of the turbulent kinetic energy k and the turbulent dissipation ε have been made.

The turbulence intensity is given by:

$$I_u = \sqrt{u_i'^2} \qquad\qquad\qquad 6.14$$

From the literature, a turbulent intensity of 10% has been assumed. [Stormvloedkering Oosterschelde 1980]

So $I_u = \sqrt{u_i'^2} = \dfrac{1}{10} U$ and this leads to $u_i'^2 = \left(\dfrac{1}{10} U\right)^2 = \dfrac{1}{100} U^2$

The turbulent kinetic energy can be expressed as follows:

$$k \approx u'^2 \qquad\qquad\qquad 6.15$$

Combined with the turbulence intensity this leads to the following expression for k

$$k = \frac{1}{100} U^2 \qquad\qquad\qquad 6.16$$

The equation for the turbulent dissipation rate is:

$$\varepsilon = C_\mu \frac{k^2}{\nu_t} \qquad\qquad\qquad 6.17$$

With: $\nu_t = \dfrac{1}{6} \kappa u_* h$ for the turbulent eddy viscosity

When $C_\mu = 0.09$, $u_* = 1/15U$ and $\kappa = 0.4$ expressions for the turbulent kinetic energy and the turbulent dissipation rate have been derived.

With the above formulas, values for the parameters in the general settings have been calculated. In the following table, the default values for the turbulent parameters in the general settings as well as the calculated values are shown.

	U (m/s)	**h (m)**	**k (m^2/s^2)**	**ε (m^2/s^3)**
Default general settings	-	-	1	1
Adapted general settings	10	20	1	0.10

Table 6-1 Turbulent parameters in general settings

From calculations executed with the default values, the average flow velocity at the inflow boundary is 2.5 m/s and the average depth is 10m. The average flow velocity at the outflow boundary is 6.5 m/s and the average depth is 13m. The following table gives an overview of the values of turbulent parameters that have been assigned to the boundaries.

	U (m/s)	**h (m)**	**k (m^2/s^2)**	**ε (m^2/s^3)**
Default boundary settings	-	-	1	1
Adapted boundary settings inflow	2.5	10	0.0625	0.00316
Adapted boundary settings outflow	6.5	13	0.4225	0.04278

Table 6-2 Turbulence parameters in the boundary conditions

6.4.5 Goals

To speed up the calculation, goals have been implemented. These goals indicate to which parameter the solution must converge. Two goals have been assigned to the inflow face, the average static pressure and the average total pressure. At the outflow face, a discharge goal have been assigned. When all the boundary conditions and goals have been assigned, the calculation can start. First, the mesh will be generated and subsequently the actual calculation continues. After 300 to 500 iterations, goals have been reached and the calculation stopped. The total calculation time varied between 24 to 32 hours, depending on the calculation.

6.5 Adapting the water level

EFD.lab model is not capable of executing calculation with a free water surface. The water level course, assigned in the water level part, needs to be adapted to the results of the calculation after every calculation until the results of the calculation correspond to the imposed water level in the water level part.

From the results of the first calculation, the pressure at a horizontal line in the model has been exported to a spreadsheet. The pressure can be recalculated to a pressure height and together with the height of the horizontal line, the water level in that point has been calculated. In this way the water level course for the total model can be composed. This has been done by using the following formula:

$$h = z + \frac{p}{\rho g}$$

6.18

where:

h = water level (m MSL)

z = place height of the line at which the pressure is calculated (m MSL)

p = pressure at line z (Pa)

ρ = mass density of the fluid (1000 kg/m^3)

g = 9.81 m/s^2

The calculated water level has been compared with the imposed water level. When the imposed water level has been adapted to the calculated water level course, the same calculation has been executed. After three calculations, the imposed water level corresponded relative well with the calculated water level. In Figure 6-6, the imposed water level and the calculated water level for four calculations are showed. The C stands for calculated water level and the E for imposed water level, the B plus the number stands for the number of the calculation.
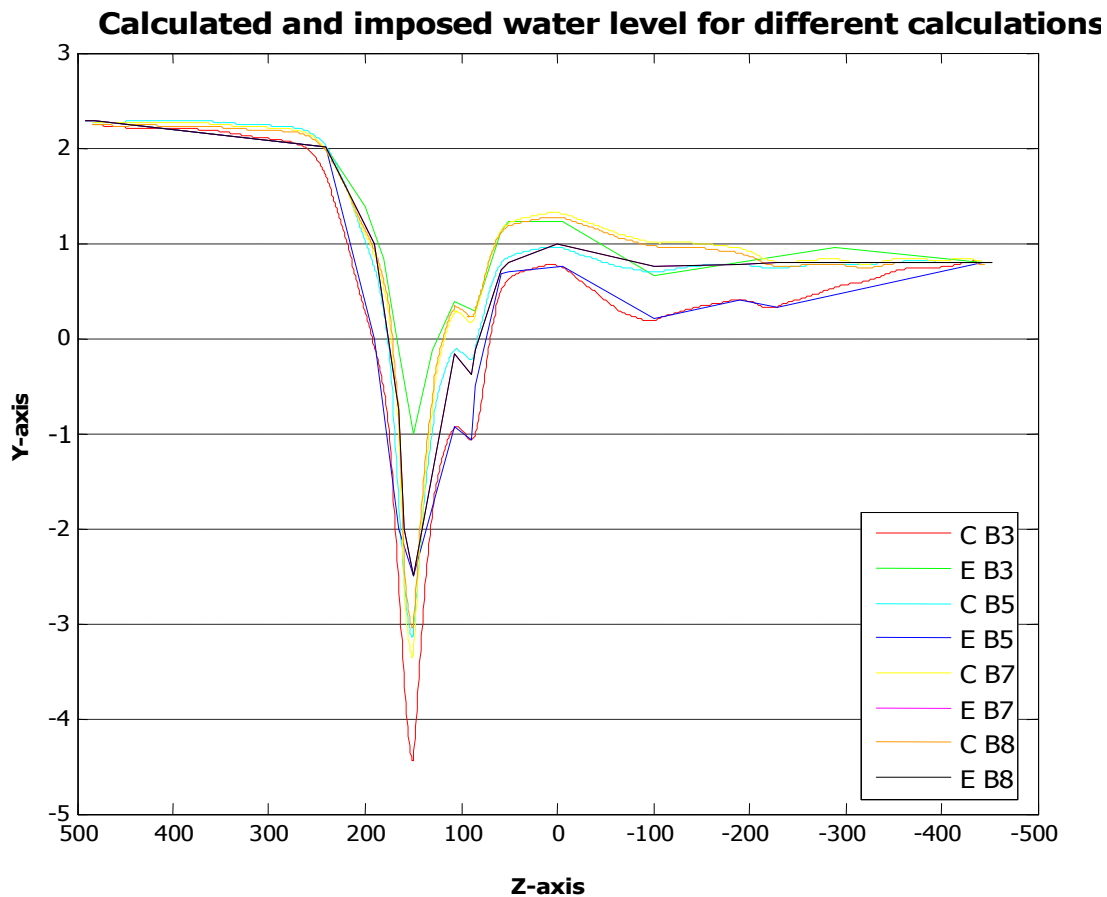
Figure 6-6 Calculated and imposed water level for four calculations

The figure shows the water level course over the cross section. When the fluid flow reaches the bottom protection (z=250m), the flow area becomes smaller and the flow will accelerate. This can be seen in the figure. The water level fall that starts at z=250 m and ends at z=155 m. This is the location of the sill on top of the bottom protection. When the flow has passed the sill, the flow will decelerates, looses energy and the water level will rise again. At some distance from the closure gap, the water level becomes horizontal again.

The water level above the sill in the final calculation is located at a level of -2.3 m MSL. The top of the sill is located at a level of -4 m MSL so the water depth above the sill is 1.7 m. The value for the gravitational acceleration g is 24.525 m/s^2 because the model is a scaled model and the water depth is a scaled water depth. The maximum mean flow velocity above the sill is 11 m/s so the Froude number is:

$$Fr = \frac{V}{\sqrt{gh}} = \frac{11}{\sqrt{24.525 * 1.7}} = 1.7 \qquad\qquad 6.19$$

The Froude number is larger than 1 so the flow above the sill is supercritical. This may be the reason why the calculated pressure above the sill is too low. The imposed water level above the sill is higher than the calculated water level above the sill. This can be seen in Figure 6-6 where the calculated water level of 'Basis 8' is 30 cm lower than the imposed water level. When the imposed water level was lowered to the level of the calculated water level, the flow opening above the sill became smaller and the flow velocity became higher. This implied a higher Froude number and a supercritical flow again. In that case the calculated water level was, again lower than the imposed water level. Therefore, the imposed water level of calculation 'Basis 8' has not been adapted anymore.

6.6 Results

As explained in the previous section the water level of the model needs to be adapted several times before the results can be used. Therefore, the results of calculation 'Basis 3' and 'Basis 5' shall not be discussed. These calculations were necessary to adapt the water level and attain calculation 'Basis 8', for which the imposed water level correspond with the calculated water level. The results of the calculation will be discussed in section 0.

To investigate the influence of different parameters on the results of the EFD.lab calculations, different calculations with different boundary conditions have been executed and the results have been compared. The influence of the gravitational acceleration has been investigated. Two calculations have been executed, 'Basis7' and 'Basis8'. The only difference between these two calculations is the value for the gravitational acceleration. These two models will be discussed in section 0. Subsequently, the influence of the value for the turbulent parameters in the boundary conditions and in the general settings on the calculation results has been investigated. Three calculations have been executed, one with the default values for both the boundary conditions and the general settings, one with adapted turbulent parameters in the boundary conditions and one with the turbulent parameters in the general settings changed as well. The differences between the results of these three calculations will be discussed in section 0. In section 6.6.4, the influence of a rough bottom geometry on the calculation results will be discussed. Two calculations have been executed, one without a bottom roughness applied to the bottom geometry and one with a bottom roughness of 2 m.

6.6.1 Results of 'Basis 8'

After several calculations, the water level input corresponds to the calculated water level and the results of the calculations will be investigated. The results of calculation 'Basis 8' will be treated and explained in the section. For all figures, the flow direction is from the bottom to the top.

For the calculation, a scaled model has been used. The gravitational acceleration has been scaled so the results of the calculation do not have to be scaled as well. The scaled water level at the inflow is 0.916 m MSL and the outflow water level is 0.32 m MSL. Because the calculation area of EFD.lab is limited to an area of 1 by 1 km, the walls of the model lie relative close to the gap. In the real situation, the area in front of the dam and behind the

dam is unlimited and not bounded by a wall. In the model, the water can only flow through the inflow part and the outflow part, which both lie parallel to the dam and perpendicular to the flow direction. Through the walls parallel to the flow direction, no water can flow in or out the model. In the real situation, the approaching flow will be wide and water will flow from all sides. In the outflow area, the real situation flow will experience no influence of the walls. The eddies occuring in the results did not occur in the real situation.

At one side of the gap, just before the right dam head, a shallow area is located. This is according the real situation and due to this shallow area, the main flow through the closure gap is concentrated more to the left side of the closure gap.

The results of the calculation give a maximum mean flow velocity of 11 m/s. The maximum velocity occurs above the sill, placed on top of the bottom protection. This maximum mean flow velocity occurs locally and the maximum mean flow velocity above the rest of the sill is lower. Figure 6-7 shows the mean flow velocity distribution through the closure gap at a level of y=-1 m MSL. The figure on the right shows the flow lines through the closure gap. As explained above, the walls influence the flow pattern. At the inflow side of the dam, the lower part of the figure, the flow lines all start parallel to the wall although this may not be the case in the real situation. In the outflow area, due to the wall eddies are formed that have not been observed in the real situation.
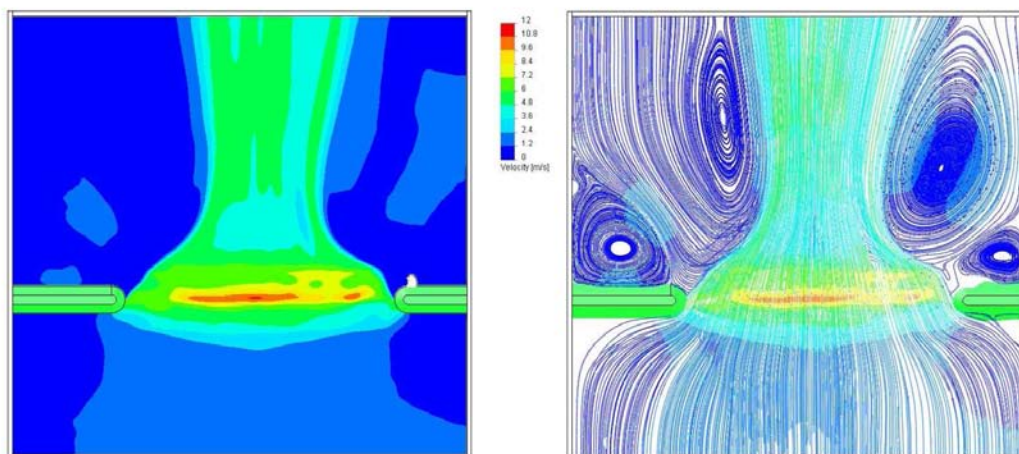
Figure 6-7 Mean flow velocity and flow lines of mean velocity, calculation 'Basis 8'

Due to the deep scour hole, that is located directly behind the bottom protection the flow stays concentrated and does not spread easily. This is according the observed situation. The following figure shows a picture of the real situation. It can be seen that the flow through the closure gap is very concentrated and stays concentrated over a long distance.

Important for the stability of a bottom protection is the velocity at the bottom profile. The following figure shows the mean flow velocity at the bottom. On both sides of the dam, the mean flow velocity is relative low compared to the flow velocity in the centre of the closure gap. The maximum mean flow velocity occurs at the top of the sill and is about 11 m/s.
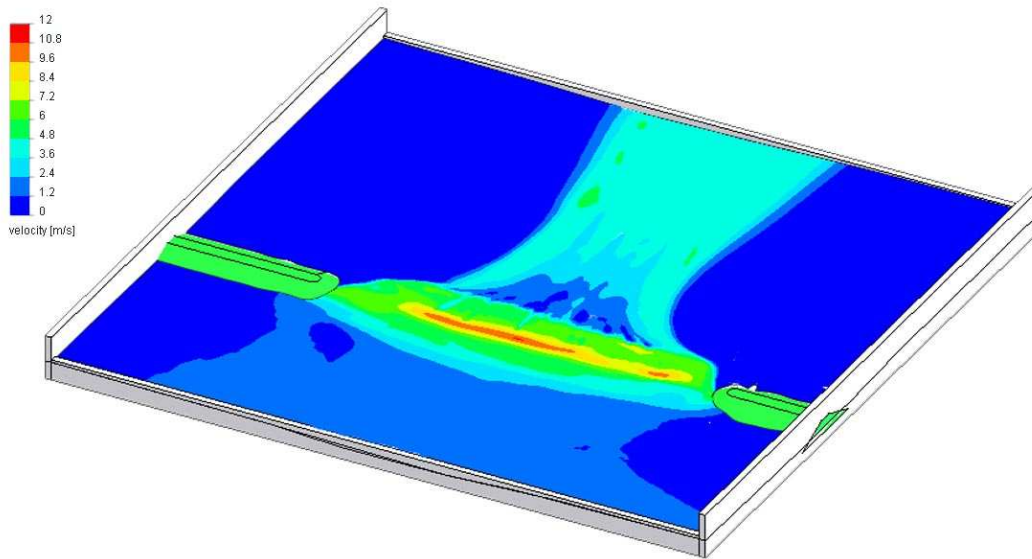
Figure 6-8 Mean flow velocity at bottom, calculation 'Basis 8'

Behind the closure dam, a deep scour hole is located and the velocities at the bottom of this scour hole are low. Because the sudden change of flow profile between the centre of the closure gap and the scour hole, eddies will be formed at the lower side of the flow. The following figure shows a detail of the calculated flow velocity over the dam.
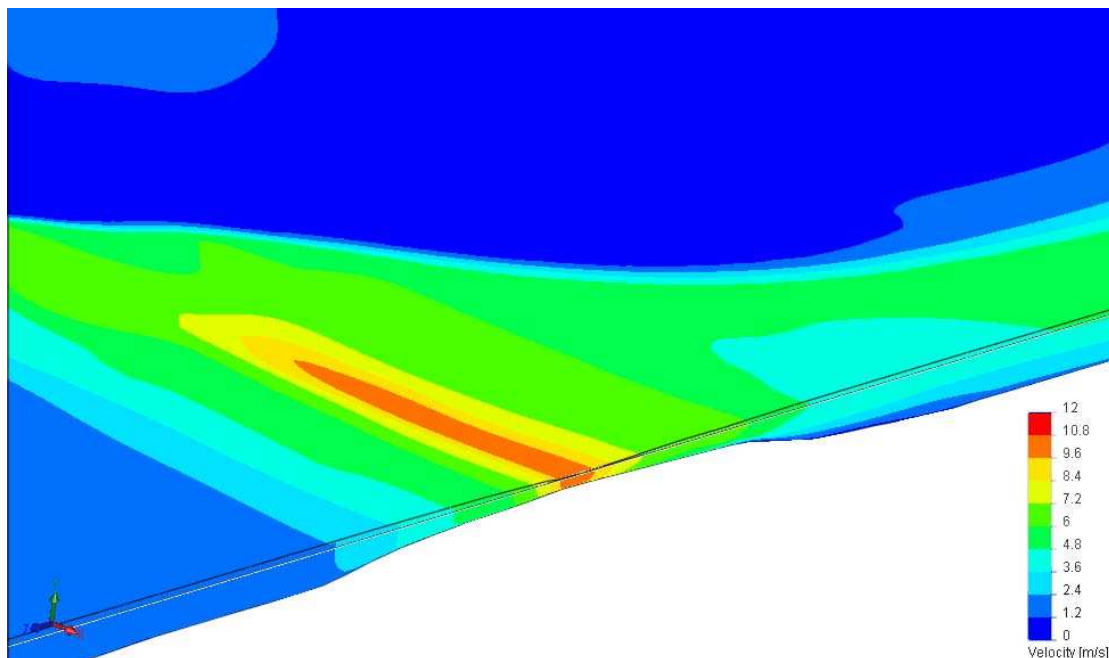
Figure 6-9 Detail of mean flow velocity over sill, calculation 'Basis 8'

It can be seen that the maximum flow velocity occurs at the end of the sill and that the flow velocity at the slope of the scour hole as well as in the scour hole itself are relative low.

By adapting the pressure in the boundary conditions for the inflow and outflow, the pressure distribution over the vertical has been assumed hydrostatic. To check whether this assumption was justified the pressure distribution over the length axis of the model has been investigated. The following figure shows the pressure distribution over the line x=0 m MSL. It can be seen that the assumption of a hydrostatic pressure distribution was justified.
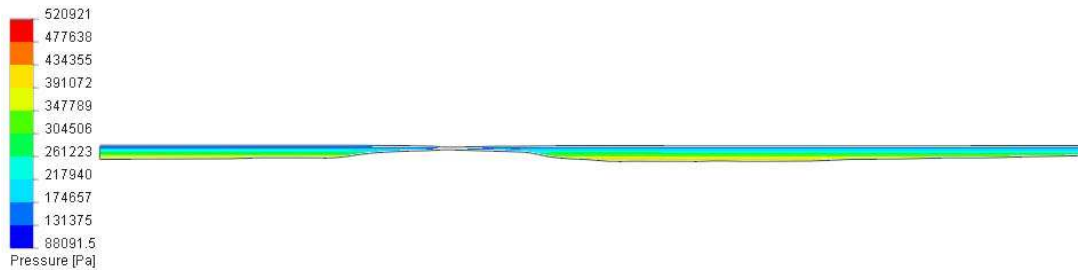
Figure 6-10 Pressure at cross section x=0m, calculation 'Basis 8'

Besides the mean flow velocity, the turbulent parameters are important for the determination of the flow load on the bottom protection and the dam heads. The turbulence intensity as calculated in the EFD.lab model gives the changes of the velocity lined out with the mean velocity. This means that when the mean velocity is low, a small change has more influence and thus a higher intensity, than when the mean velocity is large. This can give a distorted image of the turbulence intensities. To show the turbulence in the flow, a new parameter in EFD.lab has been created that resembles the turbulent velocity fluctuations. This has been done in the following way:

$$I = 100\% \frac{\sqrt{\frac{2}{3}k}}{\overline{V}} = 100\% \frac{\sqrt{\frac{1}{3}}V'}{\overline{V}} - > V' = \frac{I\sqrt{3}\overline{V}}{100\%}$$ 6.20

in which:

I = turbulence intensities (%)
k = turbulent kinetic energy (m^2/s^2)
V = mean velocity (m/s)
V' = turbulent velocity fluctuation (m/s)

Figure 6-11 shows the turbulent kinetic energy and the turbulent velocity fluctuations for the calculation. The turbulent kinetic energy is given by the square of the turbulent velocity fluctuations.
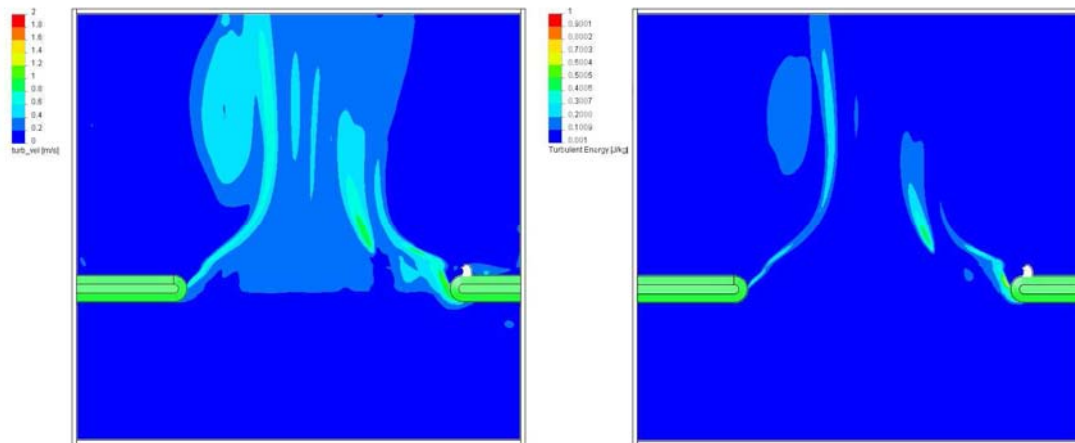
Figure 6-11 Turbulent velocity fluctuation and turbulent kinetic energy, calculation 'Basis 8'

The highest values for the turbulent velocity fluctuations and for the turbulent kinetic energy occur at the separation between the high velocities in the centre of the fluid flow and the low velocities at the sides of the fluid flow. Turbulent velocity fluctuations and turbulent kinetic energy mainly is found in the deceleration zone behind the dam. In acceleration zone in front of the closure gap, no turbulent velocity fluctuations are found and the turbulent kinetic energy is very low.

For the stability of the bottom protection, the maximum occurring velocity is normative. This characteristic velocity exists of a static component (the mean flow velocity) and a dynamic component (the turbulent velocity fluctuations) given by the following formula:

$$V_{max} = \overline{V} + \alpha V' \qquad\qquad 6.21$$

where:

V_{max} = the characteristic velocity (m/s)
V = the mean velocity (m/s)
α = variable for the standard normal (-)
V' = turbulent velocity fluctuation (m/s)

When a normal distribution has been assumed, the probability of exceeding of the characteristicvelocity depends on the value of α. For the calculation of the characteristic velocity, the variable is set to 3, which implies a probability of exceeding of 0.13%. To be able to plot the characteristic velocity an extra parameter has been created in the EFD.lab model that resembles this characteristic velocity.

The following figure shows the characteristic velocity at two heights in the model. The figure at the left shows the characteristicvelocity at a level of y=-1 m MSL and the right figure shows the maximum velocity at y=-3 m MSL. In the brown parts of the figure no values for the characteristic velocity has been calculated because the bottom at those location has been located higher than - 3m MSL.
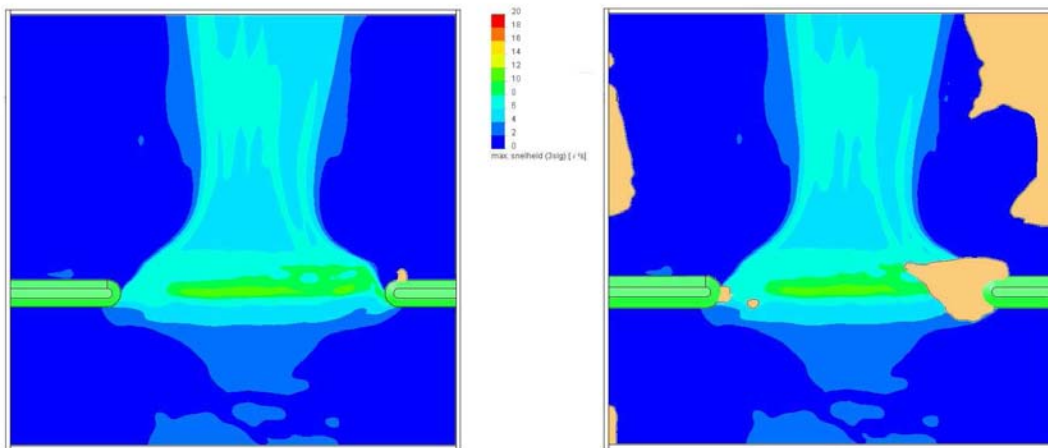
Figure 6-12 Characteristic flow velocity at two levels in the model, calculation 'Basis 8'

In contrast with the mean flow velocity, where the characteristic value occurs locally, the maximum value for the characteristic flow velocity occurs over a larger area. The mean velocity had a maximum value of 11 m/s in one small section of the closure gap. The characteristic velocity has a maximum value of 11 m/s as well but this value occurs not only in a small section of the closure gap but also in almost the total closure gap. This may seem strange but at the location where the mean velocity was high, only little turbulence was found. This is shown in Figure 6-11. At the locations where the turbulent fluctuations were high, the mean flow velocity was lower. This means that the characteristic velocity as calculated above occur over a larger area than only that area where the mean flow velocity was 11 m/s.

This shows the importance of the characteristic velocity for the design of bottom protections. When only the mean flow velocity is taken into account the bottom protection over a significant part of the closure gap will be designed with a too low velocity. Therefore, it is important to consider the turbulent fluctuations of a flow in the design.

6.6.2 Influence of gravitational acceleration

During a calculation in EFD.lab, the gravitational acceleration can be adapted. When a model has been scaled, the Froude number of the model and the prototype has to correspond. This means that:

$$Fr = \frac{V}{\sqrt{gh}} = constant \hspace{6cm} 6.22$$

where:
Fr = Froude number (-)
V = mean velocity (m/s)
g = gravitational acceleration (m/s^2)
h = vertical velocity scale (m)

When the normal gravitational acceleration has been used during a calculation, the results have to be scaled afterwards to keep the Froude number constant. However, the gravitational acceleration being scaled during the calculation the Froude number stays the same and the results do not have to be scaled afterwards.

To investigate the influence of the changing of the gravitational acceleration, the same calculation has been executed with different gravitational accelerations. By changing the gravitational acceleration, the boundary conditions change as well. The water level enforcement at both sides of the dam stays unchanged during the two calculations. The following table gives an overview of these two calculations:

Model calculation	Gravitational acceleration (m²/s)	Pressure at inflow boundary (Pa) ($p_{atm}+h_b*g*\rho$)	Pressure at outflow boundary (Pa) ($p_{atm}+h_b*g*\rho$)
Basis 7	9.81	110311	104464
Basis 8	24.525	123790	109173

Table 6-3 Overview of calculations with different gravitational acceleration

The results of the two calculations have been compared. Before the velocities of the different calculations can be compared, the calculated velocity of calculation 'Basis 7' needs to be scaled. In EFD.lab a new parameter has been created. This parameter is called ´real velocity´ and has been created by multiplying the calculated velocity by the square root of the scale factor. The following figure shows the real velocity of calculation 'Basis 7' and the velocity of calculation 'Basis 8' at y=-1m MSL.
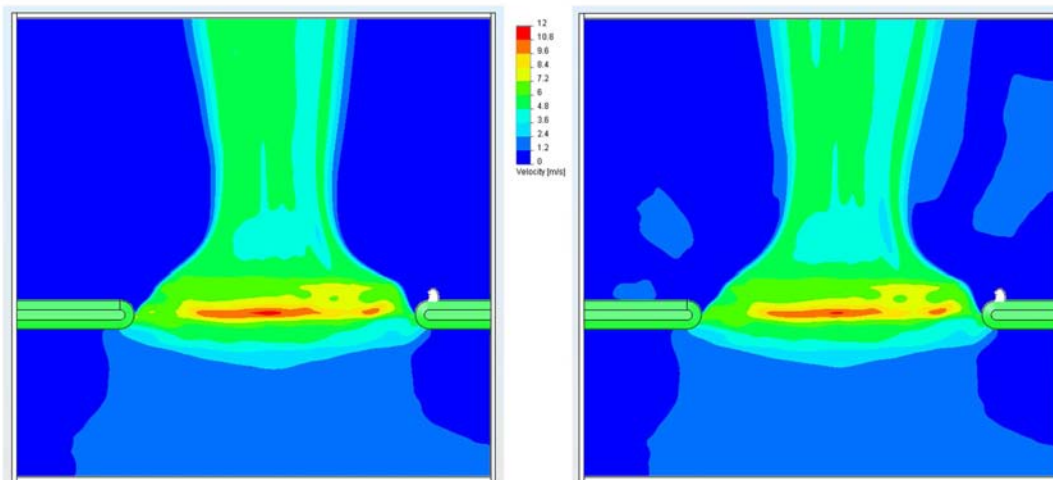
Figure 6-13 Mean flow velocity, calculations 'Basis 7' and 'Basis 8'

The figures above show that the flow velocities correspond well. Some small differences in the flow pattern have been observed, mainly in the area behind the dam. This is the area where the flow decelerates and when solving turbulent flows with computational models, small variations in the results can appear even when two exactly the same calculations have been executed twice.

Besides the results of the flow velocities, the results of the turbulent parameters have been compared to investigate the influence of the gravitational acceleration on the results. Before the results of the different calculations could be compared, the results of calculation 'Basis 7' has to be scaled. The following figures show the results for the turbulent energy and the turbulent dissipation of the two calculations 'Basis 7' and 'Basis 8'. In both figures are the results of calculation 'Basis 7'given at the left hand side and the results of calculation 'Basis 8' at the right hand side.
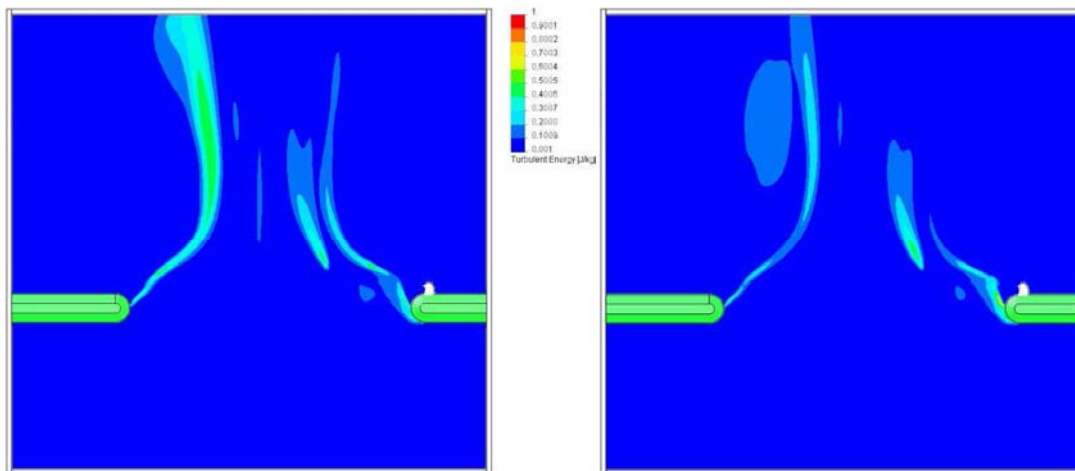
Figure 6-14 Turbulent energy at y=-1m MSL, calculations 'Basis 7' and 'Basis 8'
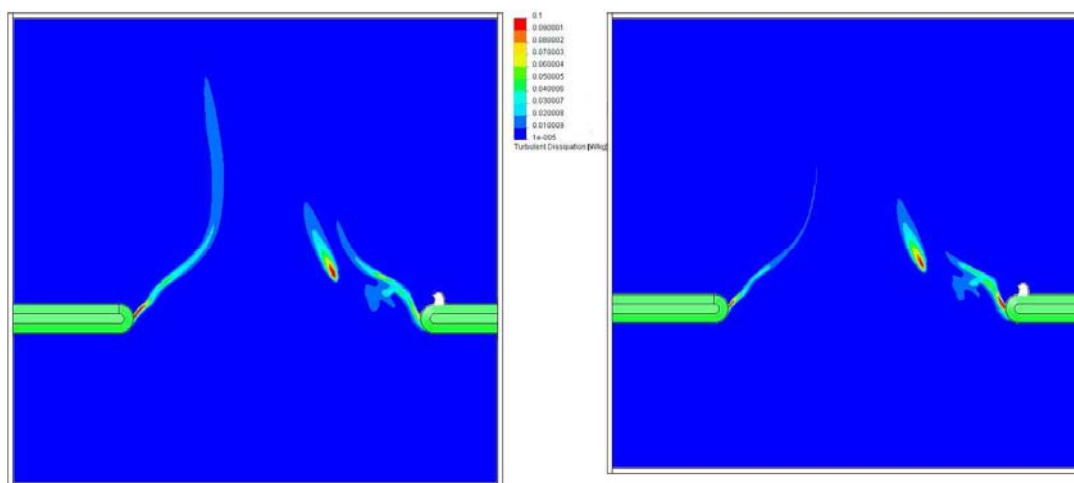
Figure 6-15 Turbulent dissipation at y=-1m MSL, calculations 'Basis 7' and 'Basis 8'

Figure 6-14 shows the results for the turbulent kinetic energy. The turbulent kinetic energy in calculation 'Basis 7' is slightly higher than the turbulent kinetic energy calculated with calculation 'Basis 8'. The location where the turbulent kinetic energy is observed corresponds well. The turbulent kinetic energy occurs at the boundary between the fast flowing fluid flow in the centre of the gap and the relatively slow flowing fluid at the sides. At the right hand side, the turbulent kinetic energy is located near the dam head and at the end of the shallower part that is located in front of the dam head.

Figure 6-15 shows the turbulent dissipation for the two calculations. The dissipation in calculation 'Basis 7' is slightly higher than in calculation 'Basis 8' but the location where the dissipation takes place corresponds well. It can be seen that near the dam heads the dissipation is high and at the end of the shallow are at the right side of the closure gap as well.

6.6.3 Influence of changing the turbulent parameters

In the two calculations discussed above, "Basis 7' and 'Basis 8', the values of the turbulent parameters have not been adapted. The default values for the turbulent kinetic energy k and the turbulent dissipation ε have been used in the general settings as well as in the boundaries of the model. The values for the turbulent parameters in the general settings are start values and the values for the turbulent parameters at the boundaries of the model are fixed values and keep that value during the calculation. The turbulent kinetic energy k and the turbulent dissipation ε are calculated in the flow. The following table provides an overview of the default values for the parameters.

	General Settings		**Values at the boundaries**	
	ε (W/kg)	k (J/kg)	ε (W/kg)	k (J/kg)
Default value	1	1	1	1

Table 6-4 Default values for turbulent parameters

To investigate the influence of changing the turbulent parameters at the boundaries of teh model and in the general settings, three calculations have been executed with the same model set up. Calculation 'Basis 8' is the basis for this investigation and the turbulent parameters in the general setting and at the model boundaries have been adapted. The first calculation is 'Basis 9' and in this calculation, only the turbulent parameters at the model boundaries have been changed. The second calculation is 'Basis 10' and in this calculation, the general settings as well as the values at the boundaries of the model have been adapted. The calculation of the values for the turbulent parameters at the boundaries has been explained in section 6.4. The following table gives an overview of the values for the turbulent parameters used in calculation 'Basis 9' and 'Basis 10'.

'Basis 9'					
General Settings		**Values at the boundaries**			
ε (W/kg)	K (J/kg)	Inflow ε (W/kg)	Inflow k (J/kg)	Outflow ε (W/kg)	Outflow k (J/kg)
1	1	0.00316	0.0625	0.04278	0.4225
'Basis 10'					
General Settings		**Values at the boundaries**			
ε (W/kg)	K (J/kg)	Inflow ε (W/kg)	Inflow k (J/kg)	Outflow ε (W/kg)	Outflow k (J/kg)
0.10	1	0.00316	0.0625	0.04278	0.4225

Table 6-5 Values for turbulent parameters in calculations 'Basis 9' and 'Basis 10'

To investigate the influence on the results of changing only the turbulent parameters at the model boundaries, the results of calculation ´Basis 8´ have been compared with the results of calculation ´Basis 9´. In Figure 6-16, the calculated mean flow velocity of the two

calculations has been compared. The results of calculation ´Basis 8´ are showed on the left hand side and the results of calculation ´Basis 9´ have been showed on the right hand side.
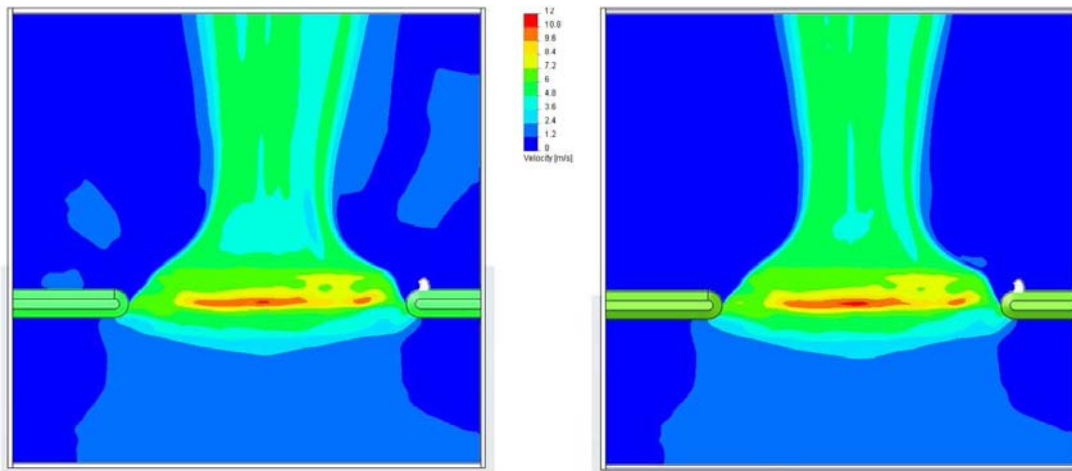
Figure 6-16 Mean flow velocity, calculations 'Basis 8' and 'Basis 9'

Figure 6-16 shows that changing the turbulent parameters at the model boundaries does not influence the mean flow velocity. The maximum mean flow velocity occurs at the same location above the sill and has the same value. The following figure shows the result of the turbulent velocities for calculations ´Basis 8´and calculation ´Basis 9´. The left frame in Figure 6-17 shows the results of calculation ´Basis 8´ and the right hand frame the results of calculation ´Basis 9´.
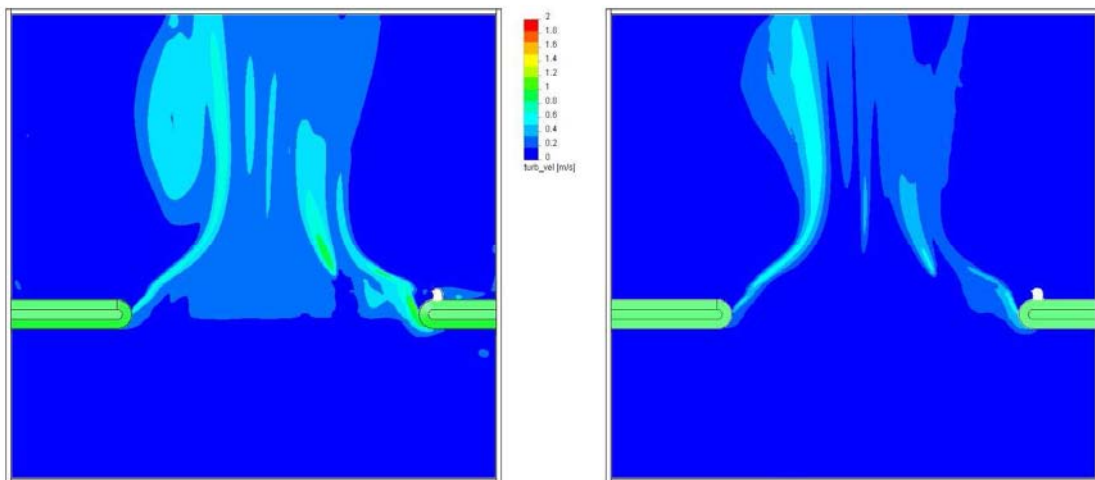
Figure 6-17 Turbulent velocity fluctuations calculations, ´Basis 8´ and ´Basis 9´

The turbulent velocity fluctuations in the results of calculation ´Basis 8´ are significant higher than the turbulent velocity fluctuations from the results of calculation ´Basis 9´. The locations where the turbulent velocity fluctuations are observed do correspond. ´Basis 8´ has been executed with the default values for the turbulent parameters at the model boundaries, which are higher than the adapted values for the turbulent parameters in ´Basis 9´. This has been showed in Table 6-4 and Table 6-5.
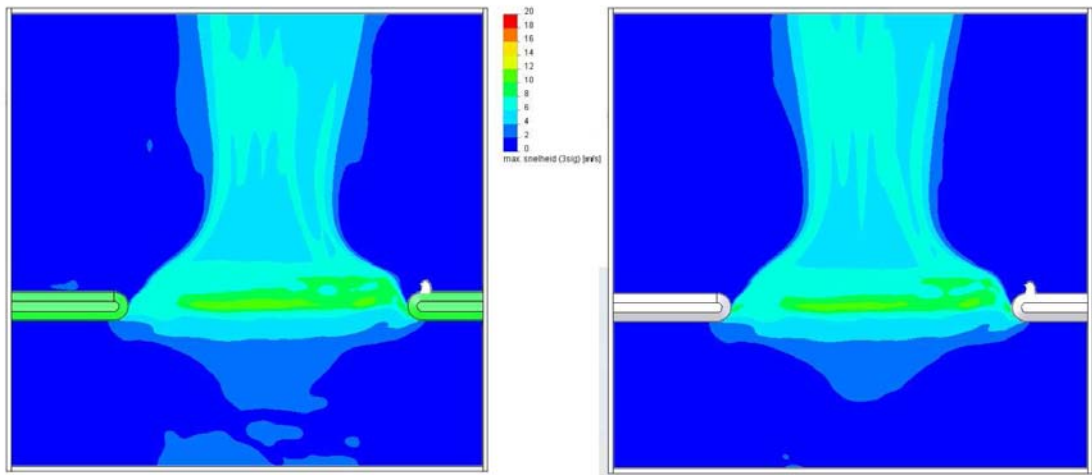
Figure 6-18 Characteristic flow velocity, calculations 'Basis 8' and 'Basis 9'

Figure 6-18 shows the characteristic velocity calculated with calculation 'Basis 8' and 'Basis 9'. The right frame is the characteristic velocity calculated with 'Basis 9' and shows that the characteristic velocity as lower and occurs over a smaller area then calculated with 'Basis8'.

To investigate the influence of changing the turbulent parameters in the general settings as well, a new calculation has been executed with adapted turbulent parameters in the general settings as well as at the model boundaries. The values used for the turbulent parameters are listed in Table 6-5. In the following figure, the flow velocity calculated with ´Basis 8´ and ´Basis 10´ are showed. The frame at the left hand side shows the calculated mean flow velocity with calculation ´Basis 8´ and the frame at the right hand side shows the with calculation ´Basis 10´ calculated mean flow velocity.
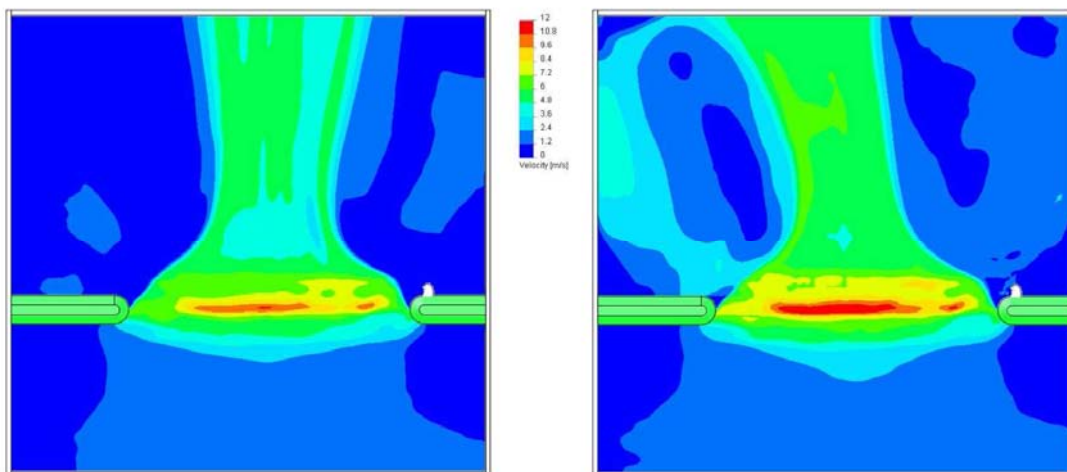
Figure 6-19 Mean flow velocity, calculations 'Basis 8´ and 'Basis 10´

The results from calculation ´Basis 10´ does not correspond with the results of calculation ´Basis 8´. The mean flow velocity in ´Basis 10´is higher and occur over a larger area. The fluid flow in calculation ´Basis 8´ evolves more or less perpendicular to the closure dam. The fluid flow in ´Basis 10´ evolves under an angle and the flow velocities at the left side of the fluid flow are improbable high.
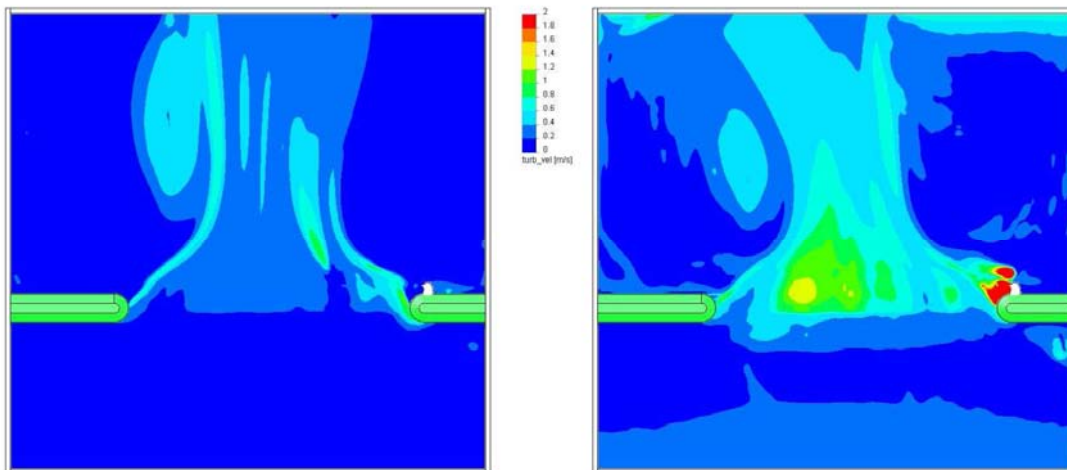
Figure 6-20 Turbulent velocity fluctuations, calculations ´Basis 8´ and ´Basis 10´

In Figure 6-20 the turbulent velocity fluctuations are given for ´Basis 8´ and ´Basis 10´. The frame at the left hand side gives the results of calculation ´Basis 8´ and shows that the turbulent velocity fluctuations mainly occur at the boundary between the fast flowing fluid flow in the centre of the gap and the slow flowing fluid flow at the sides. In the frame at the left hand side of Figure 6-20 the result of calculation ´Basis 10´ is shown. In this situation, the maximum values for the turbulent velocity fluctuations have been observed above the sill and at the downstream side of the right dam head. This seems unrealistic because above the sill, the flow is still accelerating. In general, the turbulent velocity fluctuations in the area where the flow is accelerating are lower than in the decelerating part of the flow. The results of ´Basis 10´ do not correspond with this.
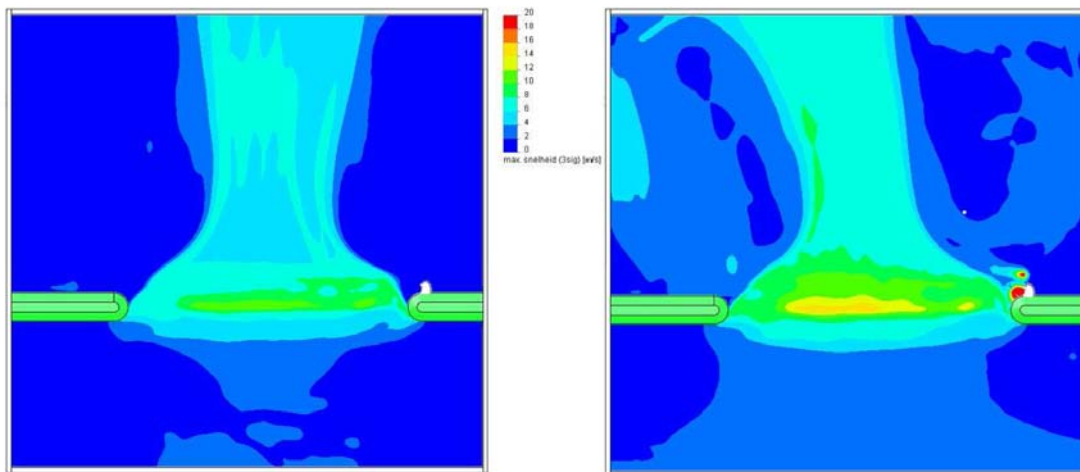
Figure 6-21 Characteristic flow velocity, calculations 'Basis 8' and 'Basis 10'

Figure 6-21 shows that by changing the turbulent parameters at the model boundaries and in the general settings, the characteristic flow velocities change drastically. The characteristic velocity calculated with 'Basis 10' is showed in the right frame and above the sill the calculated characteristic velocity reaches a value of 14 m/s while in calculation 'Basis 8' the maximum value does not get larger then 11 m/s.

6.6.4 Influence of the bottom geometry roughness

The bottom geometry in the closure gap is very rough. The bottom geometry used for the creation of the model is a measured bottom geometry and as can be seen in Figure 6-3 the surface of the bottom geometry is not smooth. Nevertheless, the gabions and rocks that are located in the closure gap are not modelled very accurate. The EFD.lab has the opportunity to assign a specific roughness to a surface. It is assumed that the bottom geometry in the surrounding of the closure gap is very rough. The influence of assigning a bottom roughness height of 2m to the bottom geometry has been investigated. This means that the bottom roughness has a Chézy factor of 32 $m^{1/2}$/s. Calculation 'Basis 8' has been adapted with the new bottom roughness and changed in calculation 'Basis 11'. The following figure shows the calculated mean flow velocity compared with the calculated mean flow velocity of 'Basis 8'.
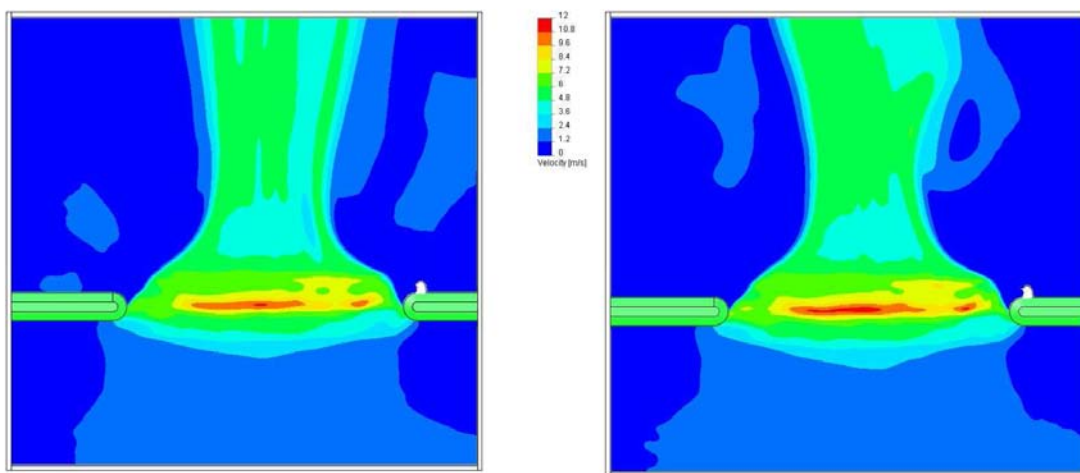
Figure 6-22 Mean flow velocity, calculations 'Basis 8' and 'Basis 11'

Figure 6-22 shows that the calculated mean flow velocity in 'Basis 8' is slightly smaller then the calculated mean flow velocity with 'Basis 11'. Above the sill the characteristic flow velocity in 'Basis 11' is higher and occurs over a larger area. Figure 6-23 shows the comparison of the turbulent velocity of 'Basis 8' and 'Basis 11'.
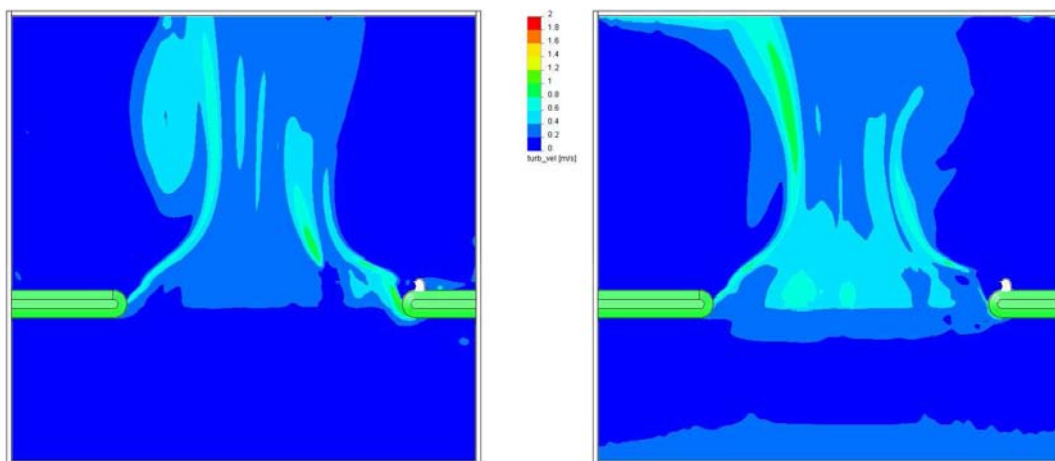
Figure 6-23 Turbulent velocity fluctuations, calculations 'Basis 8' and 'Basis 11'

The turbulent velocity fluctuations are larger in calculation 'Basis 11' then they are in calculation 'Basis 8'. At the end of the sill and at the borders between the fast flowing fluid and the slower flowing fluid, the turbulent fluctuations have their maximum value.
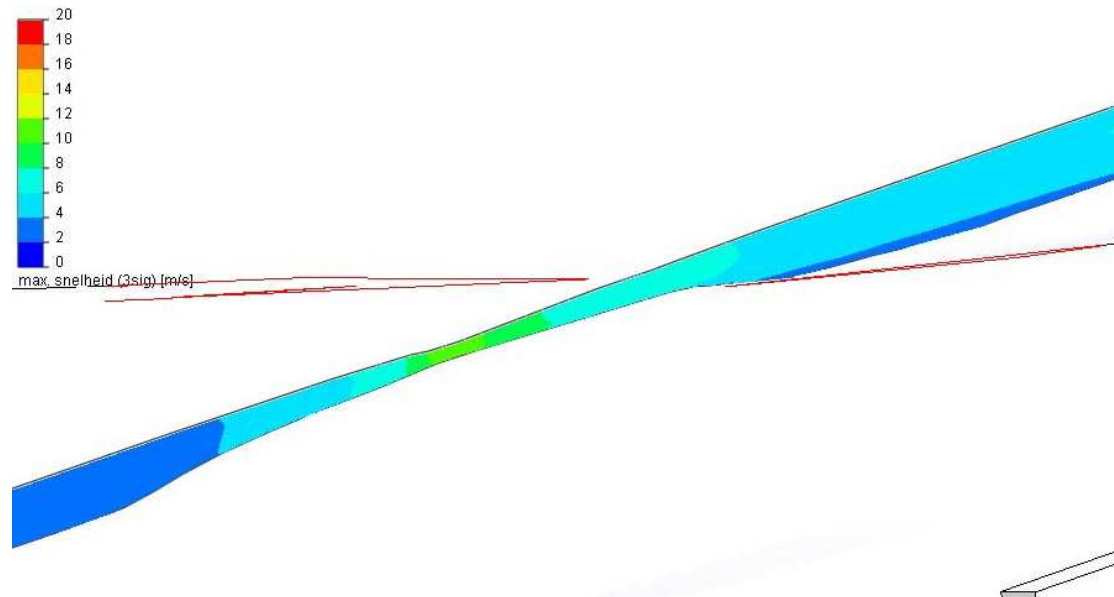
Figure 6-24 detail of characteristic flow velocity over sill, calculation 'Basis 8'
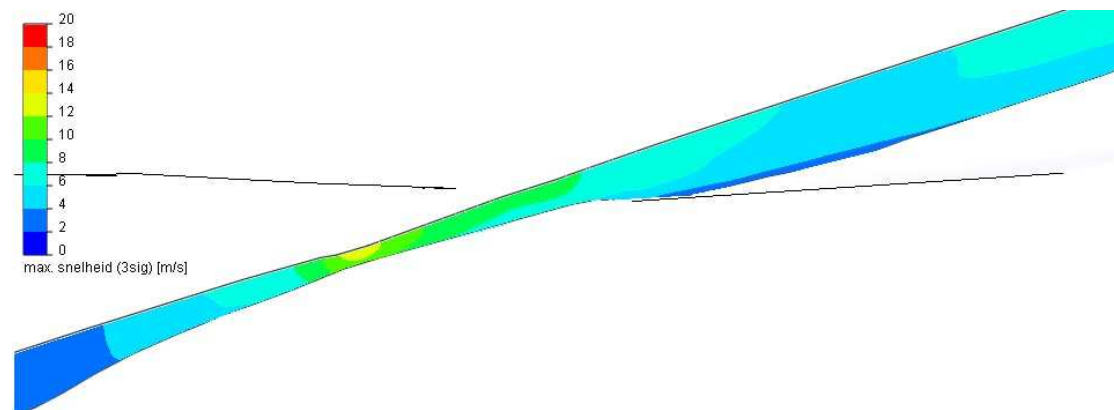
Figure 6-25 Detail of characteristic flow velocity over sill, calculation 'Basis 11'

Figure 6-24 and Figure 6-25 show the characteristic flow velocity over the sill. It can be seen that due to the extra bottom roughness in calculation 'Basis 11' the characteristic flow velocity does not reach to the sill. In calculation 'Basis 8', the flow velocity above the sill is the same over the vertical. In 'Basis 11', the characteristic flow velocity occurs at a certain distance from the bottom. A boundary layer has developed, in which the mean flow velocity is lower then at the outside of this layer. Because the water level is fixed in the model, it may be the case the because of the developing of this boundary layer the free flow area becomes smaller and the mean flow velocities increase.

7 Comparison of the different models

To investigate the accuracy of the models used in the research they will be compared with each other and with the scarce measurements obtained from the Korean counterpart. With the storage area approach the water level at the basin side of the dam and the average flow velocity through the closure gaps have been calculated. The water level inside the basin is presumed to be horizontal and the water level will be calculated at one location, namely inside the basin. Waqua calculates the flow velocity and the water level in every grid point in the computational domain. The computational domain encloses the total estuary and a significant part of the foreshore. With the EFD.lab model, a small part of the estuary has been taken into account. Only one of the closure gaps has been modelled and in contrast to the storage area approach and the Waqua model, not the depth average flow velocity but a detailed flow pattern through the closure gap has been calculated.

This chapter elaborates on the comparison of the three models. The results of the calculations have been compared with measurements and with each other. In the first section, the results of the water level calculations have been compared with the measurements executed in Korea. In the second section of this chapter, section 7.2, the calculated flow velocities have been compared with the measurements and with each other. There are no data available about the discharges through the closure gaps to compare the model results with, so the results of the discharge calculations will be compared with each other.

7.1 Water level

The basin side water level calculated with the storage area approach does not discern different locations. Only one basin side water level has been predicted. The Waqua model however does discern different locations. In every grid point, the water level has been calculated so at different locations inside the basin a prediction of the water level has been made. EFD.lab does not make a prediction of the water level. The water level in the EFD.lab model is imposed and the results of the calculations can be recalculated to a water level but this is only to check whether the imposed water level was correct.

The water level in the surrounding of the closure gaps has been monitored closely during the closure. Unfortunately, the Korean counterpart has made only a small amount of data available. Every day, an overview of the current situation has been created, which contained information about the predicted water level and the measured water level at both sides of the dam. These data are only available for two days. For March 27 the measured and predicted water levels at the seaside and basin side of Gap 1 and Gap 2 are available. For April 1, the predicted and measured water levels at the seaside and basin side of Gap 2 are available. For March 26, some data about measurements at the basin side of Gap1 are available. This data originates from a picture of the measuring file taken during a site visit at the measuring location. In Appendix VI. the original data as obtained in Korea are enclosed.

7.1.1 Measurements and the storage area approach

The storage area approach does not make a distinction between the water level near Gap 1 and near Gap 2. The water level inside the basin is assumed horizontal so at every moment

the basin side water level near Gap 1 is the same as the basin side water level near Gap 2. In the following figure, the data of the measured basin side water levels near Gap 1 and Gap 2 have been compared with the basin side water level predicted with the storage area approach.
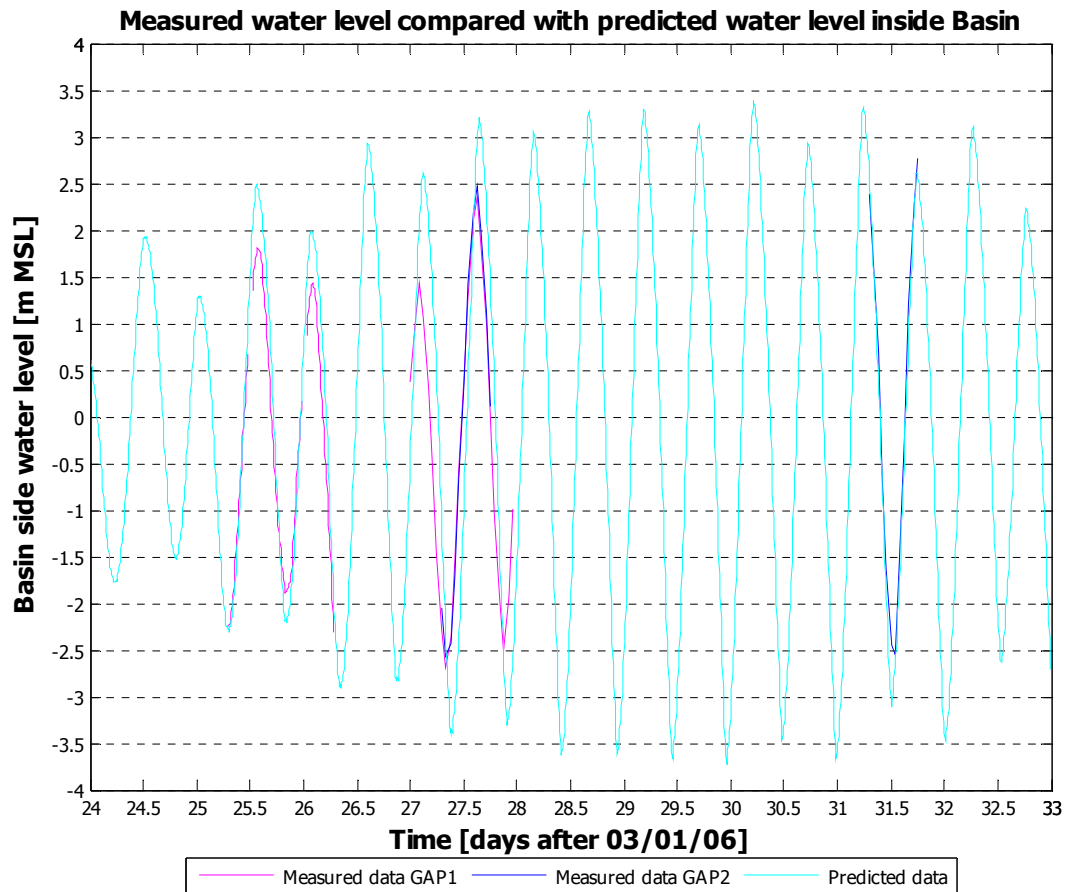
Figure 7-1 Measured and predicted (with storage area approach) water level inside basin

In the figure the pink lines are the data measured near Gap 1, the dark blue lines are the data measured near Gap 2 and the light blue line is the prediction of the basin side water level executed with the storage area approach method.

The moments of high and low water inside the basin correspond well but the level of the water at these moments does not. The water level of the prediction is too high during high water and too low during low water. The difference between the prediction and the measurements is at least half a meter and at one point almost one meter.

Measured water level compared with predicted water level at seaside
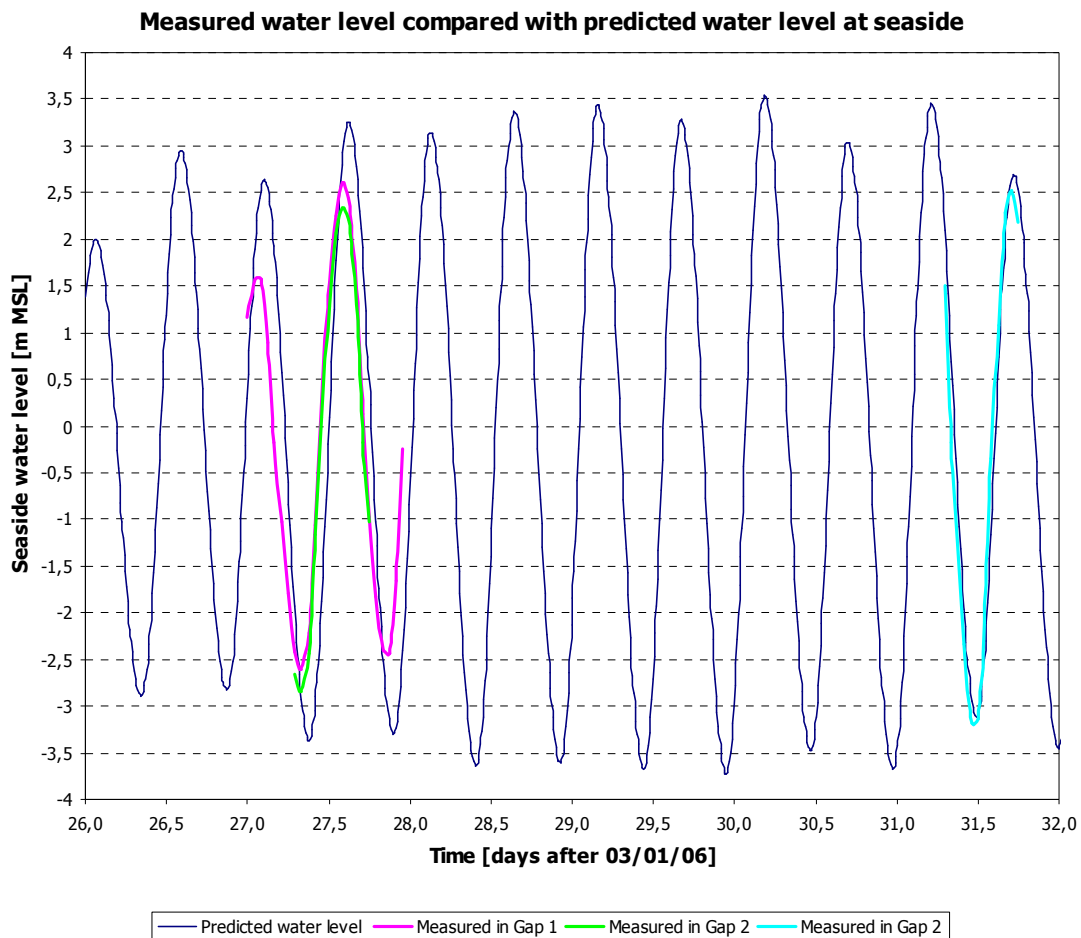
Figure 7-2 Measured and predicted (with storage area approach) water level seaside dam

In Figure 7-2 the measured and the predicted water levels at the seaside have been compared. The dark blue line is the predicted seaside water level used in the storage area approach. The pink line is the measured water level near Gap 1 during March 27. The green and the light blue line are the measured water levels near Gap 2 during March 27 and April 1. The measurements of the water level at March 27 in Gap 1 and Gap 2 do not correspond well with the predicted water level. The measured water level is significant lower during high water and higher during low water. The measurements near Gap 2 during April 1 correspond well with the predicted water level.

The storage area approach is a very crude approximation of the real situation so differences with the real situation are to expect. The basin side water level prediction with the storage area approach can be influenced by adapting some parameters. By lowering the discharge coefficients of the closure gaps and the sluices, the amplitude of tidal elevation inside the basin will decrease. Enlarging the basin wet surface area makes the water level inside the basin varying less as well. However, when these parameters are adapted the graph of the water level inside the basin will shift to the right because the water will experience more resistance when flowing in and out of the basin. Because of this shift to the right, the moments of high and low water will no longer correspond with the measured moment of high and low water. This has been explained in section 0.

Measured water level difference compared with predicted water level difference
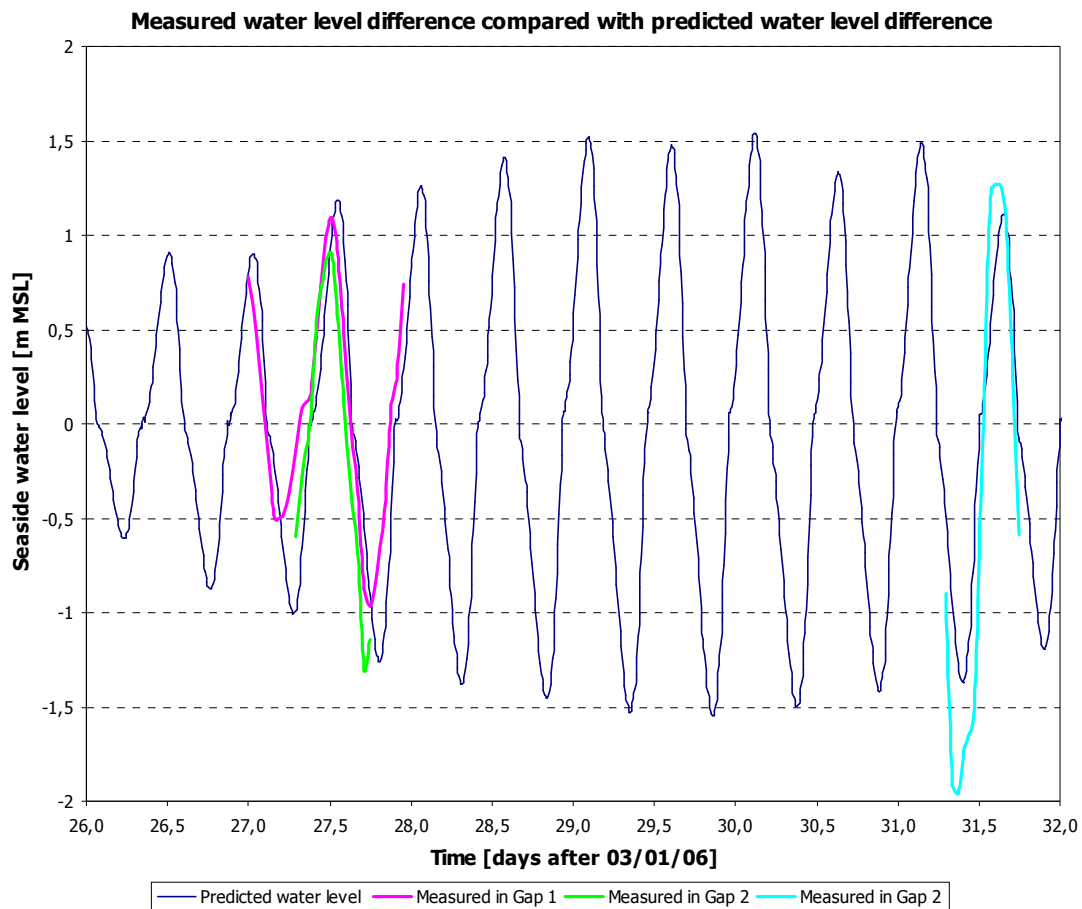
Figure 7-3 Measured and predicted (with storage area approach) water level difference

For the calculation of the flow velocity, the water level difference between the two sides of the dam is important. In Figure 7-3 the predicted water level difference and the measured water level difference have been compared. The dark blue line is the predicted water level difference, the pink line the measured water level difference in Gap 1 and the green and the light blue lines the measured water level difference in gap 2.

Because the measurements of the water level were higher during low water and lower during high water at the seaside as well as on the basin side, the measured water level difference does correspond reasonably well with the predicted water level differences. The difference between the measured and the predicted water level difference during April 1 is quite big during low water. The measured water level inside the basin at April 1 varied more then 0,5m with the predicted water level inside the basin. The measured water level at the seaside almost followed the predicted value for the water level. Therefore, the measured water level difference during April 1 varies also half a meter with the predicted water level difference.

7.1.2 Measurements and the Waqua model

Unlike the storage area approach, Waqua does calculate the water level at different locations in the estuary and the area around the estuary. The storage area approach only gives a water level for the basin side of the closure dam and no difference is made between the water level

near Gap 1 and Gap 2. Waqua calculates a water level for every grid cell of the computational domain and thus a different water level is calculated near Gap 1 and Gap 2.

7.1.3 Measurements and the EFD.lab model

In contrast to the storage area approach and the Waqua model, the EFD.lab model does not calculate the water level inside the basin on basis of a known seaside water level. The water level in the EFD.lab model is imposed and the flow properties for this particular situation are calculated.

Because the Waqua model calculates a water level in every grid point, the imposed water level can be compared with the calculated water level by the Waqua model.

7.2 Flow velocity

With the storage area approach a depth average flow velocity has been calculated, which is the same for the two closure gaps and the sluice gates. No distinction has been made between the closure gaps and the sluices and for the prediction of the flow velocity, the total flow area of the two closure gaps and the two sluices have been added together. This has been explained in section 4.2.

The flow velocity calculated with the Waqua model is a depth average flow velocity as well. The difference with the storage area approach is that Waqua has calculated a flow velocity at the border of every grid cell. The velocity consists of a component in the x-direction and a component in the y-direction.

The EFD.lab model calculates a detailed flow pattern through the closure gap. This has been done for only one situation so the flow velocity pattern for one head difference over the dam has been investigated.

Some measurements on the flow velocity have been collected in Korea. During the closing of the dam, the surface flow velocity through the centerlines of the closure gaps have been measured with GPS floaters every day. Data about these GPS floater measurements on April 16 are available for Gap 2. During the waiting periods, the flow velocity has been measured with an ADCP measuring instrument as well. For March 30, the output of this ADCP measurement in Gap 2 is available. Every day, the in Korea predicted flow velocity has been compared with the measured data. For March 26, this form is available and contains the flow velocity during ebb tide and flood tide in Gap 1 and Gap 2. The original forms of the measurement as obtained in Korea have been enclosed in Appendix VII.

7.2.1 Measurements and the storage area approach

The flow velocity, calculated with the storage area approach is the depth average flow velocity through the closure gaps. All the measurements on the flow velocity have been executed during a period of maximum flow velocities. The following figure shows the measurements together with the storage area approach predicted flow velocities.

Measured and predicted flow velocity through closure gaps
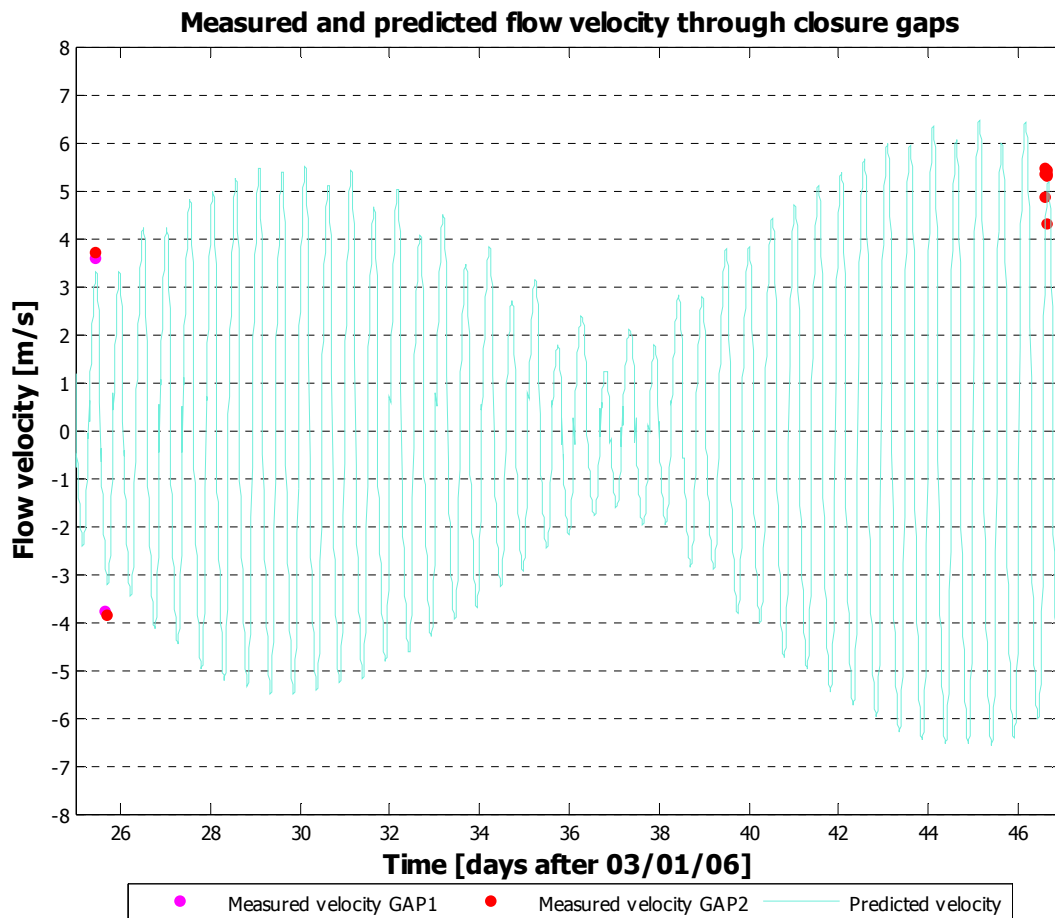
Figure 7-4 Measured and predicted (with storage area approach) flow velocities

The pink dots are the measured flow velocities through Gap 1, the red dots are the measured velocities through Gap 2 and the blue line gives the with the storage area approach predicted flow velocity. The measured velocities at March 26 have been obtained with GPS floater measurements thus the measured flow velocity is the flow velocity at the surface. The measured values for the flow velocity at April 16 are values for the surface flow velocity as well.

The differences between the measured flow velocity at March 26 in Gap 1 and Gap 2 are small. The flow velocity in Gap 1 is 3.59 m/s during flood and 3.77 m/s during ebb and in Gap 2 the flow velocity is 3.69 m/s during flood and 3.84 m/s during ebb. The predicted flow velocities are lower. For that day, the predicted flow velocity is 3.29 m/s during flood and 3.23 m/s during ebb. The difference between the predicted flow velocity and the measured flow velocity during flood is 0.3m/s for Gap 1 and 0.4 m/s for Gap 2. During ebb, the difference is larger, 0.57 m/s for Gap 1 and 0.61 m/s for Gap 2. The storage area approach calculates the depth average flow velocity which is lower than the flow velocity at the surface. This difference can be 10%.

The flow velocity measured with the GPS floaters at April 16 is also higher than the predicted flow velocity. The following figure shows a detail of Figure 7-4.

Measured and predicted flow velocity through closure gaps
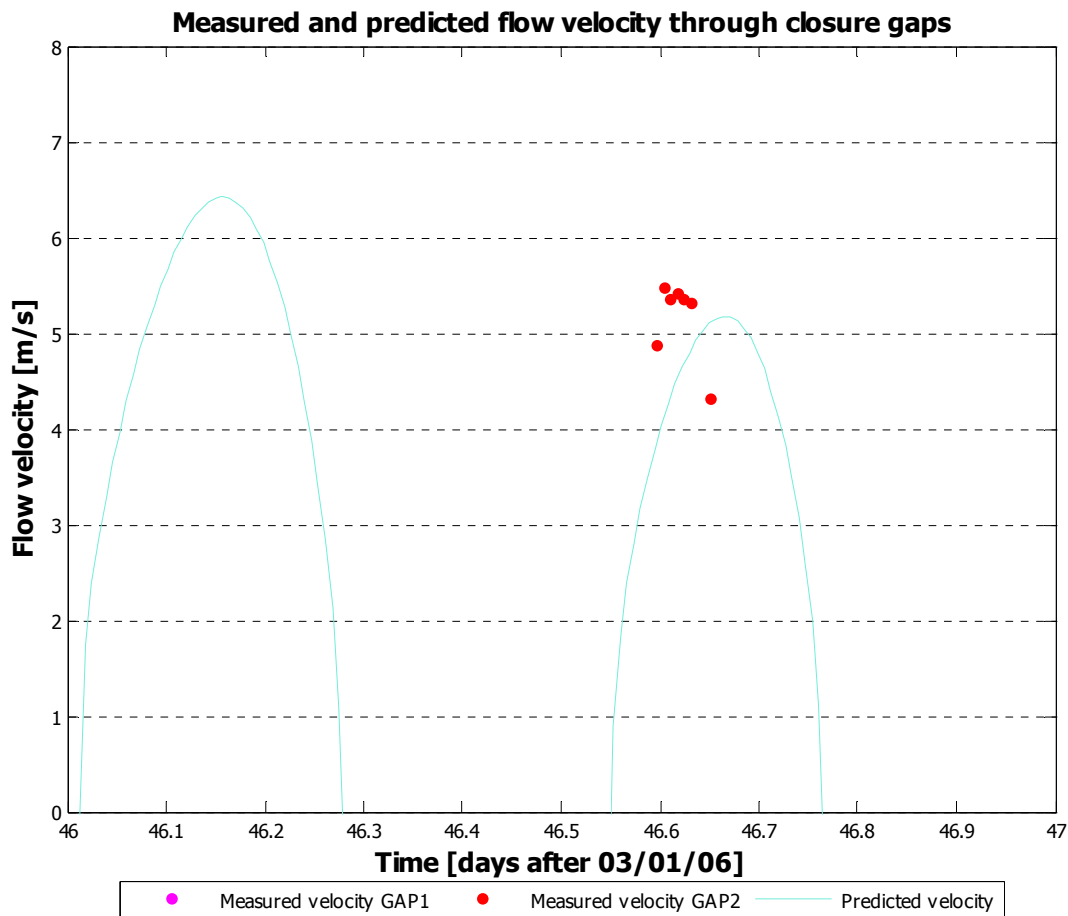
Figure 7-5 Predicted (with storage area approach) and measured flow velocity April 16

The blue line in Figure 7-5 shows the predicted depth average flow velocity and the red dots the with the GPS floaters measured flow velocity. With GPS floaters the surface water velocity is measured and the surface flow velocity is larger then the depth average flow velocity. The difference between the measured flow velocity and the predicted maximum flow velocity is less then 10% but the moment of occurring of the maximum flow velocity seems to differ. Because no data about flow measurements later that day are available, the velocity development cannot be compared.

7.2.2 Measurements and the Waqua model

The Waqua model calculates the flow velocity in two directions at every time step and in every grid cell. The measured flow velocity were measured in the centre line of the closure gap.

7.2.3 Measurements and the EFD.lab model

The EFD.lab model calculates a detailed flow pattern of the flow through the closure gap. Because detailed data about the bottom geometry was required for the creation of the EFD.lab model, Gap1 has been modelled in EFD.lab. In the waiting periods, measurements with an ADCP measuring device have been executed in both gaps at all the moments of

maximum flow velocities. Only one of these measurements is available and has been executed at March 30 in Gap2. The following figure shows the result of this measurement.

□ GAP2 (3월30일)
1. 구간별 유속분포도
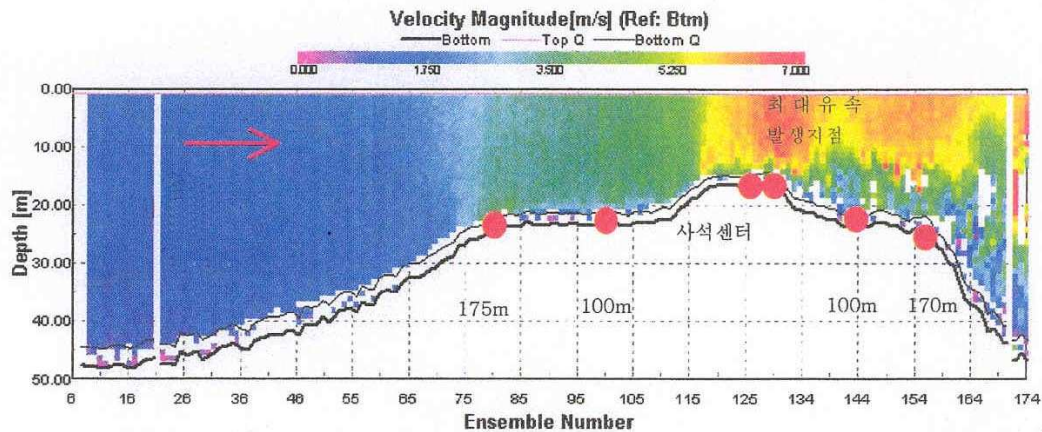
Figure 7-6 Result of ADCP flow velocity measurement at March 30 in Gap2

The figure shows a cross section through closure gap number 2. The water flows from the left side to the right side and the measurement has been executed during flood, the water flows from the seaside to the basin side of the dam. In the cross section, the two scour holes at both sides of the closure dam can be distinguished. The bottom protection and on top of the bottom protection the sill are visible as well. The red dots in the figure are the locations for which the value of the velocity has been given. This table has been enclosed Appendix VII.

In the ADCP measurement, the maximum flow velocity is 7 m/s and occurs above the sill. The flow starts to accelerate above the bottom protection and reaches its maximum value above the sill. This has been observed in the EFD.lab calculations as well. In the deceleration zone at the downstream side of the sill, the flow velocity gradient over the vertical is large and thus the turbulence as well. At the slopes and the bottom of the scour hole, the flow velocity is low. This has been concluded for the EFD.lab calculations as well.

Because the ADCP measurement has been executed in closure Gap2 and the in EFD.lab modelled closure gap resembles closure gap number 1, the results cannot be compared directly. Nevertheless, it is interesting to compare measured flow pattern and the calculated flow pattern.

The following figure shows a cross section of the results of an EFD.lab calculation. The bottom protection and on top the sill are shown together with the calculated flow velocity through the centreline of the closure gap.
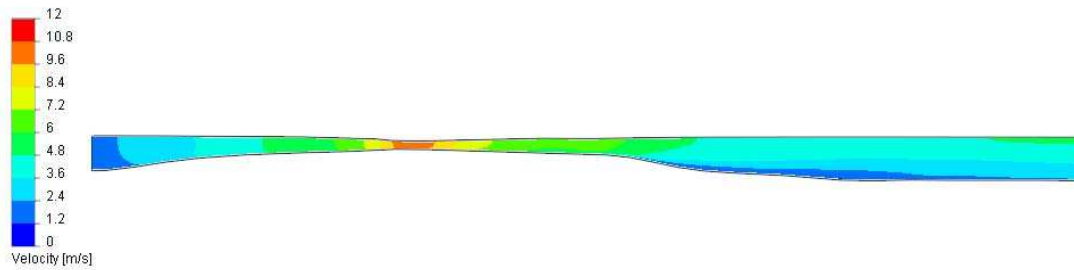
Figure 7-7 Detail of calculated flow velocity through centreline of closure gap

When the measured and the calculated flow patterns are compared, some similarities are observed. From the measurements, it can be concluded that the flow starts to accelerate when the bottom protection is reached. The flow accelerates and the flow more or less has the same velocity over the total vertical. Towards the sill, the flow accelerates more and reaches its maximum value at the end of the sill. At a line through the centre of the closure gap the flow velocity has been exported from the EFD.lab model.

Flow velocity in centre line of closure gap
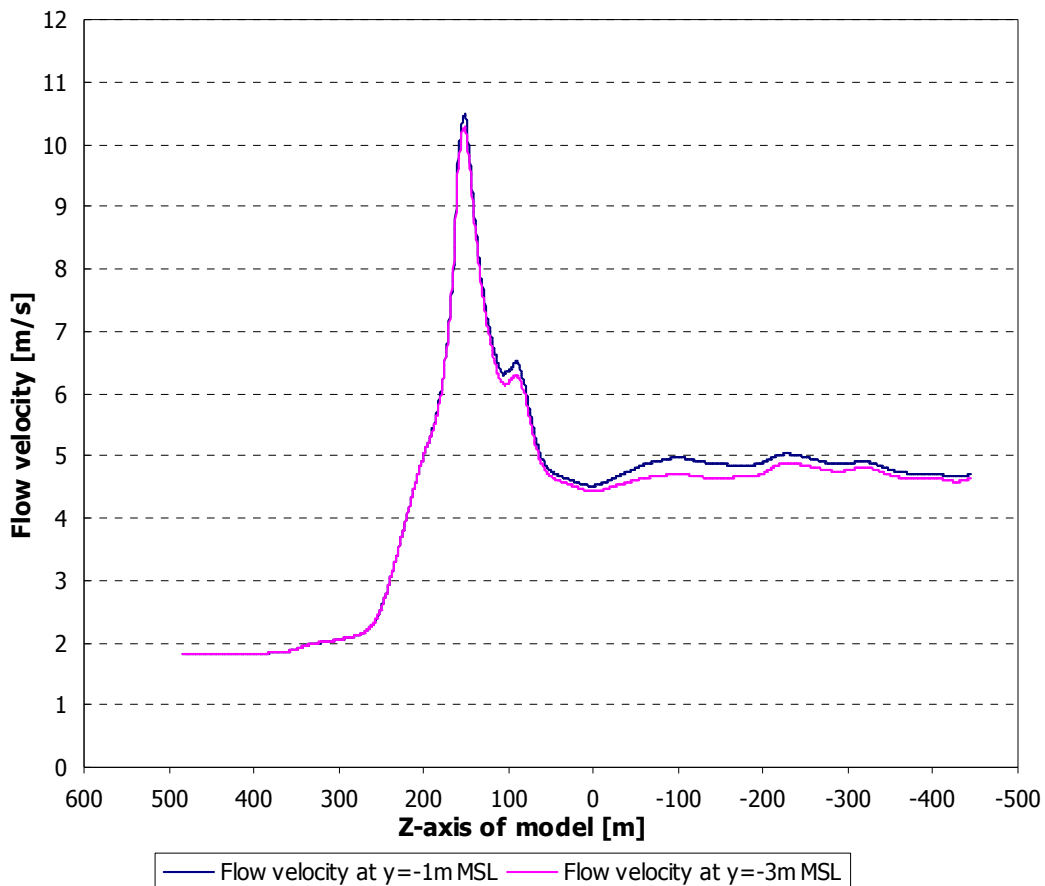
Figure 7-8 Flow velocity at different heights in the centre line of closure gap

In Figure 7-8 gives the exported flow velocity at two levels in the model. The pink line shows the calculated flow velocity at a level of y=-3m MSL and the blue line represents the calculated flow velocity at a level of y=-1m MSL. Both lines lie in the centreline of the closure

gap. The maximum velocity occurs at the end of the sill, which is located between z=150 m and z=160 m. The flow velocity in front of the closure dam is 1.9 m/s and the flow velocity at some distance from the closure gap is 4.8 m/s. Compared with the ADCP measurement through Gap 2 these values correspond. In Figure 7-6 it can be seen that in front of the closure gap the flow velocity is 1.75 m/s. The original measurement (see Appendix VII. it shows that at a distance of 170 m from the centre of the sill, the average flow velocity is 5.3 m/s. The calculated flow velocity with the EFD.lab model is slightly lower, 4,7 m/s. Only directly above the sill, the calculated flow velocity is significantly larger than the measured flow velocity. Because the measurement has been executed in closure gap number 2, and the calculation executed in EFD.lab was for closure gap number 1.

During the EFD.lab calculation with the extra bottom roughness, a roughness height of 2m has been assigned to the bottom surface. With a water level of 10 m in the closure gap, the Chézy coefficient is 32 $m^{1/2}$/s. During the closure of the Saemangeum dam, no measurements on turbulence have been executed. During the closure of the Eastern Scheldt in the Netherlands, measurements on the turbulence intensities have been executed and investigated. [Waterloopkundig laboratorium, 1986] The turbulence intensities of the flow in the Eastern Scheldt have been investigated and for several flow situations, measurements have been executed and compared with literature values of measured turbulent intensities in a flume. The measured turbulent intensities near the bottom were all lower then the literature values. The used values for the turbulence intensities over he vertical measured in a flume by a Chézy value of 36.6 are given in the following table. [McQuivey, 1969]

z/h	0.10	0.40	0.70
C= 36.6 $m^{1/2}$/s	0.19	0.098	0.074
C= 61.3 $m^{1/2}$/s	0.12	0.072	0.053

Table 7-1 Relative turbulence intensities measured by McQuivey

7.3 Discharge

During the closure works, no measurements have been executed on discharges through the closure gaps. With the storage area approach the total discharges through the closure gaps together with the two sluices has been calculated. EFD.lab has calculated the discharge at the outflow plane. Because no measurements on the discharges through the closure gap are available, the real discharge is not known and the calculated discharges can only be compared with each other.

The storage area approach calculates a total discharge every ten minutes and with this total discharge, the water rise or fall inside the basin has been calculated. This total discharge is the discharge through the two closure gaps and the sluice gates. To obtain the discharge through Gap 1 the total discharge has been divided by the total flow area of all the gaps together and subsequently multiplied by the flow area of Gap 1.

The EFD.lab model calculates the discharge through the total outflow surface. Because the length scale of the model has been scaled the results for the discharge calculated by the EFD.lab model needs to be scaled as well. For calculation ´Basis 7´, the gravitational acceleration has not been changed during the calculation and thus the results of the EFD.lab

model needed to be scaled with the scale factor as deducted in section 2.2.1. For the discharge, this scale factor corresponds to the length scale factor to the power 2,5. For the other calculation, the gravitational acceleration has been adapted during the calculations and thus the calculated discharge needs to be scaled by multiplying the results two times with the length scale factor.

The following table gives an overview of the results for the calculated discharges through the closure gap.

Storage Area Approach		EFD	Basis 7	Basis 8	Basis 9	Basis 10
Q_{total} (m^3/s)	140283	Q_{total} (m^3/s)	8030		12692	14168
$A_{flow,total}$(m^2)	29980	$A_{outflow}$ (m^2)	6067,4	6067,4	6067,4	6067,4
$A_{flow,Gap\ 1}$(m^2)	12400	Scale factor	$2,5^{2,5}$	$2,5^2$	$2,5^2$	$2,5^2$
$Q_{Gap\ 1}$(m^3/s)	**58022**	**$Q_{Gap\ 1}$ (m^3/s)**	**79351**		**79325**	**88552**

Table 7-2 Calculated discharges through Gap 1

The calculated discharge through Gap 1 with the storage area approach is one third smaller than the calculated discharge with EFD.lab. The calculate discharge with the EFD.lab model is the discharge through the total outflow plane and not only the discharge through the centre line of the closure gap.

8 Conclusions and recommendations

8.1 Conclusions

In order to summarise the conclusions in a clarifying way, they have been organized according to the different models. Some general conclusions that answer the research objectives are given as well. The conclusions are based on the executed research in which only a limited number of EFD.lab calculations have been executed on one geometry.

8.1.1 General conclusions

- The EFD.lab model calculations results are according expectancy in the qualitative way. The calculated flow pattern gives a reasonable comparison with the real situation. The locations of the separation points of the flow, the turbulent intensities and the contraction of the flow are calculated according expectancy. In the quantitative way, the results are not accurate yet and more research has to be executed.
- Before the EFD.lab model can be used for stability calculations on bottom protections, more need to be known about the accuracy of the results concerning the turbulent parameters but for a first estimate of the flow pattern through a closure gaps the EFD.lab model may by suitable.
- The adaptation of the water level, by means of the pressure ceiling, is not very efficient and the influence of the imposed pressure ceiling at the location where the flow becomes supercritical is yet indistinct.

8.1.2 Storage area approach

- The water level prediction at the seaside of the dam, which is created with the prediction for the water levels in the Gunsan Outer Port, gives a water level during high water that is too high and a water level during low water that is too low, compared with measurements executed at the project location. The storage area approach gives a water level prediction inside the basin that is too high during high water and too low during low water.
- The calculated water level difference between the seaside and the basin side of the dam does not differ much with the measured water level difference.
- The calculated flow velocity through the closure gaps corresponds reasonably well with the measured flow velocities.
- The result of the storage area approach gives a reasonably accurate first estimate of the flow velocity through the closure gap. When the seaside water level at the project location is known, the calculation of the basin side water level will be reasonable accurate as well.

8.1.3 Waqua model

- The prediction of the tidal wave, which is created with four constituents, and has been used for the initiation of the Waqua model, differs with the predicted water level in the Gunsan Outer Port.

8.1.4 EFD.lab model

- In a scaled model, scaling the gravitational acceleration during a calculation keeps the Froude number constant during the calculation. This implies that the results do not have to be scaled afterwards. Changing of the gravitational acceleration does not influence the results of the calculation.

- The flow above the sill became supercritical. It was not possible to match the pressure ceiling with the calculated pressure at this location. Therefore, the imposed water level is located at a higher level then the calculated water level at this location. This may cause a higher flow velocity at this location.

- Changing the turbulent parameters at the model boundaries does change the turbulence in the fluid flow. The turbulent velocity fluctuations are lower when the turbulent parameters at the model boundaries are also lower.

- When the overall start values for the turbulence parameters as well as the turbulent parameters at the model boundaries are adapted, the results of the calculation no longer give explicably results. The maximum mean flow velocity becomes higher and turbulent velocity fluctuations are perceived at locations where they are not expected, namely in the acceleration area above the sill.

- Discharges calculated with the storage area approach and the EFD.lab model do not correspond. The calculated discharge with the storage area approach is one third smaller than the calculated discharge with the EFD.lab model. The EFD.lab model has calculated the discharge at the total outflow plane so this can be influenced by flows that enter via the outflow plane.

- It is not possible to execute post-processing without using the implemented graphic tools. Only at lines through the model, numerical results can be subtracted from the EFD.lab model.

8.2 Recommendations

During the execution of this research, some aspects have not been treated or were not fully investigated yet. Recommendations for further research are formulated here. For the surveyability the recommendations have been listed point by point.

- The results of EFD.lab calculations for situations with a free surface flow should be compared with measurements so the accuracy of the results can be defined.
- The Waqua calculations should be executed with a prediction of the water level at the boundary of the model created with all the tidal constituents for a more accurate result.
- The results of the Waqua calculations should be compared with the measurements. Only when the predicted water level at several locations correspond with the measured water level, the water level course through the closure gap can be used as an input for the EFD.lab model.
- The influence at the results of the calculation of the supercritical flow above the sill has to be investigated, because this phenomena may influence the accuracy of the model results for the mean flow velocity.
- The influence on the calculation results of changing the turbulence properties should be investigated for a simple geometry for which turbulent measurements are available as well.

- Because scaling the model appeared to have no influence on the results, a larger area should be modelled such that the influence of the walls on the flow pattern through the closure gap becomes less.
- New calculations should be executed using the results of the Waqua model as input for the water level.

9 References

D'ANGREMOND, K. AND VAN ROODE, F.C. (2001) Breakwaters and closure dams, engineering the interface of soil and water 2, *DUP Blue Print, Delft*

BATTJES, J.A. (2001) Vloeistofmechanica. *Course notes for the course CT2100, Technical University Delft*

CHANSON, H. (1999) The hydraulics of open channel flow: an introduction. *Elsevier Butterworth-Heinemann, Oxford*

CHOI, B.H. AND HONG, S.J. (2005) Modelling of tides in the Yellow Sea and the east China Sea using dynamically interfaced nested tidal model

DALRYMPLE, R.A. (1985) Physical modeling in coastal engineering. *A.A.Balkema, Rotterdam*.

DIJKZEUL, J.C.M., KLATTER, H.E., THABET, R.A.M. AND HARTSUIKER, G. (1988) Storm surge barrier Eastern Scheldt, Evaluation of water movement studies for design and execution of the barrier. *Delft Hydraulics, Delft*

EO, D.S. AND KIM, J.S. (2003) Hydraulic studies and engineering application for Saemangeum project. *Proceedings Hydro-environmental impacts of large coastal developments, Seoul*, 11-24

H.R.WALLINGFORD, (2002) Computational and physical modelling on Samenageum closure works

H.R.WALLINGFORD, (2005) Engineering review on the final closure of Samenageum dike

HUIS IN 'T VELD, J.C., STUIP, J., WALTHER, A.W. AND VAN WESTEN, J.M. (1987) The closure of tidal basins, closing of estuaries, tidal inlets and dike breaches, *Delft University Press, Delft*

MCQUIVEY, R.S. AND RICHARDSON, E.V. (1969) Some turbulence measurements in open channel flow *Journal of Hydr. Div. ASCE, Volume 95 number hy1*

MILLER, D.S. (1994) Discharge characteristics. *A.A.Balkema, Rotterdam.*

MOHAMMADI, B. AND PIRONNEAU, O. (1994) Analysis of the k-epsilon turbulence model. *John Wiley & Sons and Masson, Chichester and Paris*

NIEUWSTADT, F.T.M. (1998) Turbulentie, inleiding in de theorie en toepassingen van turbulente stromingen. *Epsilon Uitgaven, Utrecht.*

SCHIERECK, G.J. (2001) Introduction to bed, bank and shore protection. *Delft University Press, Delft*

SCHWANENBERG, D. AND JAGERS, B. (2003) CFD for hydraulic structures. *WL/Delft Hydraulics, Delft*

TENNEKES, H. AND LUMLEY, J.L. (1972) A first course in turbulence. *The Massachusetts Institute of Technology Press, Massachusetts*

UIJTTEWAAL, W. (2006) Turbulence in hydraulics. *Course notes for the course CT5312, Technical University Delft*

VERSTEEG, H.K. AND MALALASEKERA, W. (1995) An introduction to computational fluid dynamics, the finite volume method. *Addison Wesley Longman Limited, Harlow*

WATERLOOPKUNDIG LABORATORIUM (1986), Stormvloedkering Oosterschelde, oriënterend onderzoek naar de turbulentie structuur in de monding van de Oosterschelde, *Waterloopkundig laboratorium*

WATERLOOPKUNDIG LABORATORIUM (1980), Stormvloedkering Oosterschelde, turbulentie metingen in de monding van de Oosterschelde, *Waterloopkundig laboratorium*

WILCOX, D.C. (1993) Turbulence modeling for CFD, *DCW Industries, La Cañada*

ZIJLEMA, M. (1996) Computational modeling of turbulent flow in general domains. *Technische Universiteit Delft, Delft*

USER MANUAL EFD.LAB

USER MANUAL WAQUA

USER MANUAL DELFT3D

www.fluent.com/about/cfdhistory.htm

www.wikipedia.com

www.efdlab.com

www.getij.nl

List of Appendices

Appendix I.   List of Korean signs

The following list contains the most important Korean signs and the English translation.

Most important Korean signs and the English translation

Appendix II.   Turbulence and turbulence modelling

Almost all flows in nature and in the world of civil engineering are turbulent flows. A flow is called turbulent when the dimensionless Reynolds number (*Re=UL/v*) is larger than 1000. This Reynolds number can be expressed as a ratio between the non-linear advection term and the diffusion term. When the Reynolds number is smaller than 1000 the flow is laminar. This can be seen as an exception. In a laminar flow, the viscous forces dominate over the inertial forces.

Because of the huge complexity, it is not possible to give a precise definition of turbulence. It is however possible to point some of the essential qualities of turbulence [Tennekes 1972]

- Irregularity: Turbulent flows are irregular and therefore a deterministic approach is not possible and one has to use statistical methods.
- Diffusivity: The diffusivity of a turbulent flow takes care of the rapid mixing and a large transport of momentum, mass and heat. A flow that looks random but that does not spread velocity fluctuations in the surrounding fluid is definitely not a turbulent flow.
- Large Reynolds numbers: a high Reynolds number characterizes a turbulent flow. Instability in the laminar flow often leads to a turbulent flow, in which the viscous forces are subordinate to the inertial forces.
- Three dimensional vorticity fluctuations: Turbulence is rotational and three dimensional, this means that the random vorticity fluctuations can maintain themselves. This would not be the case if the velocity fluctuations were two-dimensional because vortex stretching is absent in two-dimensional flows.
- Dissipation: Turbulent motions are always dissipative. Viscous shear stresses increase the internal energy of the fluid at expense of the kinetic energy of the turbulence. The energy present in the turbulent motions comes from the mean flow, when no energy is supplied anymore, turbulence decays very fast.
- Continuum: For turbulence, the length and time scales are far larger than those of the molecular scale. Turbulent motion can therefore be considered as continuum and can be described with the equations of motion for a fluid
- Turbulent flows are flows: Turbulence depends on the flow and not on the fluid. Every fluid can flow in a turbulent way; the characteristics of turbulence are not controlled by the molecular properties of the fluid but by the flow characteristics.

When instabilities arise in laminar flows at large Reynolds numbers, turbulence appears, but to maintain the turbulence, energy from the environment is necessary. Often the turbulent motions gain energy from the shear in the mean motion. When there is no energy source available for the turbulence, it shall decay rapidly. By turbulent fluctuations, a turbulent shear stress is induced in the presence of a velocity gradient. This provides the conditions for energy transfer.

Free turbulence is developed in those places where two fluid layers meet and where these two layers of the fluid have different velocities. Between those two layers a mixing layer develops in which the transfer of momentum and energy takes place.

Wall turbulence can develop near a wall if the Reynolds number is sufficiently high.

A third form of turbulence is grid turbulence. This kind of turbulence is generated in laboratory, has therefore favourable properties, and can be used for the verification of all kind of turbulence models.

To solve the Reynolds equations, it is necessary to relate the Reynolds stresses to the mean flow. This is the crux of turbulence modelling. Such an extra set of equations is a turbulence

model. It is, for most of the engineering purposes, not necessary to solve all the details of the turbulent fluctuations. It is enough to know the influences of these turbulent fluctuations on the mean motion. Turbulence models can be divided in two main groups: Classical models and Large Eddy Simulation models. The main difference between these two groups of models is that all the Classical models are based on the time average Reynolds equations and the Large Eddy Simulation models use space-filtered equations. Classical models can be classified as outlined in the following table.

Classical model	
1: one-equation model	Mixing length model
2: two-equation model	k-ε model
3: Reynolds stress equation model	
4: algebraic stress model	

Mixing length model
The largest eddies in a turbulent flow transport and take care of exchange of kinetic energy in turbulent motions. When a strong relation between the mean flow and the behaviour of the largest eddies is assumed, the characteristic velocity scale of the eddies can be linked with the mean flow properties.

From dimensional analyses, it can be stated that the turbulent eddy viscosity can be expressed as the product of the density ρ, a turbulent length scale l and a turbulent velocity scale v_{mix} and a dimensionless constant C.

$$\mu_t = C\rho l v_{mix}$$

This mixing velocity scale can be expressed via dimension analysis and the assumption that there is only one significant velocity gradient:

$$\frac{\partial U}{\partial y}$$

The turbulent velocity scale can then be expressed as follows, taking into account that the mixing length scale l is not a physical property of the fluid so the dimensionless constant C can be adapted in the mixing length scale which changes now into l_{mix}.

$$v_{mix} = l_{mix}\left|\frac{\partial U}{\partial y}\right|$$

The absolute value of the velocity gradient is taken to make sure the velocity scale is always positive irrespective to the sign of the velocity gradient. Now the turbulent eddy viscosity can be described in the following way

$$\mu_t = \rho l_{mix}^2 \left| \frac{\partial U}{\partial y} \right|$$

This is the Prandtl mixing length model.

Now it is a problem to determine the mixing length scale l_{mix}. This mixing length scale is not a fluid property but depends on the flow properties and the kind of turbulence. The following table gives some examples of how to compute such a mixing length scale.

Flow	Mixing length l$_{mix}$	L
Mixing layer	0.07L	Layer width
Jet	0.09L	Jet half width
Wake	0.16L	Wake half width
Boundary layer ($\delta p/\delta x=0$) • viscous sub layer and log-law layer (y/L$\leq$ 0.22) • outer layer (y/L$\geq$ 0.22)	Ky[1-exp(-y$^+$/26)] 0.09L	Boundary layer thickness
Pipes and channels	L[0.14-0.08(1-y/L)^2-0.06(1-y/L)^4]	Pipe radius or channel half width

Table Mixing lengths for two-dimensional flows
Source: Rodi 1980

The mixing length model is easy to implement and cheap in terms of computing resources. Another advantage is that the predictions are good for tin shear layers as jet, mixing layers and wakes. One major disadvantage is that the mixing model is completely incapable of describing a flow with separation and recirculation phenomena. The mixing length model only calculates the mean flow properties and the turbulent shear stress. [Tennekes 1972], [Wilcox 1993], [Versteeg 1995], [W.Uijttewaal 2006]

k-ε model
The most wide spread two equation turbulence model nowadays is the k-ε model. The model focuses on the mechanism that affects the kinetic energy by introducing two extra equations; one for the turbulent kinetic energy k, and one for the rate of dissipation of turbulent energy, ε. The standard k- ε model is introduced by Launder and Spalding [1972] and governs two transport equations for k and ε, based on the understanding of the relevant processes that instigate changes in these parameters.
The parameters k and ε can be used to define a velocity scale v_{mix} and a length scale l, which represents the large scale turbulent eddies, as follows:

Velocity scale: $\quad v_{mix} = k^{\frac{1}{2}}$

Length scale: $\quad l = \frac{k^{\frac{3}{2}}}{\varepsilon}$

Where:

k = turbulent kinetic energy (J/kg)

ε = turbulent dissipation rate (W/kg)

As explained in the chapter about the mixing length model (2.3.4) the turbulent eddy viscosity can be expressed in term of the velocity scale and the length scale as follows:

$$\mu_t = C\rho l v_{mix} = \rho C_\mu \frac{k^2}{\varepsilon}$$

In which C_μ is a dimensionless constant.

The equations for the transport of turbulent kinetic energy k and the transport of turbulent dissipation ε can now be subscribed in the following way:

$$\rho \frac{\partial k}{\partial t} + \rho \boldsymbol{u} \nabla k = \frac{\rho C_\mu}{\sigma_k} \nabla (\mu_t \nabla k) + 2\mu_t E_{ij} . E_{ij} - \rho \varepsilon$$

$$\rho \frac{\partial \varepsilon}{\partial t} + \rho \boldsymbol{u} \nabla \varepsilon = \frac{\rho C_\mu}{\sigma_\varepsilon} \nabla (\mu_t \nabla \varepsilon) + C_{1\varepsilon} \frac{\varepsilon}{k} 2\mu_t E_{ij} . E_{ij} - C_{2\varepsilon} \rho \frac{\varepsilon^2}{k}$$

In the above two equations the first term is the rate of change, the second term the transport of k or ε by convection, the third term is transport of k or ε by diffusion, the fourth term is the rate of production and the last term is the rate of destruction. There are five adjustable constants for which empirical values have been determined as follows:

C_μ = 0.09

σ_k = 1.00

σ_ε = 1.30

$C_{1\varepsilon}$ = 1.44

$C_{2\varepsilon}$ = 1.92

Appendix III.   RGF file of Waqua computational grid

(Only the ETA=1 and ETA=2 , of total 308 ETA, for both x- and y-direction are printed)

```
*
* WL | Delft Hydraulics, Delft3D-RGFGRID, Version 4.13.03.00; Dec 2005
* File creation date: 11:25:09, 10-10-2006
*
Coordinate System = Cartesian
     181     307
 0 0 0

 ETA=    1             0,00        0,00        0,00        0,00        0,00
                       0,00        0,00        0,00        0,00        0,00
                       0,00        0,00        0,00        0,00        0,00
                       0,00        0,00        0,00        0,00        0,00
                       0,00        0,00        0,00        0,00        0,00
                       0,00        0,00        0,00        0,00        0,00
                       0,00        0,00        0,00        0,00        0,00
                       0,00        0,00        0,00        0,00        0,00
                       0,00        0,00        0,00        0,00        0,00
                       0,00        0,00        0,00        0,00        0,00
                       0,00        0,00        0,00        0,00        0,00
                       0,00        0,00        0,00        0,00        0,00
                  278589,99   278499,97   278395,15   278283,43   278167,74
                  278049,51   277929,19   277806,59   277681,48   277553,93
                  277424,24   277292,60   277159,18   277024,34   276888,98
                  276754,52   276622,28   276492,78   276365,79   276240,73
                  276117,04   275994,17   275871,63   275748,93   275625,54
                  275501,50   275376,87   275251,90   275126,96   275002,41
                  274878,55   274755,49   274633,19   274511,38   274389,65
                  274267,38   274143,71   274017,57   273887,81   273753,80
                  273616,15   273477,57   273342,85   273217,48   273104,03
                  272997,31   272883,54   272747,94   272586,03   272407,23
                  272227,95   272062,27   271916,07   271787,06   271669,83
                  271558,20   271443,99   271318,04   271175,86   271022,73
                  270869,48   270720,65   270570,74   270412,98   270246,19
                  270073,44   269898,44   269723,73   269550,40   269378,43
                  269206,73   269032,91   268853,10   268662,36   268455,80
                  268229,89   267982,98   267714,27   267421,80   267100,57
                  266741,95   266335,02   265868,85   265335,36   264731,89
                  264062,74   263339,70   262578,92   261745,62   260895,11
                  260027,10   259121,97   258154,49   257111,17   256013,93
                  254915,64   253803,22   252670,99   251501,78   250274,45
                  248950,98   247561,59   246147,96   244724,02   243285,56
                  241825,55   240327,90   238774,56   237159,73   235487,97
                  233771,19   232023,90   230258,79   228481,27   226688,91
                  224873,32   223024,89   221137,48   219214,21   217273,13
                  215368,84
 ETA=    2             0,00        0,00        0,00        0,00        0,00
                       0,00        0,00        0,00        0,00        0,00
                       0,00        0,00        0,00        0,00        0,00
                       0,00        0,00        0,00        0,00        0,00
                       0,00        0,00        0,00        0,00        0,00
                       0,00        0,00        0,00        0,00        0,00
                       0,00        0,00        0,00        0,00        0,00
                       0,00        0,00        0,00        0,00        0,00
                       0,00        0,00        0,00        0,00        0,00
                       0,00        0,00        0,00        0,00        0,00
```

0,00	0,00	0,00	0,00	0,00
0,00	0,00	0,00	0,00	0,00
278483,11	278406,55	278315,87	278217,25	278113,22
278005,15	277893,61	277778,59	277660,02	277538,08
277413,13	277285,41	277155,25	277023,19	276890,28
276758,07	276627,91	276500,36	276375,20	276251,85
276129,73	276008,30	275887,06	275765,55	275643,20
275520,08	275396,27	275272,03	275147,72	275023,70
274900,26	274777,54	274655,46	274533,79	274412,12
274289,83	274166,08	274039,81	273909,93	273775,82
273638,13	273499,59	273364,88	273239,40	273125,60
273018,31	272903,80	272767,49	272605,09	272426,14
272246,92	272081,30	271934,94	271805,52	271687,65
271575,23	271460,15	271333,37	271190,46	271036,78
270883,09	270733,85	270583,51	270425,32	270258,15
270085,01	269909,61	269734,42	269560,50	269387,80
269215,21	269040,35	268859,33	268667,25	268459,25
268231,83	267983,38	267713,12	267419,13	267096,40
266736,39	266328,24	265861,13	265327,10	264723,49
264054,55	263331,96	262571,98	261740,51	260891,43
260024,41	259119,93	258153,21	257110,78	256014,50
254916,63	253804,38	252672,34	251503,69	250276,57
248953,44	247564,68	246151,64	244728,21	243290,08
241830,12	240332,18	238778,39	237163,02	235490,84
233773,62	232026,04	230260,63	228483,01	226690,56
224875,07	223026,76	221139,57	219216,17	217271,55

ETA=	1					
		0,00	0,00	0,00	0,00	0,00
		0,00	0,00	0,00	0,00	0,00
		0,00	0,00	0,00	0,00	0,00
		0,00	0,00	0,00	0,00	0,00
		0,00	0,00	0,00	0,00	0,00
		0,00	0,00	0,00	0,00	0,00
		0,00	0,00	0,00	0,00	0,00
		0,00	0,00	0,00	0,00	0,00
		0,00	0,00	0,00	0,00	0,00
		0,00	0,00	0,00	0,00	0,00
		0,00	0,00	0,00	0,00	0,00
		0,00	0,00	0,00	0,00	0,00
		4000137,99	4000137,69	4000137,35	4000136,98	4000136,61
		4000136,22	4000135,82	4000135,42	4000135,01	4000134,60
		4000134,17	4000133,74	4000133,31	4000132,86	4000132,42
		4000131,98	4000131,55	4000131,13	4000130,71	4000130,30
		4000129,90	4000129,49	4000129,09	4000128,69	4000128,29
		4000127,88	4000127,47	4000127,07	4000126,66	4000126,25
		4000125,84	4000125,44	4000125,04	4000124,64	4000124,25
		4000123,85	4000123,44	4000123,03	4000122,60	4000122,16
		4000121,71	4000121,26	4000120,82	4000120,41	4000120,04
		4000119,69	4000119,32	4000118,87	4000118,34	4000117,76
		4000117,17	4000116,63	4000116,15	4000115,73	4000115,35
		4000114,98	4000114,61	4000114,20	4000113,73	4000113,23
		4000112,73	4000112,24	4000111,75	4000111,24	4000110,69
		4000110,12	4000109,55	4000108,98	4000108,41	4000107,85
		4000107,29	4000106,72	4000106,13	4000105,51	4000104,83
		4000104,09	4000103,29	4000102,41	4000101,45	4000100,40
		4000099,23	4000097,89	4000096,37	4000094,62	4000092,65
		4000090,46	4000088,09	4000085,61	4000082,88	4000080,10
		4000077,26	4000074,30	4000071,13	4000067,72	4000064,13
		4000060,54	4000056,90	4000053,19	4000049,37	4000045,35
		4000041,02	4000036,48	4000031,85	4000027,19	4000022,49
		4000017,71	4000012,81	4000007,73	4000002,45	3999996,98

```
                3999991,36    3999985,64    3999979,87    3999974,05    3999968,19
                3999962,25    3999956,20    3999950,03    3999943,74    3999937,39
                3999931,16
ETA=     2          0,00          0,00          0,00          0,00          0,00
                    0,00          0,00          0,00          0,00          0,00
                    0,00          0,00          0,00          0,00          0,00
                    0,00          0,00          0,00          0,00          0,00
                    0,00          0,00          0,00          0,00          0,00
                    0,00          0,00          0,00          0,00          0,00
                    0,00          0,00          0,00          0,00          0,00
                    0,00          0,00          0,00          0,00          0,00
                    0,00          0,00          0,00          0,00          0,00
                    0,00          0,00          0,00          0,00          0,00
                    0,00          0,00          0,00          0,00          0,00
                    0,00          0,00          0,00          0,00          0,00
                3999135,45    3999138,90    3999142,58    3999146,04    3999149,13
                3999151,79    3999154,00    3999155,77    3999157,09    3999157,99
                3999158,47    3999158,59    3999158,37    3999157,87    3999157,08
                3999156,03    3999154,72    3999153,16    3999151,36    3999149,32
                3999147,06    3999144,58    3999141,89    3999139,00    3999135,92
                3999132,67    3999129,28    3999125,75    3999122,13    3999118,44
                3999114,71    3999110,97    3999107,22    3999103,48    3999099,75
                3999096,03    3999092,30    3999088,54    3999084,72    3999080,83
                3999076,88    3999072,94    3999069,13    3999065,62    3999062,50
                3999059,66    3999056,75    3999053,45    3999049,67    3999045,59
                3999041,55    3999037,83    3999034,59    3999031,83    3999029,45
                3999027,32    3999025,32    3999023,29    3999021,17    3999019,05
                3999017,04    3999015,19    3999013,41    3999011,64    3999009,86
                3999008,11    3999006,44    3999004,89    3999003,50    3999002,29
                3999001,30    3999000,55    3999000,10    3998999,98    3999000,28
                3999001,12    3999002,60    3999004,83    3999007,94    3999012,11
                3999017,56    3999024,58    3999033,40    3999044,11    3999056,54
                3999070,24    3999084,60    3999098,84    3999112,21    3999123,14
                3999132,18    3999140,01    3999146,84    3999152,28    3999155,79
                3999157,67    3999158,81    3999159,46    3999159,05    3999157,51
                3999155,02    3999150,88    3999144,72    3999136,70    3999127,27
                3999117,22    3999107,42    3999098,55    3999091,08    3999085,19
                3999080,81    3999077,73    3999075,71    3999074,46    3999073,57
                3999072,55    3999070,91    3999068,27    3999064,81    3999062,77
                3999075,82
```

Appendix IV.   Waqua input file

```
#SAEMANGEUM PROJECT
#
#TUDELFT
#
#Made by Maartje van der Sande
#
#
#model input file: siminp.saem
#calculation for water level in Saemangeum estuary
#
#


IDENTification


 WAQUA
 EXPERIMENT= 'Saemangeum1' OVERWRITE
 MODID= 'Saeman'
 TITLE= 'Saemangeum'


##end IDENTIFICATION


#DEPTH_CONtrol
 #ORIENtation= 'pos_upwards'


MESH


 GRID
  AREA
   MMAX= 182 , NMAX=308
  CURVilinear
   RGFfile= 'rgf.saem'
 POINTS
    # for dike section 1
 P 1=(M=101, N=275, NAME= 'P1')
 P 2=(M=101, N=274, NAME= 'P2')
 P 3=(M=99, N=274,  NAME= 'P3')
 P 4=(M=99, N=273, NAME= 'P4')
 P 5=(M=92, N=273, NAME= 'P5')
 P 6=(M=92, N=272, NAME= 'P6')
 P 7=(M=85, N=272, NAME= 'P7')
 P 8=(M=85, N=271, NAME= 'P8')
 P 9=(M=84, N=271, NAME= 'P9')
 P 10=(M=84, N=267, NAME= 'P10')
 P 11=(M=85, N=267, NAME= 'P11')
 P 12=(M=85, N=267, NAME= 'P12')
 P 13=(M=87, N=264, NAME= 'P13')
 P 14=(M=87, N=256, NAME= 'P14')
 P 15=(M=88, N=256, NAME= 'P15')
 P 16=(M=88, N=252, NAME= 'P16')
 P 17=(M=90, N=252, NAME= 'P17')
 P 18=(M=90, N=243, NAME= 'P18')
 P 19=(M=92, N=243, NAME= 'P19')
 P 20=(M=92, N=239, NAME= 'P20')
 P 21=(M=94, N=239, NAME= 'P21')
 P 22=(M=94, N=233, NAME= 'P22')
 P 23=(M=97, N=233, NAME= 'P23')
 P 24=(M=97, N=227, NAME= 'P24')
 P 25=(M=99, N=227, NAME= 'P25')
```

```
P 26=(M=99, N=225, NAME= 'P26')
   # for dike section 2
P 27=(M=99, N=205, NAME= 'P27')
P 28=(M=99, N=203, NAME= 'P28')
P 29=(M=101, N=203, NAME= 'P29')
P 30=(M=101, N=188, NAME= 'P30')
P 31=(M=102, N=188, NAME= 'P31')
P 32=(M=102, N=179, NAME= 'P32')
P 33=(M=103, N=179, NAME= 'P33')
P 34=(M=103, N=170, NAME= 'P34')
P 35=(M=105, N=170, NAME= 'P35')
P 36=(M=105, N=165, NAME= 'P36')
P 37=(M=107, N=165, NAME= 'P37')
P 38=(M=107, N=155, NAME= 'P38')
   # for dike section 3
P 39=(M=107, N=131, NAME= 'P39')
P 40=(M=107, N=118, NAME= 'P40')
P 41=(M=105, N=118, NAME= 'P41')
P 42=(M=105, N=116, NAME= 'P42')
P 43=(M=103, N=116, NAME= 'P43')
P 44=(M=103, N=106, NAME= 'P44')
P 45=(M=100, N=106, NAME= 'P45')
P 46=(M=100, N=105, NAME= 'P46')
P 47=(M=98, N=105, NAME= 'P47')
P 48=(M=98, N=101, NAME= 'P48')
P 49=(M=96, N=101, NAME= 'P49')
P 50=(M=96, N=97, NAME= 'P50')
P 51=(M=94, N=97, NAME= 'P51')
P 52=(M=94, N=80, NAME= 'P52')
P 53=(M=91, N=80, NAME= 'P53')
P 54=(M=91, N=69, NAME= 'P54')
P 55=(M=87, N=69, NAME= 'P55')
P 56=(M=87, N=50, NAME= 'P56')
P 57=(M=82, N=50, NAME= 'P57')
P 58=(M=82, N=46, NAME= 'P58')
P 59=(M=78, N=46, NAME= 'P59')
P 60=(M=78, N=36, NAME= 'P60')
P 61=(M=72, N=36, NAME= 'P61')
P 62=(M=72, N=31, NAME= 'P62')
P 63=(M=68, N=31, NAME= 'P63')
P 64=(M=68, N=27, NAME= 'P64')
P 65=(M=65, N=27, NAME= 'P65')
P 66=(M=65, N=26, NAME= 'P66')
P 67=(M=57, N=26, NAME= 'P67')
P 68=(M=57, N=25, NAME= 'P68')
P 69=(M=54, N=25, NAME= 'P69')
P 70=(M=54, N=24, NAME= 'P70')
P 71=(M=48, N=24, NAME= 'P71')
P 72=(M=48, N=23, NAME= 'P72')
P 73=(M=45, N=23, NAME= 'P73')
 # water level points
  #centre line GAP1
P 74=(M=104, N=215, NAME= 'P74')
P 75=(M=103, N=215, NAME= 'P75')
P 76=(M=102, N=215, NAME= 'P76')
P 77=(M=101, N=215, NAME= 'P77')
P 78=(M=100, N=215, NAME= 'P78')
P 79=(M=99, N=215, NAME= 'P79')
P 80=(M=98, N=215, NAME= 'P80')
P 81=(M=97, N=215, NAME= 'P81')
P 82=(M=96, N=215, NAME= 'P82')
```

```
P 83=(M=95, N=215, NAME= 'P83')
P 84=(M=94, N=215, NAME= 'P84')
P 85=(M=93, N=215, NAME= 'P85')
P 86=(M=103, N=215, NAME= 'P86')
  #centre line GAP2
P 87=(M=119, N=138, NAME= 'P87')
P 88=(M=118, N=138, NAME= 'P88')
P 89=(M=117, N=138, NAME= 'P89')
P 90=(M=116, N=138, NAME= 'P90')
P 91=(M=115, N=138, NAME= 'P91')
P 92=(M=114, N=138, NAME= 'P92')
P 93=(M=113, N=138, NAME= 'P93')
P 94=(M=112, N=138, NAME= 'P94')
P 95=(M=111, N=138, NAME= 'P95')
P 96=(M=110, N=138, NAME= 'P96')
P 97=(M=109, N=138, NAME= 'P97')
P 98=(M=108, N=138, NAME= 'P98')
P 99=(M=107, N=138, NAME= 'P99')
P 100=(M=106, N=138, NAME= 'P100')
P 101=(M=105, N=138, NAME= 'P101')
P 102=(M=104, N=138, NAME= 'P102')
P 103=(M=103, N=138, NAME= 'P103')
P 104=(M=102, N=138, NAME= 'P104')
P 105=(M=101, N=138, NAME= 'P105')
P 106=(M=100, N=138, NAME= 'P106')
P 107=(M=99, N=138, NAME= 'P107')
P 108=(M=98, N=138, NAME= 'P108')
P 109=(M=97, N=138, NAME= 'P109')
P 110=(M=96, N=138, NAME= 'P110')
P 111=(M=95, N=138, NAME= 'P111')
  #measuring points 4 location dike
P 112=(M=101, N=203, NAME= 'P112')
P 113=(M=98, N=203, NAME= 'P113')
P 114=(M=109, N=157, NAME= 'P114')
P 115=(M=105, N=157, NAME='P115')
  #tidal points for check
P 116=(M=154, N=74, NAME='P116')
P 117=(M=142, N=136, NAME='P117')
P 118=(M=157, N=285, NAME='P118')
P 119=(M=169, N=281, NAME='P119')
P 120=(M=44, N=16, NAME='P120')
P 121=(M=30, N=13, NAME='P121')
P 122=(M=60, N=20, NAME='122')
P 123=(M=141, N=140, NAME='123')
P 124=(M=38, N=13, NAME='124')
  #begin and end point open boundary
P 125=(M=182, N=2, NAME='P125')
P 126=(M=182, N=307, NAME='P126')
  #Sluice complex points
P 127=(M=94, N=235, NAME='P127')
P 128=(M=94, N=238, NAME='P128')
P 129=(M=107, N=123, NAME='P129')
P 130=(M=107, N=126, NAME='P130')

CURVES
  # GAP1
C 1=LINE(P 26,P 27, NAME='GAP1')
  # GAP2
C 2=LINE(P 38,P 39, NAME='GAP2')
  #for output
C 3=LINE( P 74, P 86, NAME='centreline GAP1')
```

```
  C 4=LINE( P 87, P 111, NAME='centreline GAP2')
   # for sluices
  C 5=LINE(P 127, P 128, NAME='Gareyok sluice')
  C 6=LINE(P 129, P 130, NAME='Sinsi sluice')

 BOUNdaries
  ENCLosures

E=(182,1),(182,307),(101,307),(101,297),(47,297),(47,289),(101,289),(101,275),(1,275),
(1,190),(2,190),(2,185),(3,185),(3,175),(13,175),(13,155),(17,155),(17,135),(21,135),(
21,115),
(25,115),(25,95),(13,95),(13,75),(6,75),(6,35),(41,35),(41,31),(45,31),
(45,16),(29,16),(29,12),(61,12),(61,1),(182,1)
  OPENings
   OPEN 1=LINE(P 125, P 126, NAME='tidal forcing')
  BARriers
   B 1: C 1
   B 2: C 2
   B 3: C 5
   B 4: C 6

 BATHYMETRY
  GLOBAL
   LAYOUT=2
   #DEPMultipl=1.00, THREshold=0.0, LAYOUT=2
   METH_DPS = 'MEAN_DPD'
  LOCAL
   BOX MNMN=( 1, 1) ( 182, 308)
   VARIABLE_values= 999 999 999 999 999 999 999 999 999 999 999 999
999 999 999 999 999 999 999 999 999 999 999 999
999 999 999 999 999 999 999 999 999 999 999 999
999 999 999 999 999 999 999 999 999 999 999 999
999 999 999 999 999 999 999 999 999 999 999 999
9.2050266 9.2087667 9.2172208 9.2302314 9.2475899 9.269131 9.2948065 9.3247348
9.3592095 9.3986459 9.4434489 9.4938079
999 999 999 999 999 999 999 999 999 999 999 999
999 999 999 999 999 999 999 999 999 999 999 999
999 999 999 999 999 999 999 999 999 999 999 999
999 999 999 999 999 999 999 999 999 999 999 999
999 999 999 999 999 999 999 999 999 999 999 999
999 999 999 999 999 999 999 999 999 999 999 999
999 999 999 999 999 999 999 999 999 999 999 999
999 999 999 999 999 999 999 999 999 999 999 999
999 999 999 999 999 999 999 999 999 999 999 999
999 999 999 999 999 999 999 999 999 999 999 999
999 999 999 999 999 999 999 999 999 999 999 999
999 999 999 999 999 999 999 999 999 999 999 999
999 999 999 999 999 999 999 999 999 999 999 999
999 999 999 999 999 999 999 999 999 999 999 999
999 999

 DRYPOINTS
  DAMPoints
   COORDinates =
    # dam section1
   (101, 275) (101, 274)
   (99, 274) (99, 273)
   (92, 273) (92, 272)
   (85, 272) (85, 271)
```

```
   (84, 271) (84, 267)
   (85, 267) (85, 264)
   (87, 264) (87, 256)
   (88, 256) (88, 252)
   (90, 252) (90, 243)
   (92, 243) (92, 239)
   (94, 239) (94, 238)
   (94, 235) (94, 233)
   (97, 233) (97, 227)
   (99, 227) (99, 225)
   # dam section2
   (99, 205) (99, 203)
   (101, 203) (101, 188)
   (102, 188) (102, 179)
   (103, 179) (103, 170)
   (105, 170) (105, 165)
   (107, 165) (107, 155)
   # dam section3
   (107, 131) (107, 126)
   (107, 123) (107, 118)
   (105, 118) (105, 116)
   (103, 116) (103, 106)
   (100, 106) (100, 105)
   (98, 105) (98, 101)
   (96, 101) (96, 97)
   (94, 97) (94, 80)
   (91, 80) (91, 69)
   (87, 69) (87, 50)
   (82, 50) (82, 46)
   (78, 46) (78, 36)
   (72, 36) (72, 31)
   (68, 31) (68, 27)
   (65, 27) (65, 26)
   (57, 26) (57, 25)
   (54, 25) (54, 24)
   (48, 24) (48, 23)
   (45, 23)
  #sheet in u direction
   #CLOSEU
     #MNNLINE
 #WEIRS
    #W: #####insert weirs

## end MESH


GENERAL

 #DIFFusion
  #GLOBAL
   #LAYOUT = 1
   #CDCON = 0
   #CONST_values=###############
 PHYSICALparameters
  GRAVity = 9.813
  WATDENsity = 1023
  AIRDENsity = 1.2050
  DYNVISCOsity = 0.001
 ### WIND no wind influence
 ### SPACE_VAR_wind
 ### KALMAN
```

```
 ### CORIolis
 ### SPACE_DEP_CD

## end GENERAL


FLOW

 PROBlem
   TIMEFRame
    DATE = '14 MAR 2006'
    TSTART = 0
    TSTOP = 66240
   METHODvariables
    TSTEP = 10 ############
    CHECKCont = 'WL'
    ITERCON = 20
    ITERMOM = 2
    ITERACCuracy = 0.10E-04
   # ITERACCURVEL = ####
   # ITERACCURWL = ####
   # THETA = only in Triwaq
  SMOOTHING
   TLSMOOTH = 180.0
  DRYING
   CHECK_WL='YES'
   #IDRYflag = 1
   DEPCrit = 0.3
  FRICTION
   GLOBAL
    TICVal = 10
    FORMula = 'Manning'
   UDIRec
    GLOBAL
     CONST_value = 0.026
   VDIRec
    GLOBAL
     CONST_value = 0.026
  VISCOsity
   EDDYviscositycoeff = 1
  BARRIERcoefficients
   B 1: CONTRSUBcritical = 0.9 0.9
        CONTRSUPERcritical = 0.9 0.9
        REStricting = 0.9 0.9
   B 2: CONTRSUBcritical = 0.9 0.9
        CONTRSUPERcritical = 0.9 0.9
        REStricting = 0.9 0.9
   B 3: CONTRSUBcritical = 1 1
        CONTRSUPERcritical = 1 1
        REStricting = 1 1
   B 4: CONTRSUBcritical = 1 1
        CONTRSUPERcritical = 1 1
        REStricting = 1 1
  #DISCHARGEcoefficients
   #SCALE_model
   #COEFFicients
  #WEIRS
   #THETAC =
   #GROYNES_reduction_factor =
   #OTHERS_reduction_factor =
```

```
##end problem FLOW


FORCings

 INITial
  WATLEVel
   GLOBAL CONST_value = 2.0
  UVELOCity
   GLOBAL CONST_value = 0.0
  VVELOCity
   GLOBAL CONST_value = 0.0
 BOUNDAries
 B: OPEN 1
   BTYPE='wl'
   BDEF='Fourier'
   REFL=0
   SAME
 FOURier
 GENeral
   OMEGA = 1.40519 1.45444 0.067598 0.72919
 SERIES
  S:P 125 TID=0 AZERO=0
     AMPL = 1.082 1.02 0.197 0.321
     PHASE= 3.0530 4.63156 1.75749 2.4657
 BARRIERS
 B 1 : SILL_depth: INITial 10
       GATE_height INITial  5
       BARRIER_Width INITial  1
 B 2: SILL_depth:   INITial= 16.
      GATE_height   INITial= 5.
      BARRIER_Width INITial= 1.
 B 3: SILL_depth   INITial  6
      GATE_height   INITial  5
      BARRIER_Width INITial  1
 B 4: SILL_depth   INITial  6
      GATE_height   INITial  5
      BARRIER_Width INITial  1


 ## end forcings FLOW



 CHECKPoints
 LEVELStations
  # centre line gap1
  P 74, P 75, P 76, P 77, P 78, P 79, P 80, P 81, P 82, P 84, P 85, P86
  # centre line gap2
  P 87, P 88, P 89, P 90, P 91, P 92, P 93, P 94, P 95, P 96, P 97, P 98, P 99, P
100, P 101, P 102
  P 103, P 104, P 105, P 106, P 107, P 108, P 109, P 110, P 111
  # water level around dike section2
  P 112, P 113, P 114, P 115
  # tidal points
  P 116, P 117, P 118, P 119, P 120, P 121, P 122, P 123, P 124
 #CURRENtstations
  #P # etc
 USECTions
  C 1, C 2
 VSECTions
  C 3, C 4
```

```
 ## end checkpoints FLOW

## end FLOW


# No Transport
# No Densities
# No Turbulence_model
# No Displays

SDSOUTput

 MAPS
  TFMAPs = 0
  TIMAPs = 6600
  TLMAPs = 66000
 HISTories
  TFHISto = 0
  TIHISto = 10
  TLHISto = 66000

# end SDSoutput

PRINToutput
 CONTROL
  TPRINTMAP=(16560, 33120, 49680,66240)
  TFRAMEHIST=(0,30000, 60000)

# end Printoutput
```

Appendix V. Tidal constituents at 17 locations

Point	Coordinaten x	y	M2 Amplitude M2A	M2 Phase M2P	S2 Amplitude S2A	S2 Phase S2P	O2 Amplitude O1A	O2 Phase O1P	K2 Amplitude K1A	K2 Phase K1P	Name of Location □□□□
			m	°	m	°	m	°	m	°	
1	205572,453	3992797,750	1,099	183,573	1,124	271,603	0,197	106,528	0,324	147,422	o
2	203467,063	3959331,000	1,082	174,926	1,02	265,369	0,197	100,697	0,321	141,276	p
3	202868,109	3933972,500	1,085	168,326	0,951	259,9	0,198	96,221	0,323	136,524	q
4	257735,190	3971097,150	1,959	76,8	0,791	125,3	0,246	244,1	0,323	272,3	maldo
5	266267,130	3965223,330	1,96	73,1	0,69	116,9	0,248	236,3	0,334	264,6	sunyoodo
6	255733,240	3944874,400	1,997	67,97	0,726	117,89	0,253	244,58	0,339	265,85	weedo
7	239286,940	3947469,210	1,821	69,7	0,596	112,4	0,261	237,3	0,292	261,2	HaWangdung-do
8	286589,220	3982840,810	2,201	82,2	0,816	126,3	0,262	343,9	0,344	272	gunsan Outer port
9	297283,020	3987860,250	1,923	95,5	0,663	147,6	0,24	246,2	0,332	297,8	gumgang
10	279071,050	3982934,000	2,166	79,2	0,847	120,8	0,255	246	0,36	268,7	Oshick do
11	291186,580	3986430,590	2,192	88,9	0,633	132,9	0,269	242,1	0,314	274	Janghang Port
12	266588,790	3964844,760	1,965	73,1	0,69	116,9	0,248	236,3	0,334	264,6	□□□□□□
13	291156,560	3986431,310	2,192	88,9	0,633	132,9	0,269	212,1	0,314	274	□颯□
14	286560,080	3982878,520	2,201	82,2	0,816	126,3	0,262	343,9	0,344	272	□□□·ヮヌラ
15	207776,000	3977563,500	1,104	179,708	1,09	268,628	0,198	103,777	0,325	144,524	50
16	212635,063	3951046,500	1,118	173,02	1,032	263,111	0,202	98,944	0,33	139,432	67
17	201612,406	3921536,500	1,062	164,458	0,886	257,264	0,199	93,525	0,323	133,638	68

Water level at all locations in computational grid
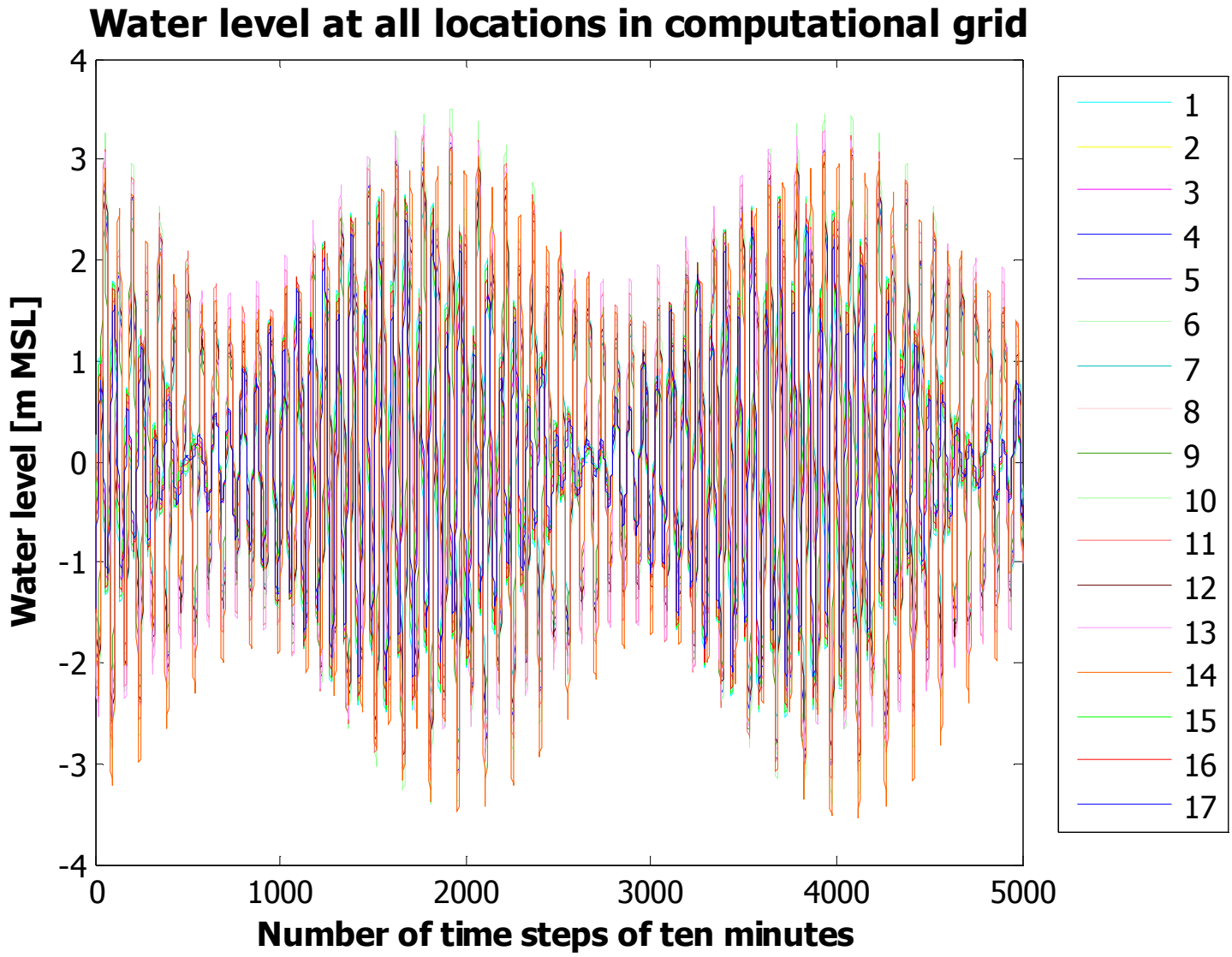
Appendix VI.   Measured data of water levels
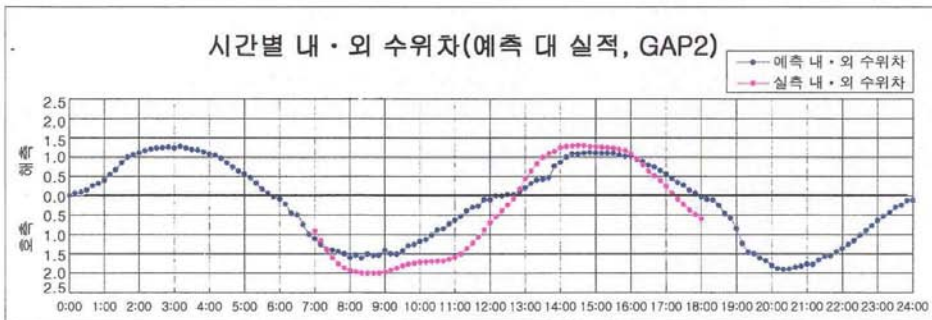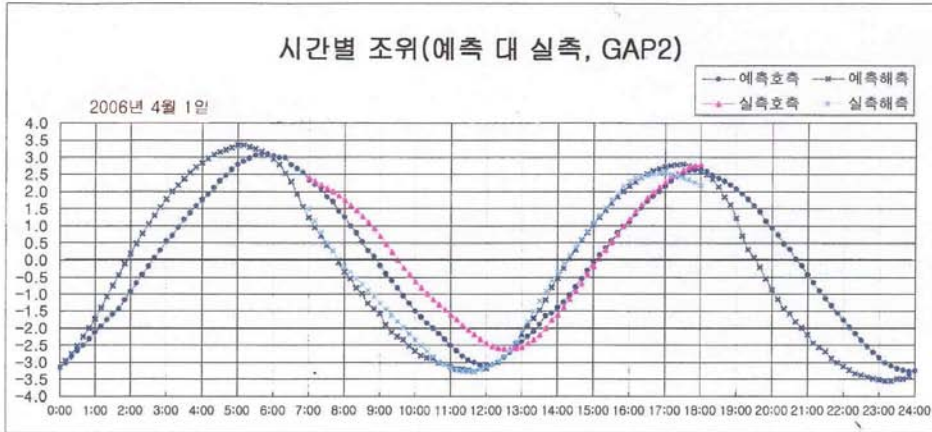
구분 \ 시간	0시	1시	2시	3시	4시	5시	6시	7시	8시	9시	10시	11시
예측(m) 호측	-3.17	-2.12	-0.92	0.54	1.75	2.78	3.03	2.34	1.25	-0.17	-1.49	-2.51
예측(m) 해측	-3.16	-1.73	0.19	1.77	2.83	3.35	2.95	1.23	-0.35	-1.58	-2.67	-3.14
실측(m) 호측								2.40	1.75	0.70	-0.63	-1.60
실측(m) 해측								1.50	-0.17	-1.26	-2.34	-3.18
내외수위차(m) 예측	0.01	0.39	1.11	1.23	1.08	0.57	0.08	1.11	1.60	1.41	1.18	0.63
내외수위차(m) 실측	–	–	–	–	–	–	–	0.90	1.92	1.96	1.71	1.58

구분 \ 시간	12시	13시	14시	15시	16시	17시	18시	19시	20시	21시	22시	23시
예측(m) 호측	-3.07	-2.40	-1.40	-0.07	1.12	2.14	2.63	2.07	0.93	-0.44	-1.76	-2.87
예측(m) 해측	-3.18	-2.20	-0.54	1.03	2.15	2.71	2.59	1.22	-0.87	-2.20	-3.13	-3.51
실측(m) 호측	-2.45	-2.55	-1.60	-0.19	1.20	2.28	2.78					
실측(m) 해측	-3.14	-2.10	-0.35	1.08	2.29	2.53	2.19					
내외수위차(m) 예측	0.11	0.20	0.86	1.10	1.03	0.57	0.04	0.85	1.80	1.76	1.37	0.64
내외수위차(m) 실측	0.69	0.45	1.25	1.27	1.09	0.25	0.59	–	–	–	–	–

Measured and predicted water levels for April 1, 2006 in Gap2
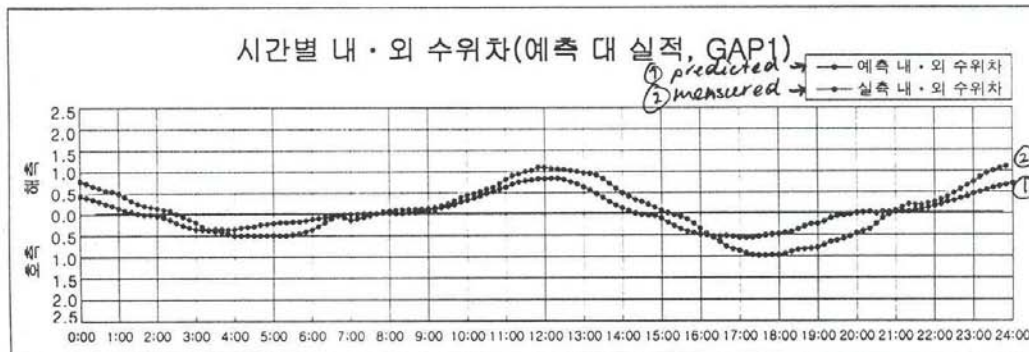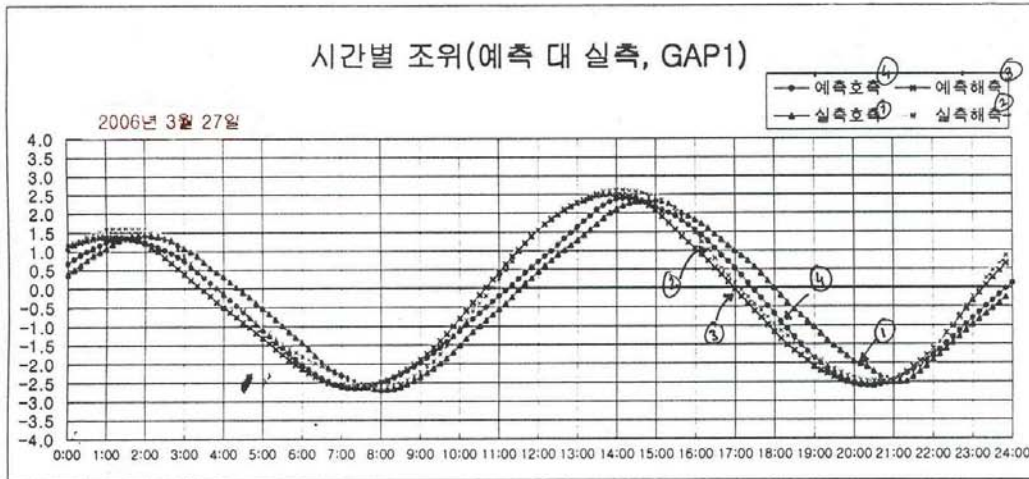
구분\시간		0시	1시	2시	3시	4시	5시	6시	7시	8시	9시	10시	11시
예측 (m)	호측	0.67	1.23	1.24	0.73	-0.15	-1.11	-2.02	-2.60	-2.52	-1.98	-1.13	-0.21
	해측	1.09	1.37	1.21	0.38	-0.50	-1.32	-2.14	-2.60	-2.49	-1.89	-0.80	0.43
실측 (m)	호측	0.38	1.07	1.43	1.08	0.32	-0.53	-1.44	-2.28	-2.69	-2.36	-1.52	-0.56
	해측	1.16	1.57	1.57	0.89	-0.18	-1.02	-1.80	-2.42	-2.61	-2.22	-1.07	0.26
내외수위차 (m)	예측	0.42	0.14	0.03	0.35	0.35	0.21	0.12	-	0.03	0.09	0.33	0.64
	실측	0.78	0.50	0.14	0.19	0.50	0.49	0.36	0.14	0.08	0.14	0.45	0.82

구분\시간		12시	13시	14시	15시	16시	17시	18시	19시	20시	21시	22시	23시
예측 (m)	호측	0.70	1.62	2.36	2.17	1.54	0.52	-0.69	-1.86	-2.55	-2.46	-1.80	-0.81
	해측	1.53	2.26	2.49	2.06	1.05	-0.04	-1.17	-2.10	-2.54	-2.43	-1.63	-0.35
실측 (m)	호측	0.44	1.28	2.11	2.35	1.82	1.00	0.00	-1.03	-1.95	-2.50	-1.92	-0.98
	해측	1.53	2.25	2.61	2.43	1.47	0.13	-0.97	-1.83	-2.41	-2.43	-1.65	-0.24
내외수위차 (m)	예측	0.83	0.64	0.13	0.11	0.49	0.56	0.48	0.24	0.01	0.03	0.17	0.46
	실측	1.09	0.97	0.50	0.08	0.35	0.87	0.97	0.80	0.46	0.07	0.27	0.74

Measured and predicted water levels for March 27, 2006 in Gap1

시간별 조위(예측 대 실측, GAP2)

2006년 3월 27일

시간별 내 · 외 수위차(예측 대 실적, GAP2)
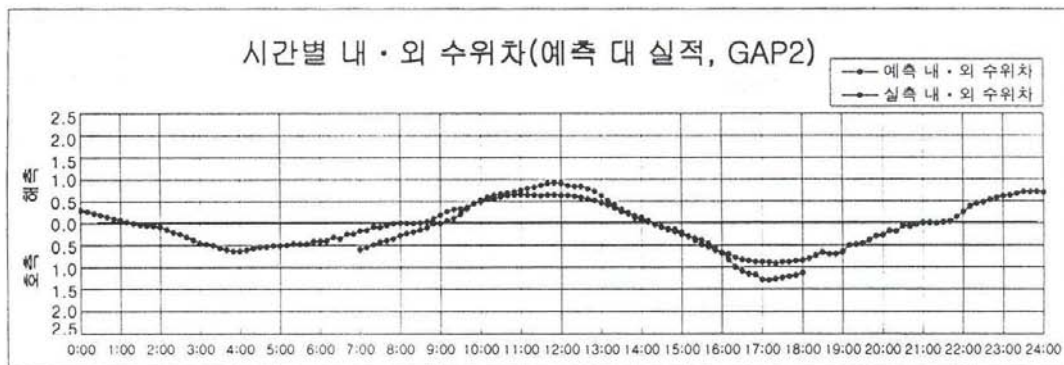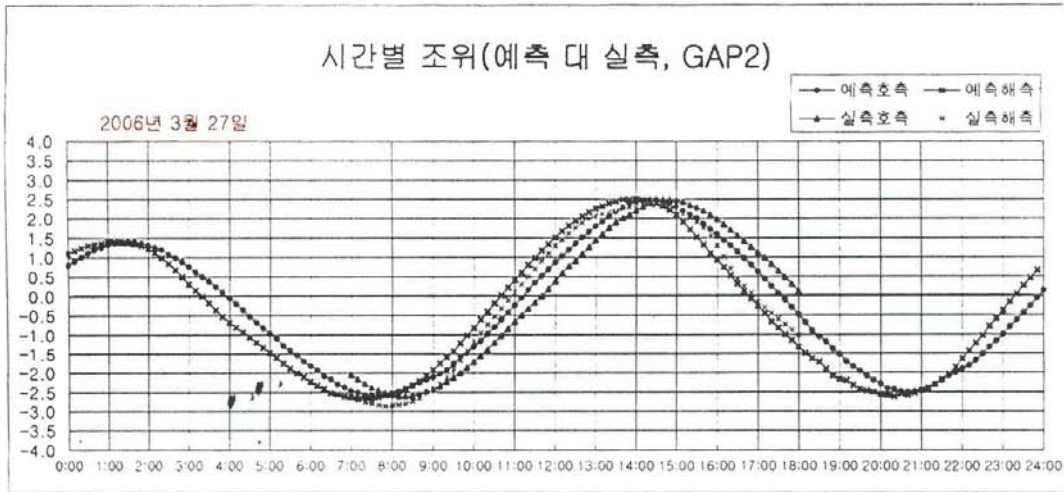
시간\구분		0시	1시	2시	3시	4시	5시	6시	7시	8시	9시	10시	11시
예측(m)	호측	0.80	1.32	1.31	0.76	−0.05	−0.97	−1.82	−2.46	−2.54	−2.11	−1.32	−0.24
	해측	1.10	1.39	1.22	0.31	−0.68	−1.48	−2.23	−2.63	−2.53	−1.92	−0.82	0.42
실측(m)	호측								−2.05	−2.57	−2.43	−1.71	−0.66
	해측								−2.65	−2.85	−2.43	−1.17	0.10
내외수위차(m)	예측	0.30	0.07	0.09	0.45	0.63	0.51	0.41	0.17	0.01	0.19	0.50	0.66
	실측								0.60	0.28	−	0.54	0.76

시간\구분		12시	13시	14시	15시	16시	17시	18시	19시	20시	21시	22시	23시
예측(m)	호측	0.87	1.79	2.43	2.29	1.59	0.62	−0.49	−1.52	−2.29	−2.46	−1.90	−1.00
	해측	1.51	2.26	2.50	2.08	0.93	−0.27	−1.33	−2.17	−2.56	−2.45	−1.64	−0.38
실측(m)	호측	0.38	1.44	2.20	2.47	1.98	1.12	0.12					
	해측	1.29	2.07	2.33	2.21	1.30	−0.17	−1.02					
내외수위차(m)	예측	0.64	0.47	0.07	0.21	0.66	0.89	0.84	0.65	0.27	0.01	0.26	0.62
	실측	0.91	0.63	0.13	0.26	0.68	1.29	1.14	−				

Measured and predicted water levels for March 27, 2006 in Gap2

Appendix VII.   Measured data of flow velocities

□ GAP2 (3월30일)

1. 구간별 유속분포도

<gap2 수심별 유속분포>
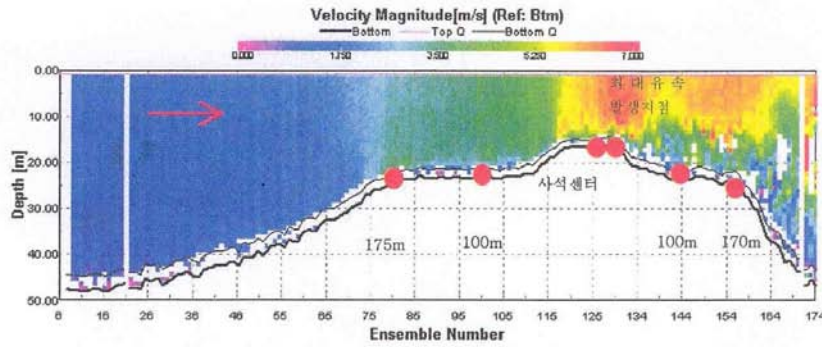
위치 수심(m)	175m(해측)	100m(해측)	사석센터	최고유속발생 12m(내측)	100m(내측)	170m(내측)
1.16	3.32	3.61	6.57	6.40	5.92	6.16
2.16	3.23	3.62	6.56	6.39	5.83	6.25
3.16	3.21	3.62	6.55	6.50	5.90	6.23
4.16	3.18	3.49	6.48	6.46	5.95	6.15
5.16	3.16	3.49	6.46	6.46	6.12	6.19
6.16	3.27	3.70	6.42	6.49	5.98	6.05
7.16	3.23	3.52	6.58	6.66	6.06	5.95
8.16	3.20	3.50	6.50	6.59	5.88	6.09
9.16	3.14	3.66	6.29	6.60	5.85	5.93
10.16	3.44	3.61	6.19	6.64	5.84	5.93
11.16	3.22	3.66	5.79	6.39	5.59	6.08
12.16	3.53	3.55	5.05	5.96	5.66	6.02
13.16	3.44	3.66	4.70	5.97	5.38	5.56
14.16	3.44	3.63	4.70		4.28	4.54
15.16	3.38	3.67			4.03	4.77
16.16	3.53	3.61			4.74	4.77
17.16	3.45	3.52			4.68	3.97
18.16	3.37	3.59			3.94	4.14
19.16	3.60	3.44			4.42	4.35
20.16	3.57	3.05			4.57	4.70
21.16	3.88	2.32				4.24
최대유속(m/s)	3.88	3.70	6.58	6.66	6.12	6.25
수심평균유속(m/s)	3.38	3.58	6.34	6.55	5.50	5.31

Measured water level with ADCP for March 30, 2006 in Gap2

시간별 유속(예측 대 실측, GAP1)

2006년 03월 26일

── 예측
── 실측
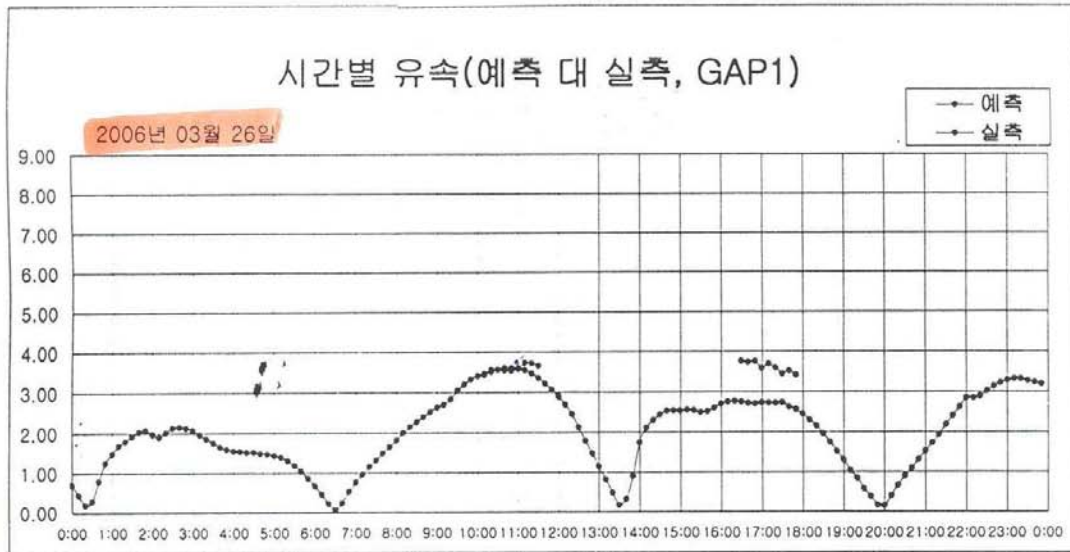
< 시간별 유속표 >

구분 \ 시간	0시	1시	2시	3시	4시	5시	6시	7시	8시	9시	10시	11시
예측 (m/s)	0.70	1.49	1.98	2.08	1.56	1.44	0.67	0.77	1.82	2.64	3.42	3.61
실측 (m/s)												3.59
유속차 (m/s)												-0.02

구분 \ 시간	12시	13시	14시	15시	16시	17시	18시	19시	20시	21시	22시	23시
예측 (m/s)	2.90	1.15	1.75	2.54	2.71	2.74	2.46	1.31	0.15	1.53	2.85	3.30
실측 (m/s)						3.59						
유속차 (m/s)						0.85						

< 일별 최대유속 >

구분		낙조1	창조1	낙조2	창조2	비 고
예측	시 각	2시 40분	10시 50분	16시 20분	23시 20분	
	유속(m/s)	2.16	3.62	2.78	3.33	
	내외수위차(m)	0.16	0.52	0.17	0.44	
실측	시 각	·	11시	16시30분		
	유속(m/s)		3.59	3.77		
	내외수위차(m)		0.6	0.33		

Measured and predicted flow velocity for March 26, 2006 in Gap1

시간별 유속(예측 대 실측, GAP2)

2006년 03월 26일

< 시간별 유속표 >

시간 구분	0시	1시	2시	3시	4시	5시	6시	7시	8시	9시	10시	11시
예측 (m/s)	0.48	1.74	3.00	2.53	2.16	2.06	1.43	0.18	2.32	2.95	3.20	3.12
실측 (m/s)											3.53	
유속차 (m/s)											0.33	

시간 구분	12시	13시	14시	15시	16시	17시	18시	19시	20시	21시	22시	23시
예측 (m/s)	2.54	0.93	1.88	3.37	3.27	3.39	3.16	2.23	0.82	1.94	2.97	3.31
실측 (m/s)					3.75							
유속차 (m/s)					0.48							

< 일별 최대유속 >

구 분		낙조1	창조1	낙조2	창조2	비 고
예측	시 각	2시 00분	10시 10분	15시 20분	22시 40분	
	유속(m/s)	3.00	3.21	3.60	3.33	
	내외수위차(m)	0.26	0.41	0.43	0.43	
실측	시 각	·	10시20분	16시40분		
	유속(m/s)		3.69	3.84		
	내외수위차(m)		0.41	–		

Measured and predicted flow velocity for March 27, 2006 in Gap2